# POLITECNICO DI TORINO

**Master of Science in**
**Mechatronic Engineering**

Master of Science Thesis

# Study and Design of a Hip Joint for Exoskeleton Applications

**Supervisor**
Prof. Luigi Mazza

**Co-Supervisors**
Prof. Terenziano Raparelli
Prof. Gabriella Eula
Prof. Alexandre Ivanov

**Candidate**
Gabriele Tilloca

December 2018

# Table of Contents

# Abstract

This work arises in the wearable robot's field, with the aim of decreasing the fatigue to the back of industrial workers in case of stooping or bending forward, leaving the possibility of walking when needed. The developed work includes a deep study of many robots available in literature, which brought to have a bird-eye view of the state of the art, allowing to understand the starting problem and set a design target and develop the optimal solution to realize it, with a particular focus on the hip joint in which the actuation system lies. The choose of the actuation unit and of its components brought to have a more realistic and detailed system, which has to work in three different modes. The first chosen working mode is the "free mode", in which the actuation unit is decoupled with the legs, allowing the user to walk. Besides, the "stooping mode" was studied to detect the trunk angle of the user and maintaining it, providing a hip torque. The last working mode, the "bending mode", has the aim of aiding the user to bringing back the trunk to the vertical position, performing the uprising. The conclusive part involves kinematic and dynamic simulations for the different operating modes of the hip joint. The control system was developed in MATLAB Simulink implementing the joint 3D models in MATLAB Simscape and allowing to simulate the controlled system behavior. Kinematics of the gait cycle, associated with "free mode", and dynamics, related to "stooping mode" and "bending mode", were then studied. In this way, all the three operating modes of the system were studied. For making this, a model composed by a four-bar linkage and the attached inertia was considered, imposing suitable boundary conditions. The employment of the series elastic actuator allowed to transform the torque control problem into a position control problem.

# Chapter 1

# Introduction

## 1.1 Motivations

The aim of this thesis is to study and design a device, able to sustain part of the weight of the upper body of an individual, in particular a factory worker, and providing help for particular movements, with the purpose to reduce the fatigue effort of the trunk during the work shift, with a special focus on the hip joint design. It’s been proved that the muscular fatigue has an extremely negative impact on people, because brings the worker to perform incorrect movements, producing both localized muscle discomfort and balance problems [1], bringing to a decrease of the working efficiency. This thesis work lies in the wearable devices branch. In particular, being conscious of the design target, devices of this kind are commonly known as wearable robots (WR) or, in similar cases, exoskeletons (EXO), devices worn by human operators for a wide range of reasons.

## 1.2 Preliminary Discussion about the Exoskeleton Design

In anatomy the human body motion is commonly decomposed in the movement into three planes (*fig.1*): the sagittal plane, the coronal plane and the transverse plane. The EXO to be designed, for assumption, will provide torques only on an axis perpendicular with the sagittal plane. The human body will often be schematized as a two-dimensional system, composed just by rotational joints and rigid links, moving only on this plane. In the anatomical terminology, the angular motions of the trunk with respect to the hip joint center (HJC) are defined as flexion (trunk forward) and extension (trunk backward). The range of motion (ROM) of the trunk was already studied [2]: the maximum flexion is around 120°, and the maximum extension is around -10°. Nevertheless, the active hip extension is not of interest for this work, and the ROM of the active hip flexion of the EXO will be for sure much less than 90°, considering the application field.

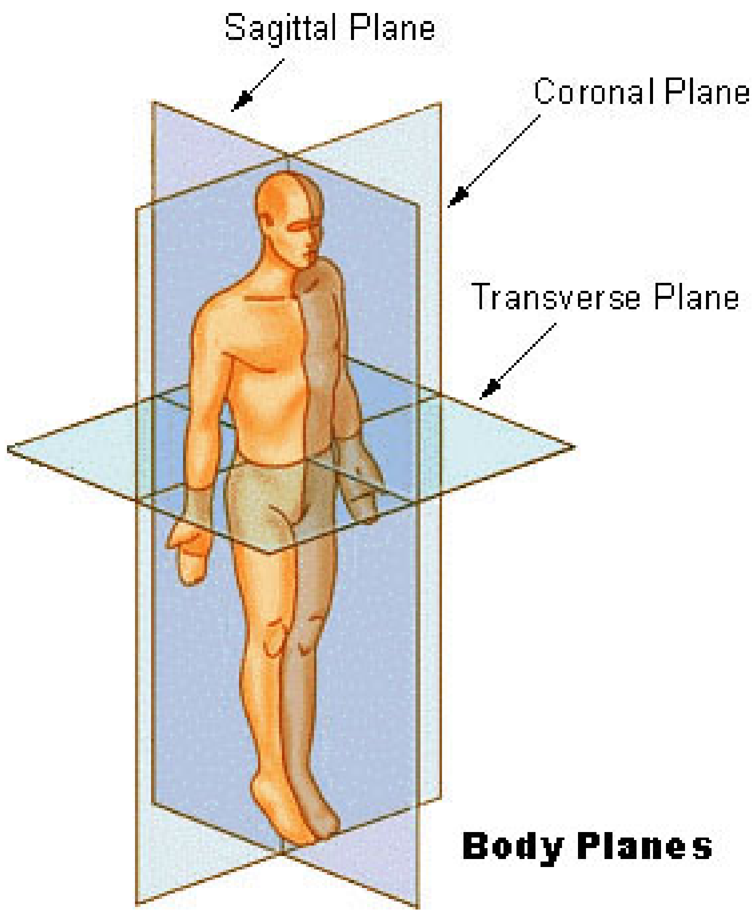


*Figure 1. Standard Body Planes [96]*

The WR to be designed is asked to provide a torque, providing a good dynamic response to the EXO-wearer system, in different operating mode. Indeed, the exoskeleton will offer support to the user when bending forward, both when the subject maintains the position and when he wants to perform the uprising, reaching the vertical position, providing a power able to partially equilibrate his upper body weight, and decreasing the fatigue. A torque will be provided by the hip joint, properly designed and actuated by a pneumatic or electric motor. An important aspect for the design of the WR is the physical human-robot interaction (pHRI), with the aim of transmitting power, with actuators and rigid structures, from the robot to the subject's musculoskeletal system.

The torque, as already mentioned, lies on the sagittal plane, and is applied to the hip joint that corresponds to the only actuated degree of freedom (DoF) of the system for each side. Nevertheless, both sides of the EXO (left and right side) will be actuated, bringing the system to have two active DoF. To avoid redundancy in this dissertation only the left side will be considered.

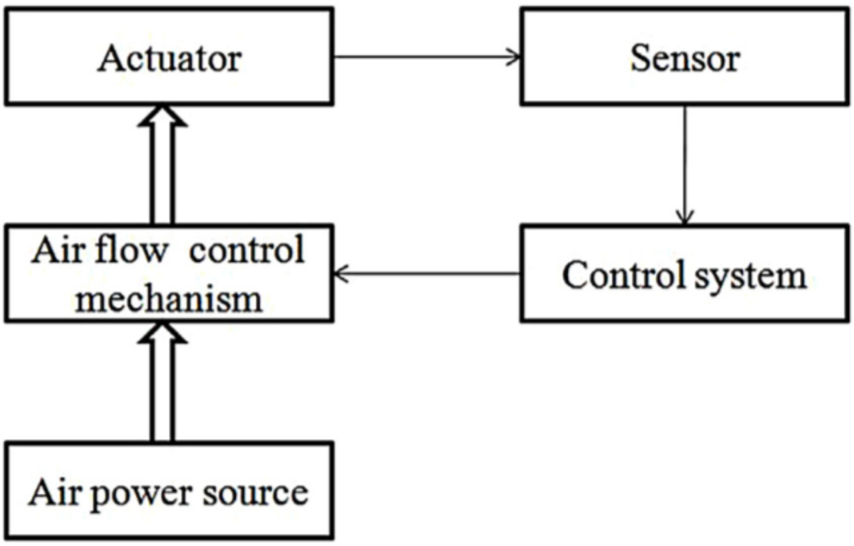


*Figure 2. Basic Structure of a Servo Pneumatic System [3]*

It's not negligible the fact that the user must be able to perform other movements, otherwise the robot acts as an obstacle, and this is not a desired behavior. It's then relevant planning other passive DoFs, corresponding to rotational/prismatic/spherical joints, with the purpose to allow not only flexion/extension movements, but also adduction/abduction (rotation in the coronal plane), which helps keep balance of body while center of gravity shifts during walking, and internal/external rotation (in the transverse plane) of the legs, to assist human to turn around during walking. The free movement of torso, chest and shoulders is also required. It’s of primary importance that the wearer would be free to perform these movements, without feeling constrained by the EXO.

It's not even to underestimate the wearability of the device, in terms of time needed to wear the EXO and in terms of number of other people needed to help the wearer to fit it. A good dressing system is important to save time for the company, and to avoid that the user senses the WR as an obstruction, beyond that a waste of time.

A control system is necessary to provide a proper torque, making it interact with the actuators and the sensors of the WR. This latter side of the WR design is also known as cognitive human-robot interaction (cHRI). An example of a typical structure of a servo pneumatic system is shown in *fig.2*. Another fundamental aspect of the design is providing a user-friendly robot, realizing a safe, easy to employ, comfortable pHRI. In fact, the main interactions between human and robot are performed by means of the sensors (cHRI) and the contact surfaces (pHRI).

One of the main issues emerged from the literature [4] is the importance of the correct alignment between the hip center axis of the user articulations, usually simplified as a “ball and socket joint”, and the HJC axis of the robot. A misalignment between them brings to discomfort or even pain. If this unpleasant interaction with the robot is reiterated over time, in application scenarios as daily living or working activities, micro/macro misalignments between the user and the exoskeleton hip axes may bring to discomfort, skin abrasions, and overloads to muscles and articulations [5-6], with a possible propagation also to knee, ankle, etc. This situation becomes more severe in applications different from the industrial ones, such as in medical environment where some users are not able to feel pain (paraplegic patients) when wearing the exoskeleton for rehabilitation purposes. A proper alignment of these axis is difficult to achieve, considering the extreme variability of the anatomy for different reference subjects. It’s then necessary to design a size adjustment mechanism, not only for the hip joint, to adapt the robot portions to many possible users. It’s possible to consider the possibility of adding not only a manually adaptable mechanism to regulate the links, but also flexible attachments or additional passive joints.

Another important factor to consider, to achieve a good comfort, passes through a suitable design of the contact zones between WR and user. It’s crucial the choice of the geometric characteristics and the material of the interaction surfaces between the wearer and the device, besides a proper mechanical design. Indeed, in order to have a safer and more comfortable device, it’s significant to have a system with a low mechanical impedance on the actuated joints. As “joint mechanical impedance” [7] we mean the relation between the force (or torque) applied to the considered element, and the correspondent linear (or angular) displacement.

A low mechanical impedance is a typical characteristic of the so-called yielding systems, in which is possible to observe variation on the linear/angular displacement, when external forces/torques are applied. This is important because a WR with a high mechanical impedance is characterized by an irreversible motion, and may hinder the wearer's movements, acting as an obstacle for him. At the contrary, a WR having a low mechanical impedance results in a more comfortable interaction with the user, especially in cases as bumps or quick movements, very common in practice.

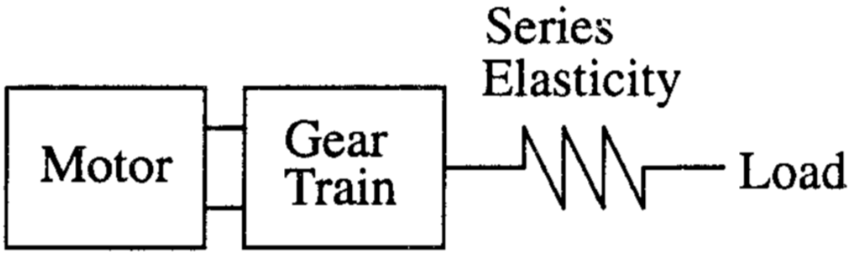


*Figure 3. Block Diagram of a Series-Elastic Actuator [8]*

It's possible to achieve a similar behavior adding to the system a compliant element (usually a spring), able to absorb high frequency loads and granting a low mechanical impedance, independently form the user's movements. In this application field it's always inadvisable connect the powertrain directly to the load, even more so the "load" is a human being.  The most common choice in literature is adding a spring element, with an intrinsic characteristic as linear as possible, in series with the mechanical output of an electric gearmotor. This configuration is known as series-elastic actuator (SEA) [8] system.

Another fundamental aspect regarding the comfort of the WR is related to the contact surfaces between user and robot. Large interaction surfaces allow a better distribution of the forces/torques applied to the anatomic portions of the subject, to limit unpleasant tissue deformations [9]. In general, the body tolerance to torques is limited, and pure forces are much better accepted. The loads are derived both from the weight of the device and from the forces/torques supplied actively by the robot [4-6]. Furthermore, the weight of the device is a problem especially for lower-limb EXOs, due to the vertical orientation of the segments: without strong translational couplings [6], the exoskeleton cuffs may slip due to gravity and cyclical inertial forces, irritating the user's skin. The weight problem is not so easy to be solved. If for the rigid parts a satisfying goal has been reached, with light but

resistant materials, it's not possible to assert the same for the actuation system (comprising not only the actuators, but also the energy source, like batteries, air power sources, etc.), due to technological and physical limits.
The research is now focusing on new actuation methods, and on the modification of the existing ones, in order to increase the efficiency, the capacity (for batteries) and decrease the weight [10]. At the moment, to have lighter actuation system is mandatory renouncing to a portion of power, and this is not always possible, depending on the application.
It's hence easy to understand the reason why the exoskeleton design must take into account not only the "purely mechanical aspect", but also a key requirement as the ergonomics, regarding a proper regulation system, the overall weight, adequate contact surfaces, and an easy dressing system.

## 1.3 Classification of the Wearable Robots

By means of the found literature, is possible to extract different schematic classifications for the WRs.

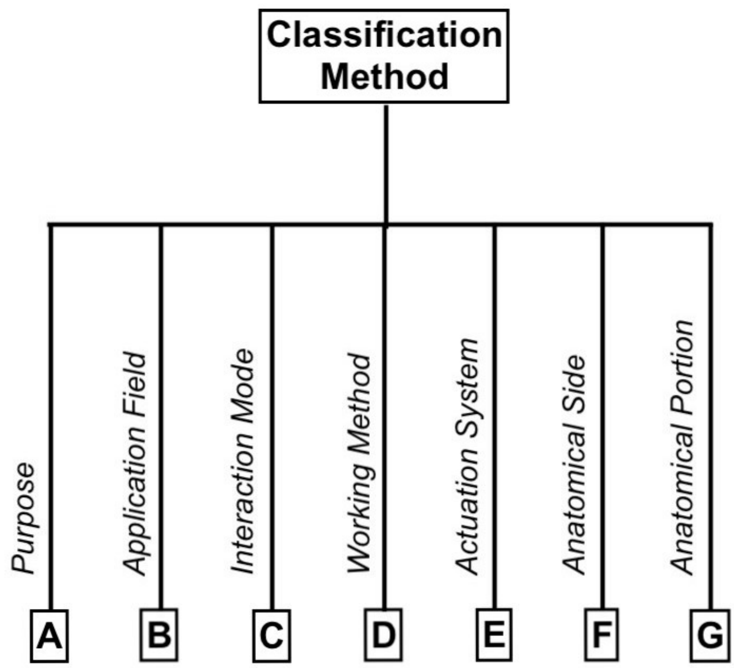


*Figure 4. Classification Methods of the Wearable Robots*

A first sorting of the exoskeletons can be made regarding their purpose (A). They can then be divided into three main categories:

A1. *Power-augmenting robots*: in this category are contained all the WRs with the aim of increasing the human capabilities, in terms of force or resistance. The exoskeleton studied in this work lies on this category, being a robot designed to support the user, increasing the human resistance related to the fatigue;

A2. *Treadmill-based rehabilitation robots*: these EXOs are fixed robots used in medical field, typically in combination with other instruments, like computers and treadmills. They are normally located in hospitals or in private clinics;

A3. *Over-ground rehabilitation robots*: even this category of robots is used in medical environment, but these can be worn by the user without a support apparatus. They may be then used both in a hospital structure and at home or in mobility, to help the subject with rehabilitation needs, to reacquire some lost capabilities or just to act as support or protection for particular movements;

A4. *Assist robots*: these are typically passive robots, with the aim to support the user without providing energy, just for safety or to induce the subject to perform correct movements.

The exoskeletons may also be categorized depending on the application field (B):

B1. *Medical branch*: nowadays the wearable robots used in medical field are the most common. Most of the requests of exoskeletons are addressed to patients who need rehabilitation;

B2. *Military branch*: the first exoskeletons are born for this application in the '60s. They are still used in the battlefield, and are typically power-augmenting robots, used to carry heavy loads;

B3. *Industrial branch*: this is the youngest application field. Some companies (e.g. Audi, Ford, BMW, etc.) have recently adopted power-augmenting robots to aid the workers, in order to increase the productivity and improve the working conditions.

A third classification takes into account the interaction mode (C) with the wearer:

C1. *Parallel coupling*: worn by the subject as anatomical supplement, in any application field. In medical field they are often called "orthosis";

C2. *Series coupling (prosthesis)*: worn by the subject as substitution of a missing anatomical portion (e.g. the amputation of a limb).

One of the main features of an exoskeleton is the working method (D), and the classification to be made is quite simple:

D1. *Passive exoskeletons*: they are the simplest robots, without an actuation system. A sub-classification of these robots can be easily made: there are “simple” passive EXOs, composed only by links and joints, and passive EXOs with an “energy storing system”, typically springs. The latter are very common;

D2. *Active exoskeletons*: at least one of the robot joints is actuated, in order to supply an external force/torque to be propagated to the rigid links and then to the user. These robots necessarily need a suitable control system, both for an adequate working of the robot and for user’s safety. The control system may be open-loop or closed-loop. A closed-loop control system requires a suitable sensorization of the device;

D3. *Hybrid exoskeletons*: this category mixes the active exoskeletons, also with different actuation methods, with the passive exoskeletons with an “energy storing system” in order to achieve an energy recovery during the actuation.

Considering only the active/hybrid exoskeletons, it is important to distinguish the WRs depending on their actuation systems (E):

E1. *Pneumatic actuation*: pneumatic actuators offer numerous advantages, such as safety, cleanliness, easy maintenance, relatively low cost, high power to weight ratio, high mechanical efficiency and long working life. For these reason pneumatic actuators are fairly adopted in the WRs. The main drawbacks are their nonlinear characteristics, which affects badly the accuracy of this actuation system, and a high noise level;

E2. *Hydraulic actuation*: this actuation system has advantages such as a very high peak power, extremely high load ratings and long working life. Unfortunately, these actuators have a high cost for purchase, operate and maintenance. Besides, there’s the problem of the hydraulic fluid leak. These actuators are the least used for the wearable robot application;

E3. *Electric actuation*: these are the most common actuators. The power is strongly dependent on their dimensions, and then to their weight, but these motors are very versatile and have a low environmental impact. Furthermore, they have a very high efficiency;

E4. *Internal combustion engine actuation*: now obsolete, this kind of actuation system is no more taken into account for WRs mainly for safety reasons, due to the high temperatures, the explosion risk, and the bad environment impact of these engines even at idling;

E5. *Hybrid actuation*: some robots combine different actuation methods in different joints, to obtain the desired behavior of the EXO.

Another usual classification, even if trivial, is made considering the body side (F) in which the robot operates, with respect to the sagittal plane:

F1. *Unilateral robots*: operates only on left or right side of the subject;

F2. *Bilateral robots*: operates on both sides of the subject. They may be symmetric or asymmetric, depending on their configuration.

A last categorization considers the anatomical portion (G) in which the robot acts:

G1. *Lower-limb exoskeletons*: they act mainly on the legs. Most of them are gait assistant with active rotational joints on the hip and/or on the knee, then the majority is bilateral;

G2. *Upper-limb exoskeletons*: they act on the arms and, being mostly rehabilitation robots, they may be unilateral or bilateral according to the requirements. Differently from other robots, these ones need an extremely high dexterity;

G3. *Upper-body exoskeletons*: these robots are studied to support the trunk or helping its movements: most of them are passive EXOs;

G4. *Full-body exoskeletons*: they cover a great portion of the body, included lower and upper limbs. All the robots found in literature belonging to this category are power-augmenting EXOs, but in a next future is easy to predict other applications for these wearable robots.

G5. *Extremities robots*: these devices act on a relatively small anatomical part (e.g. hand, ankle, neck, etc.).

By means of these classifications is possible to define almost each robot found in the current literature. The exoskeletons that are not part of these categories can be considered as "experimental" or anyway a very rare case, for which is not possible to extrapolate a defined category.

It's now necessary going into details, providing a bird-eye view of the progress of the wearable robots' field, quoting the already existing exoskeletons that could be relevant for this work, analyzing their peculiarities with a special focus on the hip joint, that will be the actual core of this thesis.

## 1.4 History and State of the Art

The first device which may be considered an exoskeleton-like device was developed in 1890 by Nicholas Yagn, and was an apparatus [11] composed by bags filled with

compressed gas, used to store energy and assist passively human movements, such as walking, running and jumping.
As already said the first true EXO was developed in the '60s, by a cooperation between the United States Armed Forces and the General Electric. It was named Hardiman I [12], was a full-body 30 DoFs (15 per side) power-augmenting exoskeleton powered by an electrohydraulic system, developed for military purposes in naval environment, and was supposed to amplify the strength of the wearer, making him lift up to 680 kg, a quantity equal to its mass. Unfortunately, the project was unsuccessful, due to the slow responses to user inputs, resulting in violent and uncontrolled motions. For these reasons it was never tested with a human inside it.

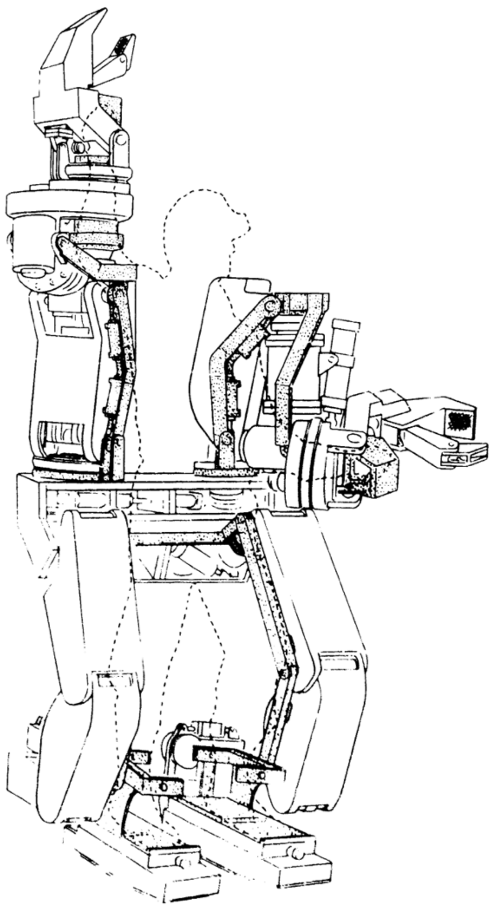

*Figure 5. Hardiman I [11]*

Starting from the '70s the research was focused not only on the military field, but also in the medical one, trying to satisfy all the needs of the people with physical issues, especially to help them with the rehabilitation of the gait cycle. This brought to the development of new technologies for the growth of active prosthesis and orthosis. In both fields have been found similar issues, mainly related to the difficulty of decreasing the weight, to the reliability, to the power supply, to the actuators and of increasing the efficiency. Some of these troubles are not solved yet, but substantial steps were made by the researchers, bringing the biomechanics technologies to be more and more common. Starting from the last years of the '90s there was a great increase of the WR study, bringing the development of robots in other application fields, such as the industrial one in the last few years.

In 2004 Pratt et al. developed the RoboKnee [13], a unilateral, performance-augmenting, lower-limb robot, with a single active DoF on the knee, which allows the wearer to climb stairs, and perform deep knee bends, even while carrying important loads in a backpack. The aim of the user is decided by the control system, which receives as input the knee joint angle and the ground reaction forces detected by different sensors. The actuation is performed by a brushless DC servo motor, placed in a SEA with two linear springs, to achieve a low mechanical impedance. The torque is applied around the knee, allowing the wearer to relax the quadriceps muscles. The desired force to provide is compared to the actual measured force. The produced error is the input of a proportional derivative (PD) controller, which output is the current needed by the electric motor.

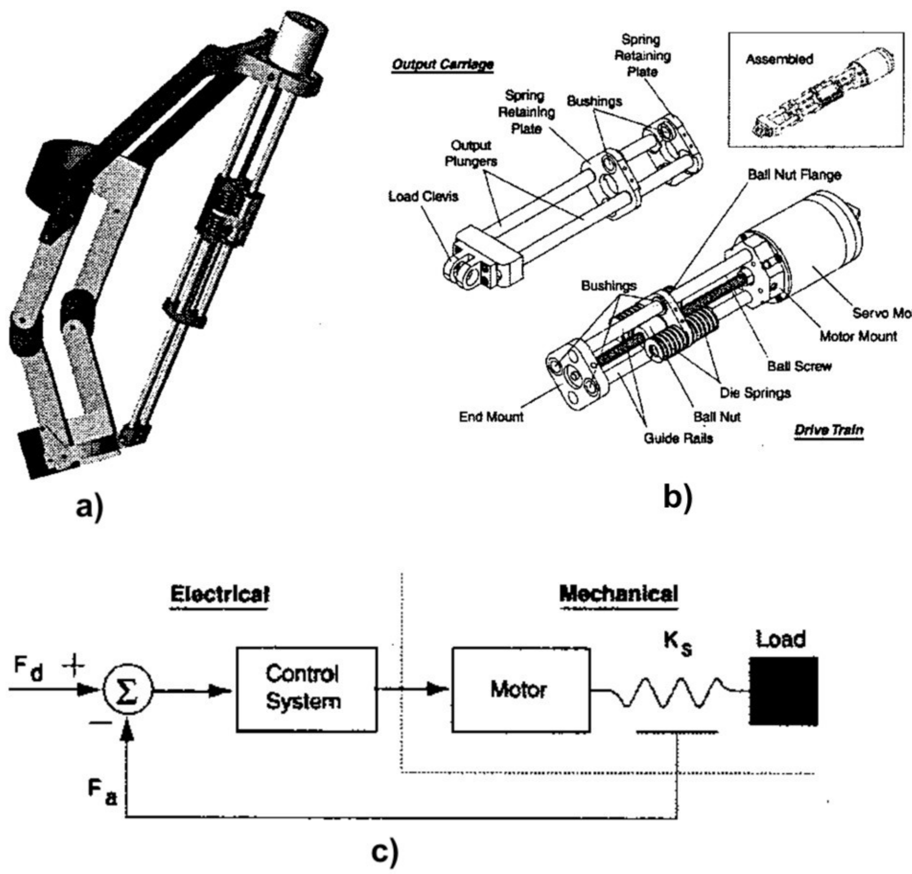


*Figure 6. a) RoboKnee b) Exploded View of the RoboKnee SEA c) RoboKnee SEA Block Diagram [13]*

In the same year at the Berkeley University of California was developed the Berkeley Lower Extremity Exoskeleton (BLEEX) [14-15], a lower-body power-augmenting robot, designed for military purposes. This can be considered the first functional load-carrying and energetically autonomous EXO. The BLEEX has 14 DoFs (7 per leg), eight of which are powered by linear hydraulic actuators, mounted in triangular configuration to provide a torque varying as a function of the angle. Wearing this robot, the user will increase his strength and his endurance during locomotion, walking at the average of 1.3 m/s while carrying a 34 kg payload. The aim of the BLEEX is to provide a versatile transport platform for mission-critical equipment. This robot implements a particular control system that doesn't require any sensor in the interface between the user and the exoskeleton, using the inverse dynamic of the robot as a positive feedback controller. The trade-off of this choice is that it requires a relatively accurate model of the whole system.

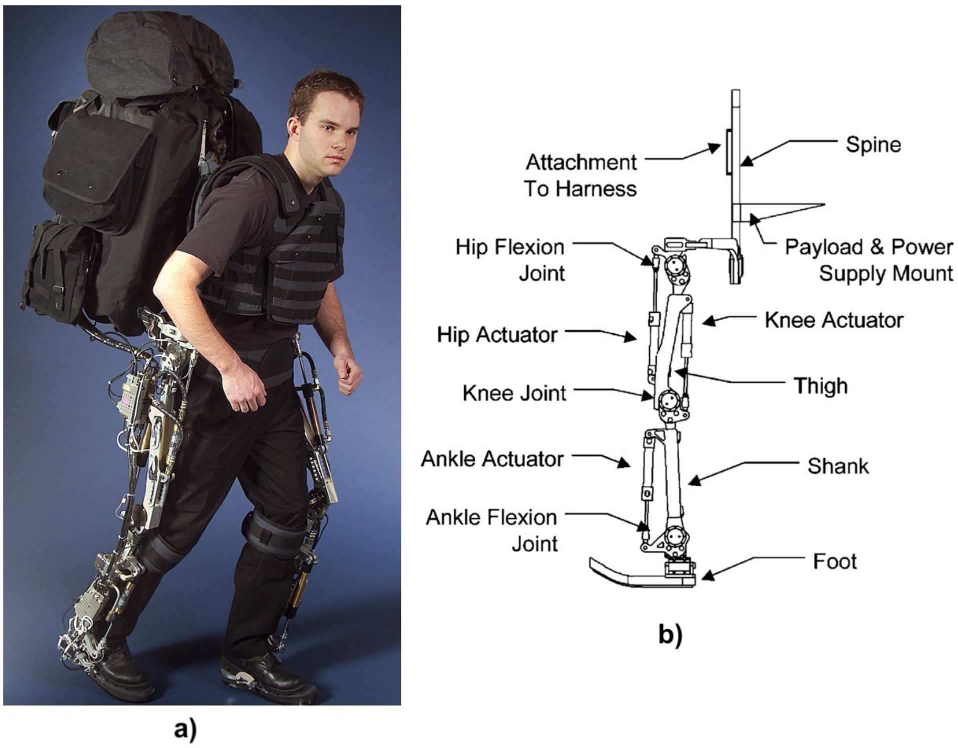


*Figure 7. a) Final BLEEX Design b) Simplified BLEEX Model [15]*

Focusing on the hip joint is possible to note that for each side there are three DoFs, corresponding to the three rotation axes. The abduction/adduction joint is placed in the back of the waist, the flexion/extension joint is positioned on the side of the hip. The rotation axis has indeed been moved from the hip side to the back of the person, to avoid problems related to the payload, and is common to both legs. The only actuated joints are the abduction/adduction and flexion/extension ones, by hydraulic cylinders connected respectively to torso and thigh modules.

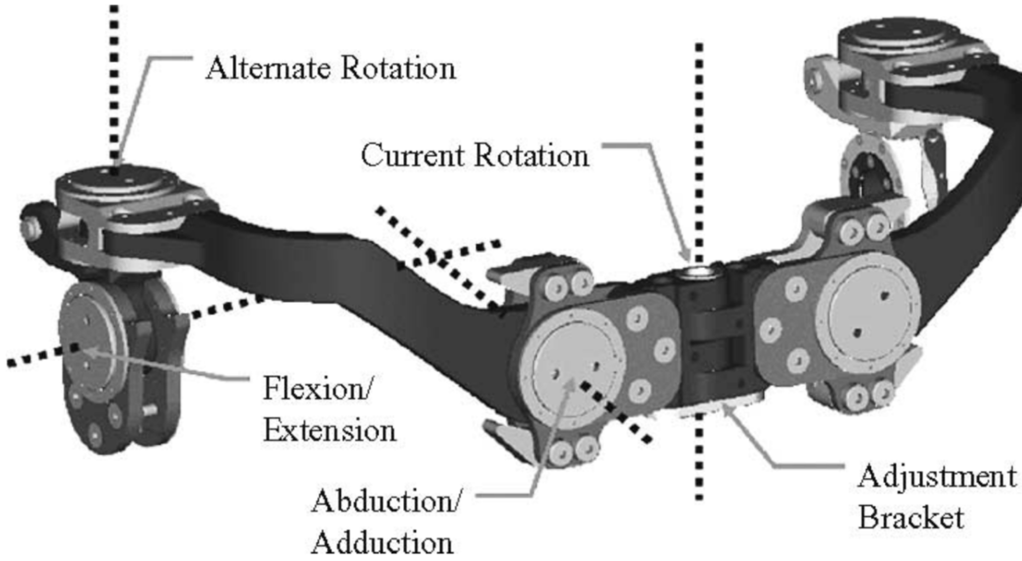


*Figure 8. BLEEX Hip DoFs (back view) [15]*

In 2006 at University of Salford (UK) was presented a 10-DoF lower limb exoskeleton [16] for force augmentation and active assistive walking training, addressed to the rehabilitation of brain/spinal injured patients, powered by pneumatic muscle actuators (PMAs). PMAs have the advantage to have low mass and volume, but relatively high power. They have the capacity to reproduce the real muscle behavior and such as can be considered a soft and biomimetic actuation system. The leg structure is made in aluminum, with some joint portions made in steel. Each leg presents 3 DoFs at the hip structure, 1 DoF at the knee and 1 DoF at the ankle. Even in this case the abduction/adduction joint is mounted on the rear of the waist. Two PMAs are mounted on each leg to perform the hip flexion/extension, and they're capable to produce a 60 Nm torque with a ROM larger than the human one. The control is performed by a proportional integral derivative (PID) controller in closed loop with the torque, but there are also inner loops that consider the pressure in the muscles. Torque sensors and pressure sensors are then used.

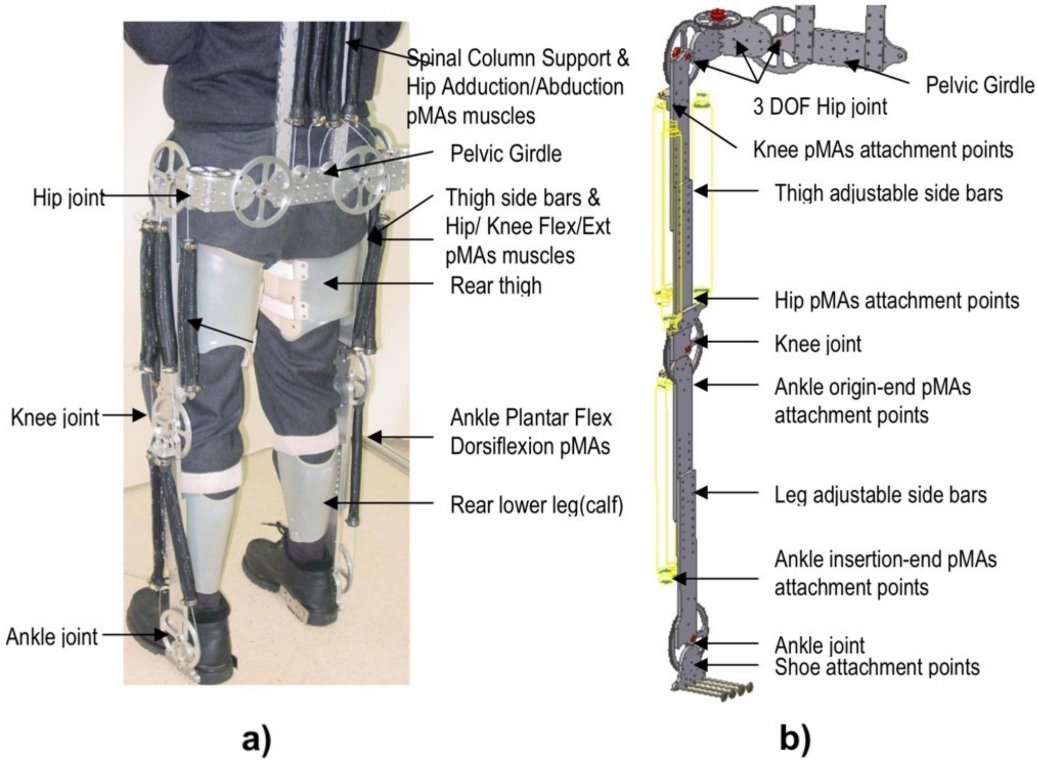


*Figure 9. a) The 10-DoFs Lower Body Exoskeleton b) 3D CAD Graphical Representation of a 10-DoFs Lower Body Exoskeleton Leg [16]*

In the same year in South Korea, at the Sogang University, was presented the EXPOS [17], a particular exoskeleton for patients with a residual degree of mobility, in which the wearable module is minimized (its mass is less than 3 kg). The wearable part is composed just by links, joints and sensors to detect motion. The actuation system is positioned in a smart caster walker, also useful to maintain a stable posture. Because it carries motors, drivers, controllers and batteries, its weight is significant. The power is transmitted from the smart caster walker to hip and knee with a tendon-driven mechanism composed by pulleys and a double-layered wire. As already said, the sensorization system is positioned on the wearable module of the EXPOS, and is composed by pressure sensors, able to detect the muscles contraction. The main disadvantages of the EXPOS are its important dimensions and the capability of working only on flat surfaces.


*Figure 10. EXPOS [17]*

Considering the treadmill-based robots, in 1999 was used for the first time on a patient the 4-DoFs robotic orthosis Lokomat [18]. It was developed for the training rehabilitation of locomotion for stroke and spinal cord injured patients. The whole system consists of a treadmill, a suspension system to provide the body-weight unloading, two PCs and the Lokomat itself. One PC runs the control task, the other one acts as graphical user interface. This robot moves only on the sagittal plane and it has only four rotational joints (two per leg at hip and knees) actuated by four linear drives, containing force sensors, and a parallelogram structure, which allows the vertical motion of the patient. The actual hip/knee joint angles are measured by precision potentiometers and computed by PD position controller to achieve the reference hip and knee joint angles. In fact, the system uses a control algorithm based on the inverse dynamics, controlling the impedance to achieve the desired torque at the joints.

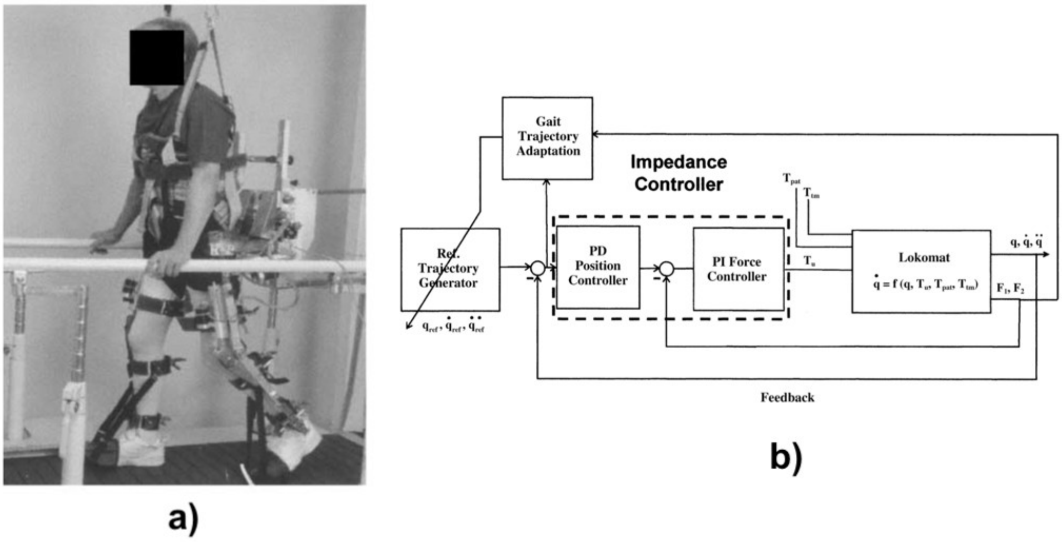


*Figure 11. a) Automated Treadmill Training with Lokomat b) Block Diagram of the Gait-Pattern Adaptation Algorithm of the Lokomat [18]*

Another important treadmill-based lower limb rehabilitation robot was presented in 2007. It is called LOPES [19] and combines a 2D-actuated pelvis segment free to translate in all three axes, and a leg EXO containing three rotational joints per leg, two at the hip and one at the knee. It is programmed to work in two ways: following the patients or guiding them. The LOPES is electrically actuated by servomotors, and the adopted control variable is the impedance as in the Lokomat case. The power is transmitted by means of SEAs driven by a flexible Bowden cable transmission.

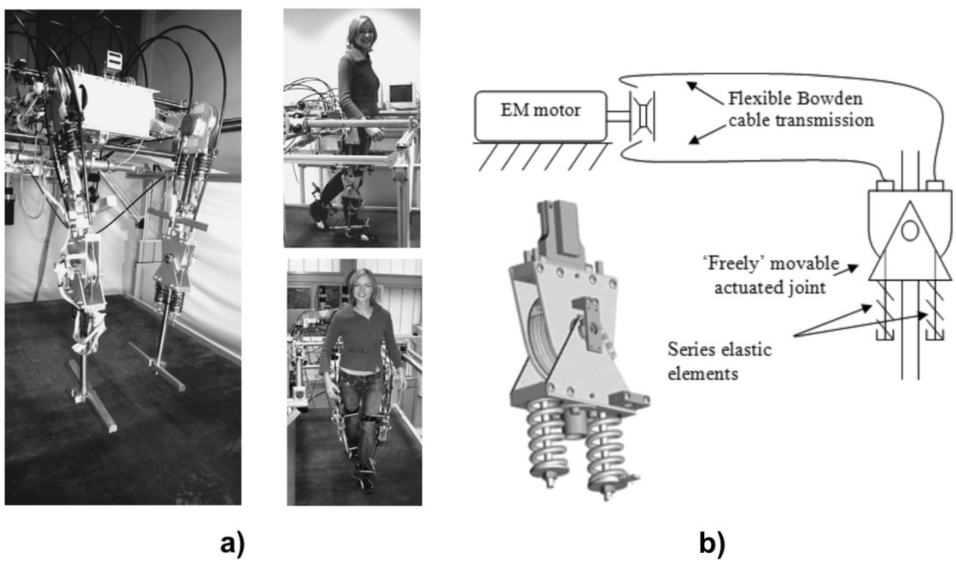


*Figure 12. a) Prototype of the LOPES b) Joint Actuators of the LOPES [19]*

In 2004 do Nascimento et al. [20-21] developed a unilateral single-DoF lower limb robot powered by PMAs, with the aim of providing gait assistance. The pelvic brace and the thigh support of the orthosis are made of polyethylene and are shaped on the patient's body; it causes a low versatility. These two parts are connected by a vertical articulated aluminum beam, constrained to avoid hyper-extension. It has just one passive DoF on the sagittal plane to allow the hip flexion/extension only. The PMA, made of an internal latex bladder surrounded by a braided nylon shell, is mounted in triangular configuration with thigh and torso. The pneumatic muscle, by means of flexible but not-extensible nylon fibers, shorten when pressurized, producing an external tension load. Of course, this tensile force heavily depends on the contraction: a PMA at its maximum displacement generates no force. This solution is interesting because the pneumatic muscles are capable to develop a rather high force maintaining a good weight/power ratio. The actuation of the PMA is controlled by a voluntary activation method based on the angular behavior of the hip joint.

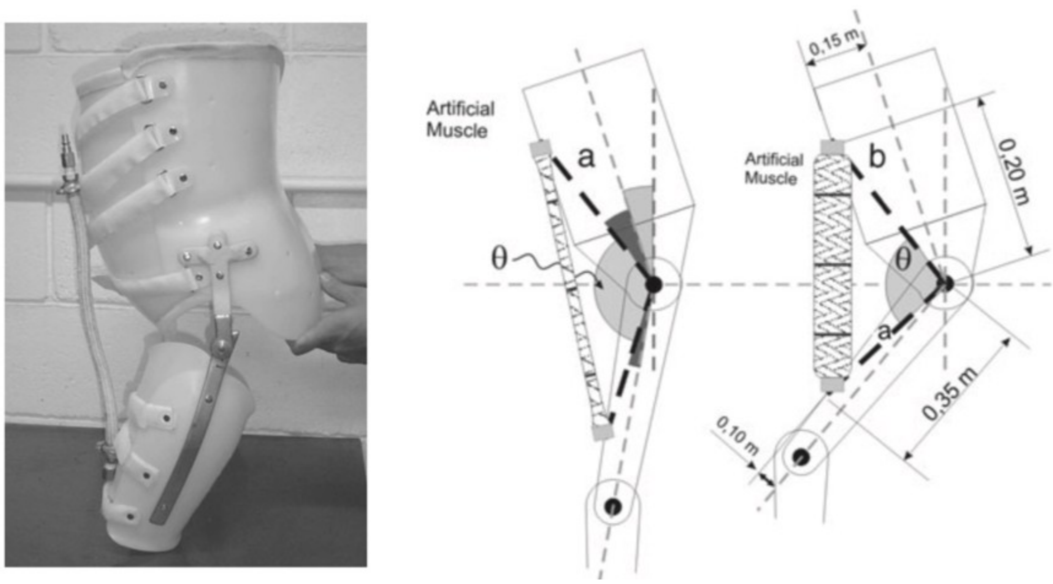


*Figure 13. Realization and Geometric Model of the Orthosis Designed by do Nascimento et al. [20]*

Returning to the treadmill-based robots, a unilateral orthosis was also created. The Active Leg Exoskeleton (ALEX) [22] is a lower limb robot for gait assistance, developed for stroke patients. Some links, such as the thigh or the shank ones, are telescopic, so that it could be adapted to different users. The EXO has a total of seven DoFs: three DoFs on the trunk (two translations and one rotation), two DoFs on the thigh (rotations in sagittal and coronal plane), one DoF on the shank and one DoF on the ankle. The hip and knee joint movement on the sagittal plane is powered by linear actuators, able to generate up to 60

Nm, with built-in encoders to determine the current position. All the other DoFs are passively held by springs. To apply normal and tangential forces to the ankle of the user, a force-field controller was developed.

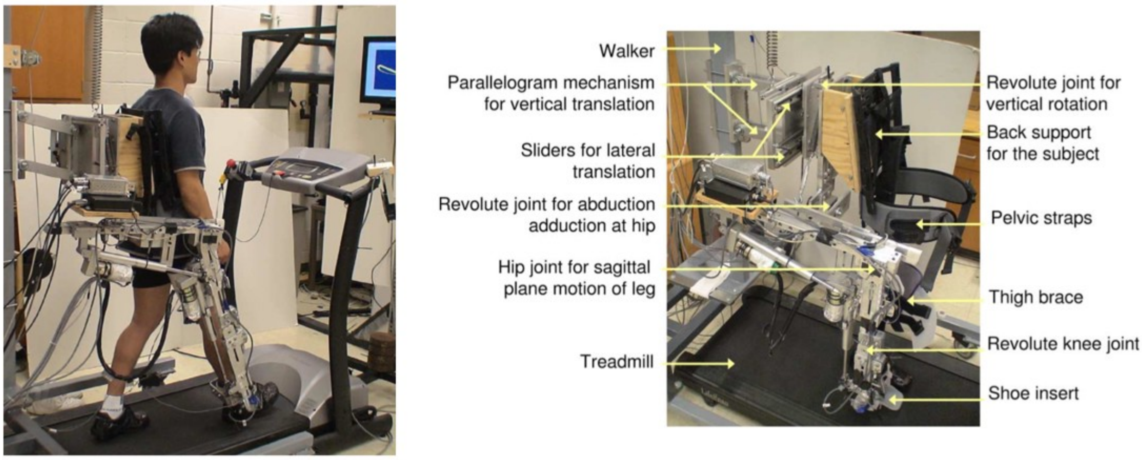


*Figure 14. ALEX [22]*

One of the most popular powered exoskeletons is for sure the Hybrid Assistive Limb (HAL) [23-26] developed by a cooperation between the Japan's University of Tsukuba and the robotic company Cyberdyne.

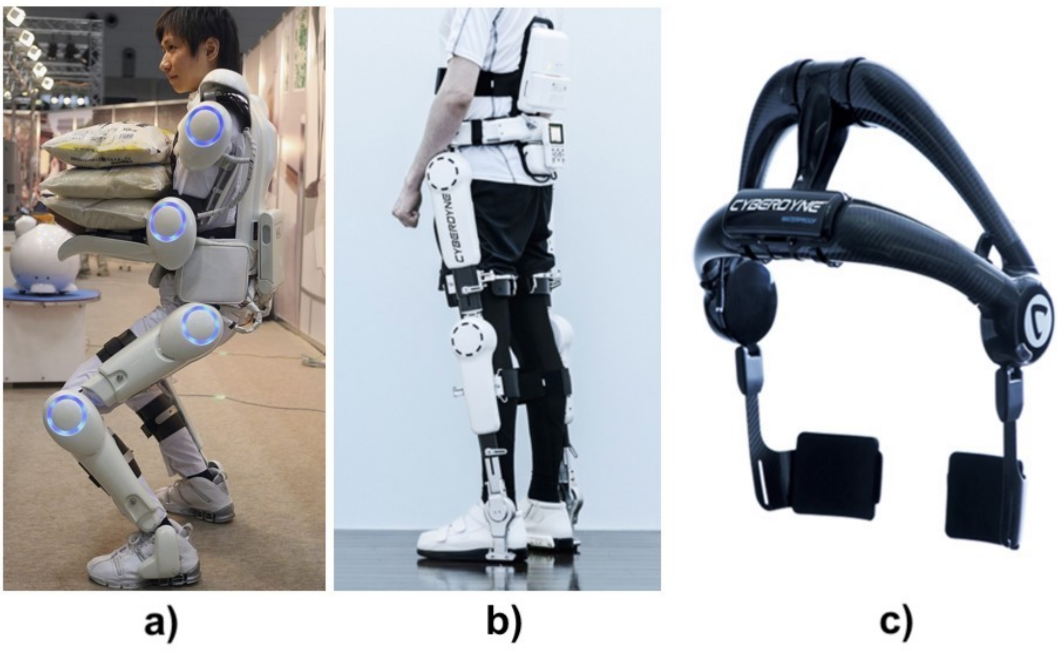


*Figure 15. a) HAL-5 Full-Body Exoskeleton b) HAL for Medical Use (Lower Limb Type) c) HAL Lumbar Type for Labor Support [27]*

HAL is a power-augmenting robot thought both for able-bodied and disabled people. Even if the studies on this WR started in 1989, the first relevant results were reached in the early 2000s with the prototype, HAL-5, a ten actuated DoFs (five per side, from which the suffix of HAL) power-augmenting full-body EXO which had the problem of a high weight. More versions of this robot were created later, such as the lower limb EXO, HAL-3, which is powered by the same technology. These exoskeletons are actuated by very compact actuation systems, composed by a DC brushless motor in series with a harmonic drive. The motion decoupling between motor and human is performed by means of a flexible friction around the motor, activated by a magnet inside a solenoid. Its input is provided by the control systems, able to translate the signals given by EMG sensors placed on the needed human muscles. In fact, HAL uses sensors able to detect biosignals sent from the brain to the musculoskeletal system. The HAL control system can operate in two different ways: robot-autonomous or user-controlled, depending on the necessity.

HAL brought great popularity to the company, which started to produce different variants of the robot, getting adopted by hundreds of medical-rehabilitative facilities, firstly around Japan and then also in the European Union.

The HAL Lumbar Type for labor support (*fig.15c*) may be interesting for this thesis. It's a nonmedical support undergoing trials at multiple sites, e.g. the baggage workers at airport, providing them assistance on each lift. In fact, its purpose is to reduce the lumbar fatigue, and the work-related low back pain produced by an overload. HAL reduces moment by supporting hip flexion/extension movement with a single actuated DoF per side. It is able to provide a torque up to 15 Nm, a remarkable result considering its compact dimensions. Measurements from different experiments confirm that lifting performances were significantly improved by using HAL Lumbar Support [28-31].

Another noteworthy WR is the Mobility Assist Exoskeleton developed by the Florida Institute for Human and Machine Cognition (IHMC) [32], a lower limb WR for strength augmentation or gait generation. This EXO allows a user to walk in a straight line for about 4.5 m. The power source, as well as the control, is off board and supplied to the robot by means of a tether system.

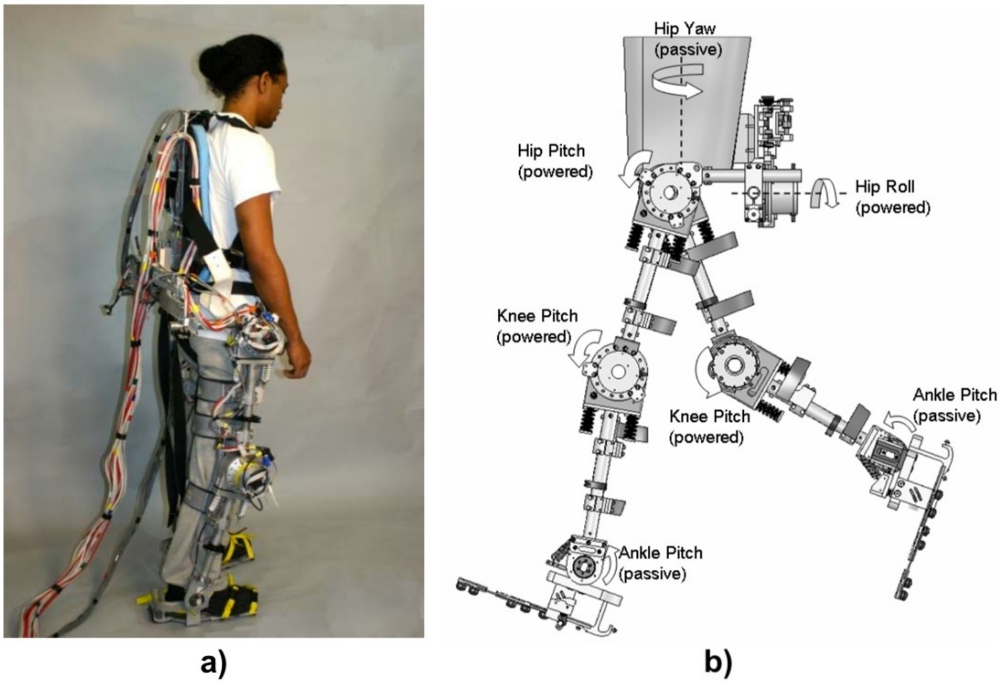


*Figure 16. a) The IHMC Mobility Assist Exoskeleton Prototype b) Side View of the IHMC Mobility Assist Exoskeleton Model [32]*

The IHMC Mobility Assist Exoskeleton has six DoFs per leg, in which three of them are actuated: hip abduction/adduction, hip flexion/extension and knee flexion. The joints are powered by means of rotary series elastic actuators (RSEAs) able to provide a peak torque up to 80 Nm. The joint angular position is read by means of optical encoders and, in combination with the springs, the actuators' embedded sensors can detect the actual torque. The control system (*fig.17*) compares the measured torque (inner loop) and the measured joint angle (outer loop) to provide the required torque to the joints.

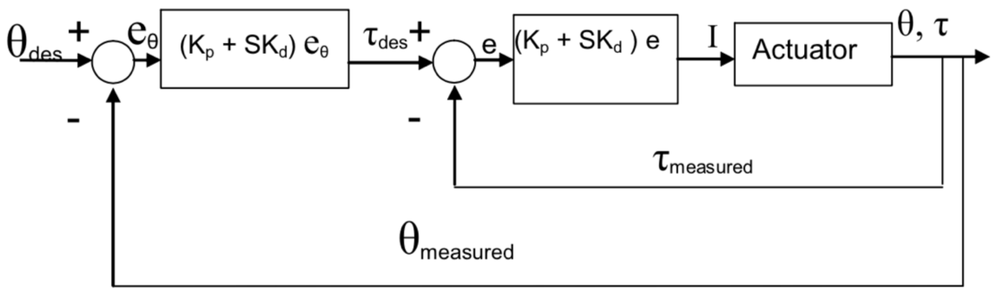


*Figure 17. Control System Diagram for an Actuator of the IHMC Mobility Assist Exoskeleton [32]*

In 2009 was also presented a treadmill-based lightweight unilateral lower limb exoskeleton known as Series Elastic Remote Knee Actuator (SERKA) [33], a device thought for people with a gait disability known as stiff-knee gait.

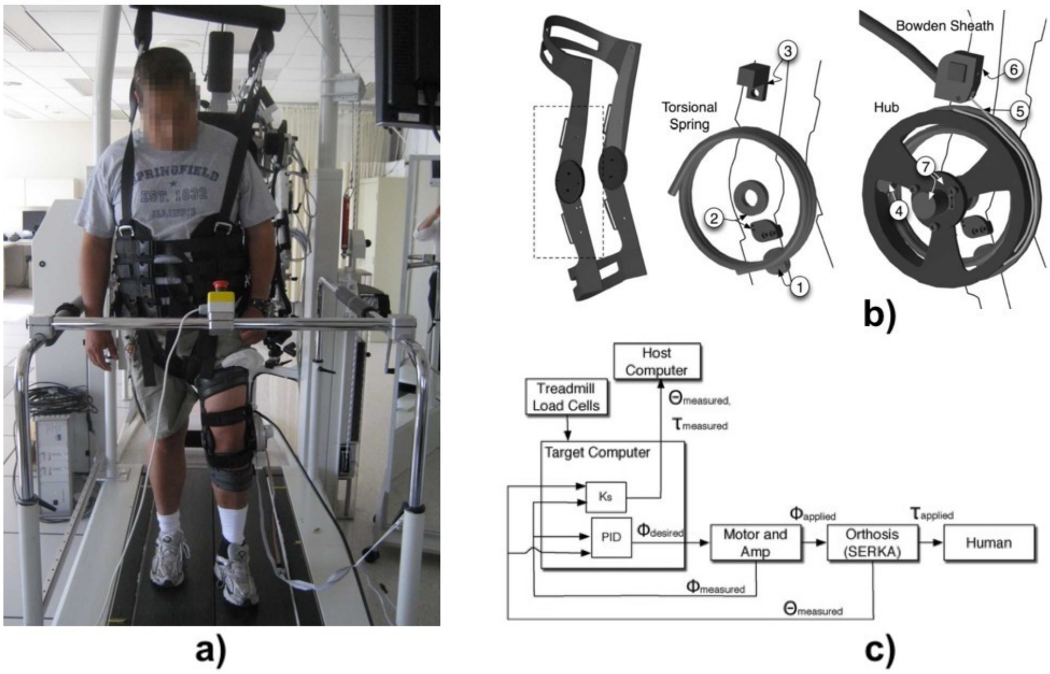


*Figure 18. a) The SERKA b) Structure of the Knee Brace c) Block Diagram of the SERKA [33]*

This robot is capable of assisting knee flexion torque before the leg swing but feeling transparent for the rest of the gait cycle. The torque is provided by a torsional spring, which deflection is controlled by a sheathed Bowden cable. The peak torque amounts to 41 Nm. The spring angular deflection is measured with an encoder mounted on a suspended platform nearby the rotating hub. The system is powered by a 1.4 kW DC servomotor with a 5:1 gear reduction, located away from the user. The control runs on a PC using MATLAB XPC: a PID controller (*fig.18c*) controls the displacement of the cable relative to the brace angle and operates the torque control.

The powered lower limb orthosis developed by Farris et al. [34-35] at the Vanderbilt University (Nashville, Tennessee) is intended to provide assistance in the sagittal plane to spinal cord injured patients, by supplying torques up to 40 Nm on both hip and knee joints. Hip abduction/adduction is also possible, to provide stability to the wearer during swing. Its mass amounts to 12 kg, comprising the actuation system and the battery capable to provide one hour of continuous walking.

*Figure 19. Vanderbilt Powered Orthosis [34]*

Each joint is powered by a brushless DC motor through a 24:1 reduction gear. Furthermore, the knee joints are equipped with a normally locked electrically controllable brake, such that the knee joints remain locked in case of power failure. The EXO is sensorized with potentiometers at both hip and knee joints, in addition to accelerometers located in each thigh link. An embedded control system controls the orthosis movements by means of a state-flow system with four states, where each state is defined by a set of joint angle trajectories, based on normal biomechanical walking trajectories, and enforced by PD control loops.

In 2011 was presented the Mina [36], a robotic orthosis built by researchers at the IHMC, which provides mobility assistance for people suffering from paraplegia or paraparesis. The Mina is powered in the sagittal plane at hip and knee joints, for a total of four actuated joints. All the actuators are identical, composed by a brushless DC motor, a 160:1 harmonic drive gear reduction and encoders. Each actuator is capable to perform both position control and torque control.

*Figure 20. The IHMC Mina [36]*

Mina does not provide hip abduction/adduction, then for paralyzed users the balance is provided with the assistance of forearm crutches. Its torso section is made by a rigid curved back plate which matches with the human spine. The Mina is adaptable to different user body sizes by means of nested aluminum tubing as the structural links. The power to motors and computers is provided by a tether system.

Within the Mindwalker Project [37] was developed a system which combines a lower limb exoskeleton for disable people rehabilitation and training, with a brain-computer interface (BCI) technology. It's been implemented a virtual reality (VR) system capable to detect the user's eyes movement, using it to control the EXO. The Mindwalker has four actuated DoFs per leg: hip flexion/extension, hip abduction/adduction, knee flexion/extension and ankle dorsi/plantar flexion. The Mindwalker exoskeleton joint [38] may be considered particularly interesting for this work. This joint is a sort of series elastic actuator that weighs just 2.9 kg, consisting of an integrated brushless DC motor, a ball-screw driven linear actuator, with the ball-screw nut directly coupled to the motor rotor, and a double spiral spring, capable to sense fine torques, and that may be considered linear, with no backlash or hysteresis. The linear actuator is connected in a sort of triangular configuration (*fig.21c*), through which can output a continuous peak torque of 100 Nm.

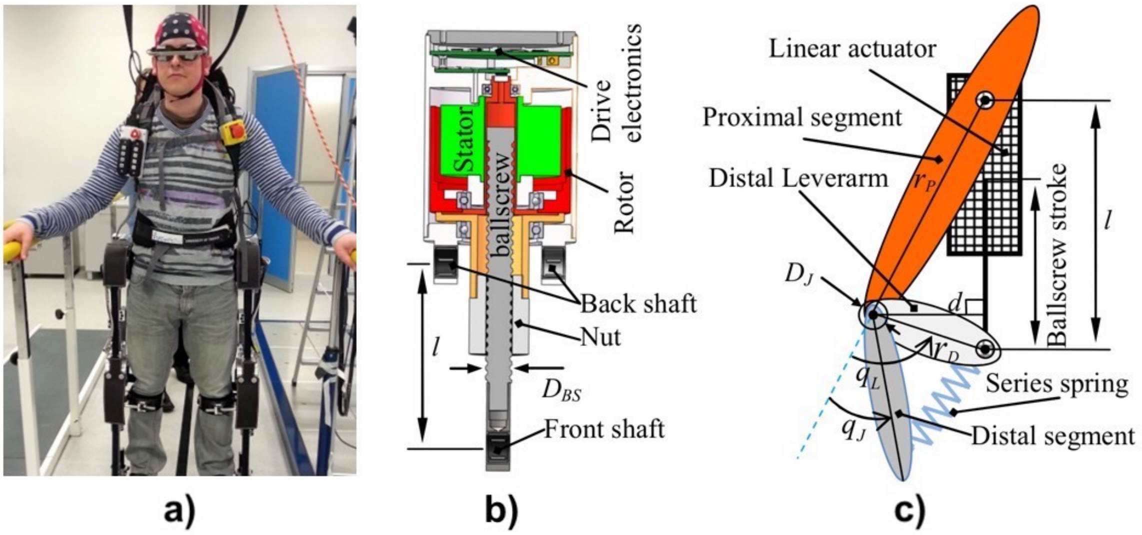


*Figure 21. a) The Mindwalker Exoskeleton b) The Mindwalker Linear Actuator Section c) Mindwalker Series Elastic Actuator Concept [38]*

The joint torque is directly measured by sensing the spring deflection with an encoder. Another encoder is implemented to detect the joint angle. The joint control is performed in three loops in series, converting the torque control problem in a motor position control problem (*fig.22*).

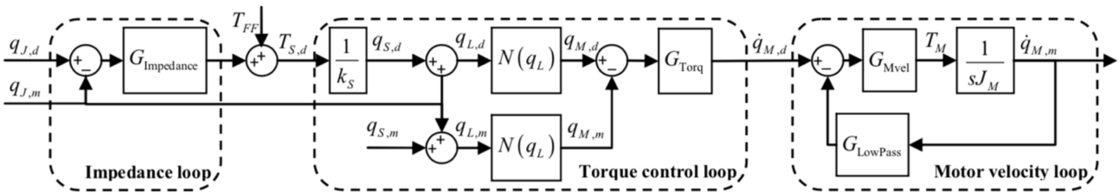


*Figure 22. The Mindwalker Joint Control Scheme [38]*

It's also noteworthy the hybrid drive lower extremity exoskeleton research platform XoR2 [39], a 20 kg WR capable to support a 30 kg payload without interfere with the user's normal walking. The robot has a total of fourteen DoFs, but only six joints are actuated, allowing the flexion/extension of hip, knee and ankle. The actuation is considered "hybrid" because combines PMAs, which can generate a relatively high force, with small high-response servo motors, capable to produce a high torque for a short period of time, with the purpose to sum the two actuator outputs and obtaining the desired torque with a peak of 60 Nm. Small custom-made inline force sensors were fabricated and applied to the PMAs, in addition to compact surface EMG sensors, in order to estimate the human motion intention and effort. Unfortunately, this robot is not power-autonomous, and it must be externally supplied.

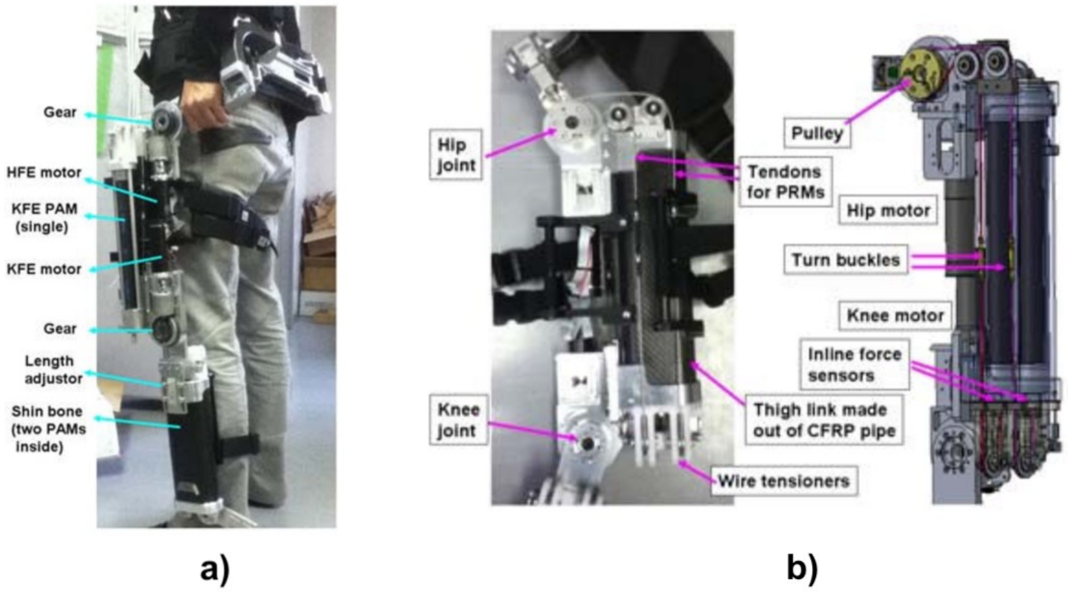


*Figure 23. a) The XoR2 b) Structure of the XoR2 Actuation Mechanism [39]*

In 2014 was presented a novel anthropomorphic lower extremity exoskeleton designed to help paralysis patients realizing ground walking rehabilitation, known as Bionic Lower Extremity Rehabilitation Exoskeleton (BLERE) [40]. Behind this project there was a great study around the calculation of the hip joint and knee joint center locations, in order to design human compatible and comfortable joints. To adapt the EXO to different users, it is provided of a size adjustment mechanism composed by a rough adjustment unit and a precise adjustment unit. The hip joint of the BLERE has three DoFs but just the flexion/extension is actuated, by means of a servo motor. The passive internal/external rotation was realized with a curved slider (*fig.24b*), to match the human center of rotation with the exoskeleton's one. The knee joint is also actuated by a servo motor.

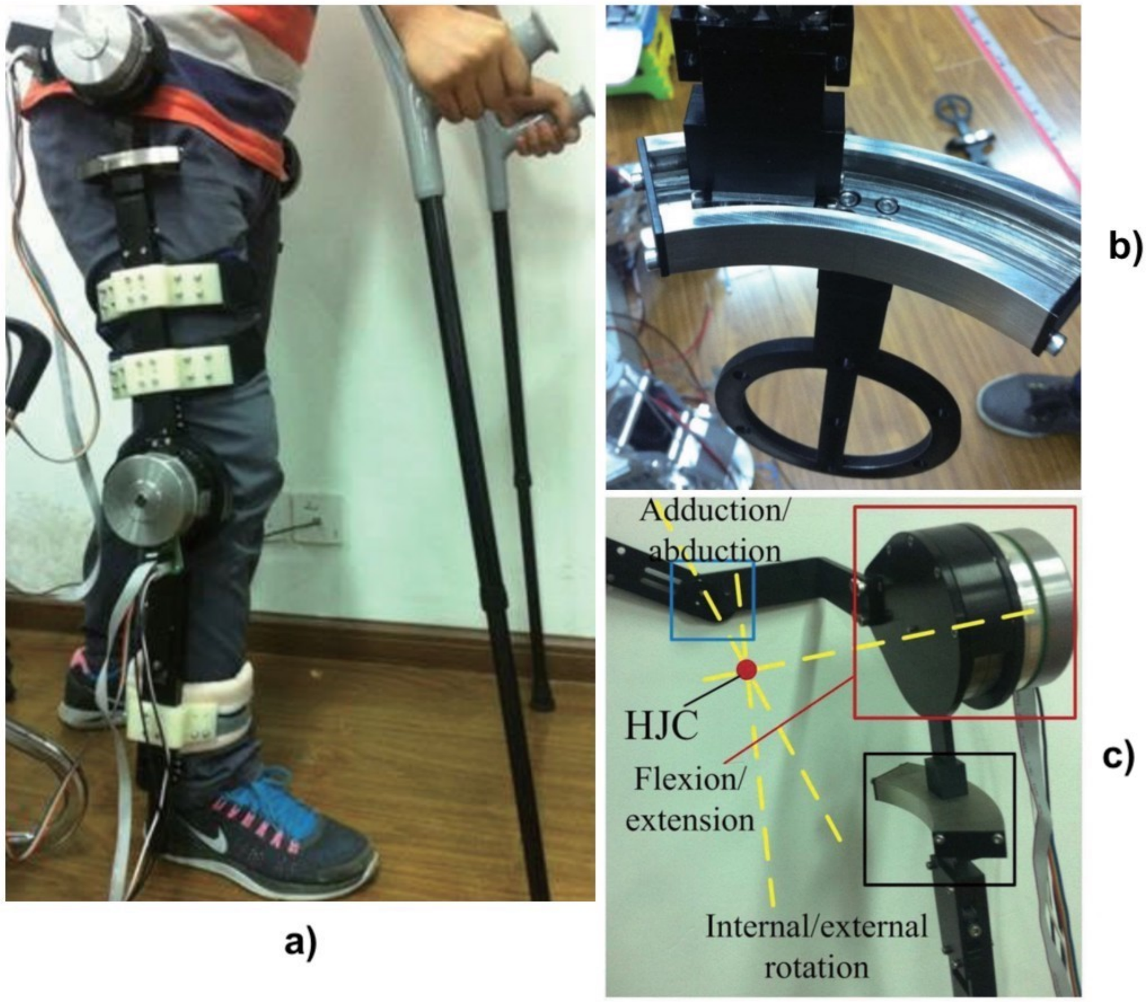


*Figure 24. a) The BLERE b) Upward View of the BLERE Hip Internal/External Rotation Mechanism c) The BLERE 3-DoFs Hip Joint [40]*

In 2015 Vitiello et al. presented the Active Pelvis Orthosis (APO) [41-43] designed within the CYBERLEGs (Cybernetic Lower-Limb Cognitive Ortho-prosthesis) Project in the Scuola Superiore Sant'Anna (Pisa, Italy). The APO is a light-weight active exoskeleton for assisting hip flexion/extension, wearable by both healthy and disable subjects, realized with materials such as aluminum and carbon fiber. It is provided of size adjustment elements, in order to adapt it to different anthropomorphic measures. As already mentioned, the device has one actuated DoF, the hip flexion/extension, but also a passive DoF, the hip abduction/adduction, to provide body balance and to be more comfortable. The device is composed by a C-shaped frame that surrounds the user's hip, connected to user's waist by means of three orthotic shells, and coupled with a thigh linkage per side, interfaced with the user's thigh with an orthotic shell and tightened around it by means of an elastic belt.

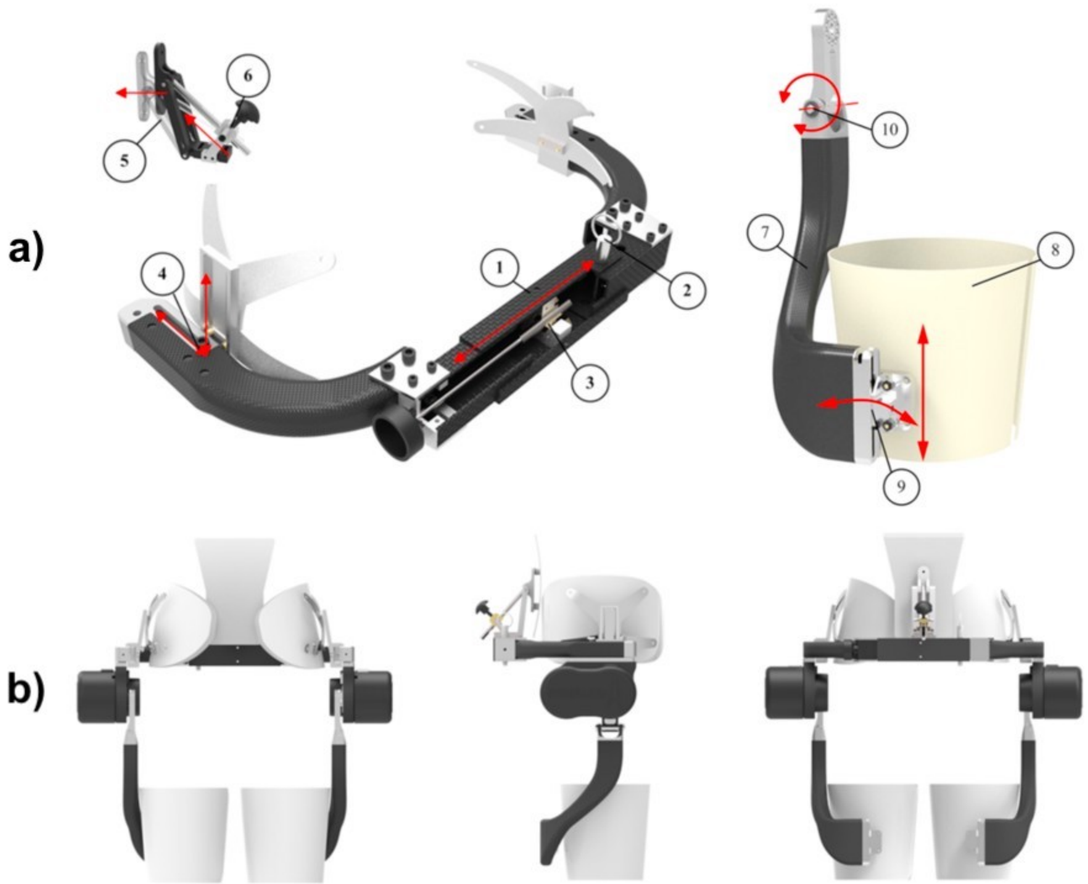


*Figure 25. a) Overview of the APO System b) Front, Lateral and Back View of the APO System [42]*

The two actuation units are carried by the frame, and each one of them is a SEA (*fig.26a*) deployed around two parallel axes to reduce the overall lateral encumbrance. This two-axes configuration has the advantage to allow the subject to freely make the so-called "swing" movement of the arms during the gait cycle. The SEA is composed by a 100 W DC motor with embedded incremental encoder, a 80:1 harmonic drive reduction stage, a custom torsional spring having a highly linear characteristic and a stiffness of 100 Nm/rad, a 32-bit absolute encoder in series with the spring to measure the absolute hip joint angle, and a transmission based on a 4-bar mechanism, able to transmit the torque between the two axes of the SEA. The whole system reaches a weight of just 4.2 kg, excluding the control unit, that is remotely located. The APO control system is based on a hierarchical architecture composed by two layers. Two independent low-level layers (*fig.26b*) deploy the torque controls in a PID closed loop architecture, measuring the actual torque by means of the torsional spring deformation. Since one of the two encoders is incremental, an initialization procedure is required at the power-on of the system to acquire the spring zero reference.

The high-level layer (*fig.26c*) performs the gait assistive control with a model-free algorithm relied on adaptive oscillators.

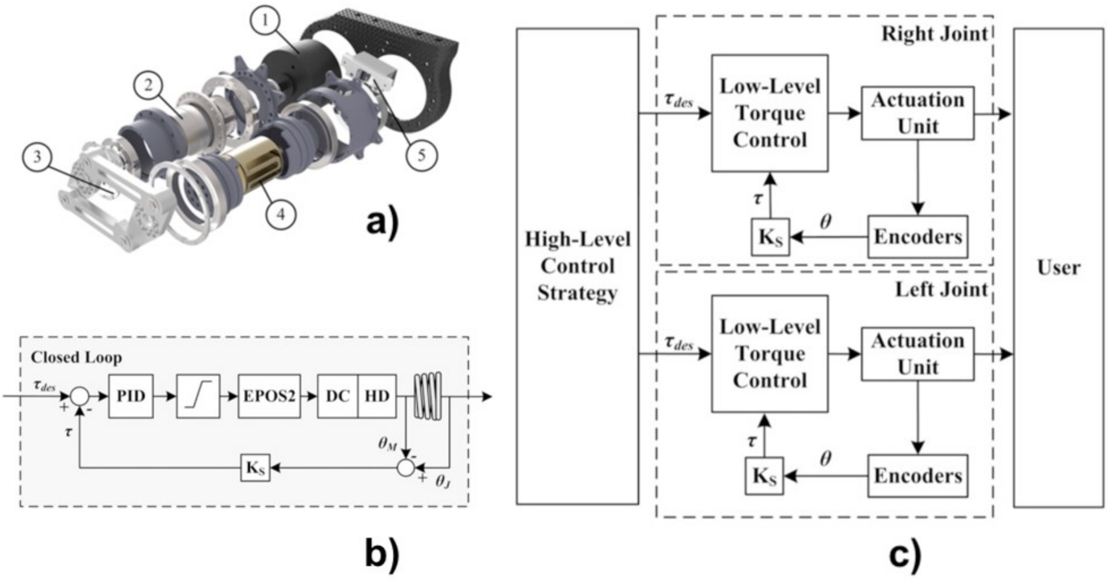


*Figure 26. a) Exploded View of the APO SEA b) Low-Level Closed-Loop Torque Control c) Block Diagram of the Hierarchical Control Architecture [42]*

An interesting project, born with an aim similar to the one of this work, was developed by Kobayashi et al. in Tokyo, for a company known as Innophys. They developed a compact and lightweight exoskeleton with a single active DoF, the Muscle Suit [44-49], for back support during lifting of heavy materials or material handling, in order to reduce the workload and decrease the probability of back pain and other work-related injuries and illnesses. Tested by means of the productivity concept, it was showed that wearing this EXO increases the working performance. The advantages of this WR were also tested by means of integral electromyography (IEMG). Indeed, the muscle suit provides direct and physical motion support using McKibben artificial muscles. These actuators were chosen due to their compactness, light weight, softness, power-to-weight ratio, reliability and waterproof finish. The power generated by the PMA is transmitted to the hip by means of a cable and some pulleys. A pulley fixed with the back frame, which contains the actuators, rotates around a pulley fixed with the thigh frame. The wire is fixed with the fixed pulley, converting the contractive force of the actuator into a torque. This system configuration includes also electric valves, pressure sensors, a microprocessor and various sensors and switches.

The Innophys muscle suit is already on the market in Japan in different versions, whose differences consider the supply type, the cHRI, and the number of PMAs. The version without reservoir and with four McKibben artificial muscles (*fig.27c*) has a mass of just 6.6 kg and is capable to produce a torque up to 140 Nm. This value was chosen considering the Labor Standard Law of Japan, which says that the limit of weight handled by humans must be less than 40% of his/her weight.

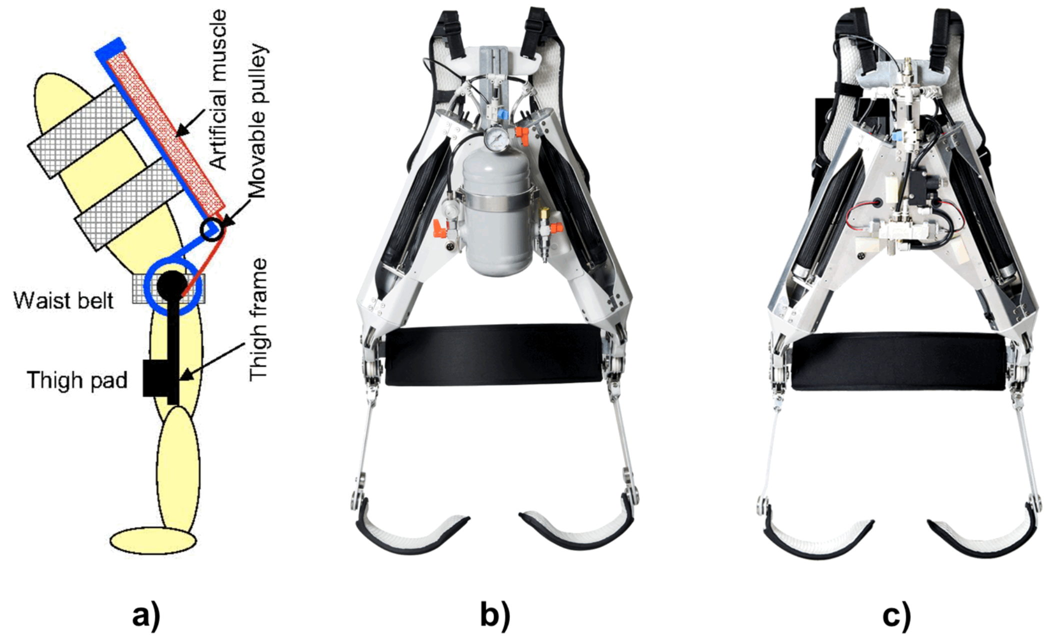


*Figure 27. a) Muscle Suit Working Principle b) Innophys Muscle Suit Standard Version with Reservoir c) Innophys Muscle Suit Standard Version without Reservoir [44-49]*

From the robots analyzed previously is possible to take into consideration various elements that may be of inspiration for this work, such as the hip joint conformation, the frame and links configuration, the degrees of freedom, the actuation system, the power source, the sensorization system, the control system, the materials, the robot-user contact surfaces, the cuffs and so on and so forth. In particular, what comes to light from the previous analysis is that, even if most of the mentioned robots were designed for purposes different from the one of this work, they have many points of view in common between them. It's then possible to extract many data by them, extremely precious considering the lack of information regarding most of the robots more similar to the one object of study in this thesis.

It's possible to note that the number of both passive and active DoFs is normally as low as possible, to reduce the complexity of the structure and avoid undesired movements. Nevertheless, at least the rotation on the three body planes is always allowed, for what regards the hip joint, and this assumption is not true only for particular reasons, far from the studied case.

In the considered robots most of the actuation systems are powered by different kinds of electric motors, typically coupled with a reduction gear. There is also a remarkable number of robots that favors the pneumatic actuation. About the transmission method, Bowden cables are widely used, but also pulleys systems and direct triangle configurations. The SEA system appears in many robots, for the advantages previously exposed.

The materials used in the studied robots are almost always the same, with aluminum and carbon fiber for links, aluminum and steel for joints and shafts, carbon fiber and polyethylene for pads and orthotic shells.

In the mentioned exoskeletons is possible to analyze many different control systems and, as it's easy to note, they all perform a closed-loop control. Different sensors were employed: potentiometers, absolute and differential encoders, EMG sensors, accelerometers and pressure sensors mainly. In the devices in which just few sensors were used, the model of the system had to be very precise. Hierarchical controls were often performed and, excluding some systems with a great complexity, most of the implemented controllers were PD or PID controllers.

Of course, the considered robots are not the only ones ever created: many other exoskeletons were developed, especially in the last twenty years. It's possible to mention some of them in case that the reader needs more information, without going into details to avoid redundancy: robots such as ReWalk [50-51] (an all-day power-autonomous lower-limb robot), Indego [52] and Berkeley eLegs [53] (lower-limb over-ground recovery platforms), Armin-III [54] and IntelliArm [55] (unilateral upper-arm rehabilitation robots), AAFO [56] and ScarlETH [57] (ankle rehabilitation robots), HONDA stride management assist [58-59] and bodyweight support assist [58,60] (power-augmenting robots). Some WRs were developed for the military environment, among which HULC [61], Sarcos XOS 2 [62], Marine Mojo [63] and PowerWalk [64]. There were also developed more particular robots, such as the power-augmenting tool-based exoskeletons for industrial workers FORTIS and Ekso Works, which sensibly reduce the user fatigue, discharging the tool's weight to the ground. Reducing the worker's fatigue is one of the main goals of the last few years, in fact the number of these devices is sensibly increasing, as a demonstration of the exoskeleton even greater diffusion. It's possible to mention the Noonee Chairless Chair

[65], the HERCULE [66], the legX [67] or the shoulderX [67]. Among these power-augmenting EXOs for factory worker there are some wearable devices designed with the aim to provide back support, a task similar to the purpose of this thesis. Some of them are certainly noteworthy, such as the already mentioned CYBERDYNE HAL Lumbar Support [27-31] and Innophys Muscle Suit [44-49].

Another robot of this kind is the ATOUN AWN-03B [68], made by ActiveLink, a branch of Panasonic. Its primary goal is to reduce the body effort when lifting and lowering heavy loads, providing a maximum assistive force equal to 150 N, with an approximate weight of 6 kg. It's waterproof and dustproof, and its integrated battery promises eight hours of continuous operating time. It can work in three different assist mode: assist off (when walking), holding the middle posture and lifting.

The SuitX backX [67] is a completely passive exoskeleton for work and industry designed to reduce some loads by an average of 60% from the spine when bending forwards, both for stooping or lifting objects. The backX is designed to be worn all day, without impeding natural movements. It further includes pouches to hold cooling and heating packs, to wear the exoskeleton with extreme weather.

The StrongArm Tech FLx [69] and V22 [69] ErgoSkeletons are exoskeletons, developed to assist the user to perform correct movements. Their focus is to keep the user safe while lifting or moving heavy objects. They apply pressure to remind the user both while over rotations and improper lifts. The FLx is totally passive, and does not perform a power-augmenting action, the V22 has two clutch controlled cable to assist moving and lifting.

The Hyundai H-WEX [70] is a lightweight, small and practical industrial exoskeleton designed to support hip and upper body, to prevent injuries for workers. A single motor provides power to both legs is controlled by a built-in control algorithm focused on the user safety.

The passive exoskeleton Laevo V2.5 [71] was designed for chest and back support. It transmits part of the user's upper body weight from the chest pad to the thighs, by means of gas springs. It decreases the risk of injuries, reducing the risk of unexpected back muscle contractions through its damping effect.

Obviously, these exoskeletons don't represent the totality of the wearable robots already developed, but it's possible to assert that, handling this knowledge, one may have a good bird eye view of the state of the art.

## 1.5 Exoskeletons in the Pop Culture

The term "exoskeleton" became known to most of the people, even people without particular skill in biomedical or robotics environment (the so called popular culture, or pop culture), due to comics/manga, television, cinema and videogames. Nowadays the word exoskeleton brings immediately to mind IronMan [72], the Marvel comics superhero created by Stan Lee in 1963. IronMan became even more famous due to a long-term project composed by a sequence of movies, also known as the "Marvel Cinematic Universe". The first movie appearance of this superhero in this cinematic series was in 2008 with the dedicated movie "IronMan" [73], directed by Jon Favreau, in which the actor Robert Downey Jr. performs Tony Stark, the man beyond the mask, a rich and brilliant war-engineer without particular physical skills, but able to design his own armor suit, becoming a superhero.

*Figure 28. IronMan [73]*

In movies there are other examples of the use of exoskeletons, among which "Aliens" [74] (1986), written and directed by James Cameron, in which is present a power-augmenting robot used by the spaceship crew to move heavy loads.

Exoskeletons have great exponents also in oriental pop culture, with animated works such as Mobile Suit Gundam [75] (Japan, 1979) and Neon Genesis Evangelion [76] (Japan, 1995).

Exoskeletons became popular in the last twenty years also due to the newest media: the videogames. One of the first videogames in which was treated the exoskeleton theme to become really famous is Metal Gear Solid [77] (1998), created by Hideo Kojima and produced by Konami. In this game there’s a character, Gray Fox, supposed to be dead, but saved by means of prothesis and orthosis, composing an actual exoskeleton. More recently, other videogames have faced this theme, such as Crysis [78] (2007), developed by Crytek and published by Electronic Arts, in which a special American military team equipped with a “Nanosuit” is dispatched to an island for a mission. The Nanosuit is a sort of armor, capable to provide them great speed, force and resistance, thanks to a particular choice of materials: nanotechnologies that composes the active component of the suit.

Even if all the mentioned works, coming from different medias and cultures, are pure fantasy works, it’s possible to note some elements that may be connected with real situations. For example, why is the IronMan suit so powerful compared with the other suits presented in the same comics/movies? The main character has discovered a brand-new source of energy, more power efficient, lightweight and portable than anything else, and this is the core of the armor suit. As already said, nowadays the optimization of the power sources is a key-element for the researchers. Furthermore, this armor was upgraded step-by-step becoming even better, also in terms of wearability. This is a genuine engineering process. Besides, the exoskeleton seen in “Aliens” can be considered anything else than a sort of a power augmenting active exoskeleton for industrial workers. In the same way, the exoskeleton seen in “Metal Gear Solid” is a full-body rehabilitation exoskeleton, and the one seen in “Crysis” is a power-augmenting exoskeleton used in military environment with a particular focus on the materials choice.

It’s possible to say that, even if these works went too far with the fantasy, they aimed a good point: what the researchers have to focus on. To have an improvement to exoskeleton’s performance and usability different requirements are needed: power sources even smaller, lighter and more powerful; exoskeletons easy and fast to wear; increasing biocompatibility in terms of materials and dimensions, obtaining suits even more anthropomorphic, shaped on the user’s body.

# Chapter 2

# Preliminary Hip Torque Calculation

The aim of this chapter is to determine the hip torque in the sagittal plane due to the weight of the upper body of the user, as a function of the angle between the subject back axis and the vertical axis, neglecting the exoskeleton weight. The user was simplified with a classical stick model, defining a reference subject and creating a free body diagram.

## 2.1 Definition of the Variables

The first important step to calculate the hip torque to be provided by the exoskeleton passes through the definition of a reference system. It's convenient simplify the system as a 2-dimensional system, due to the fact that the only motions interested by the actuation system in this case are leg flexion/extension and upper body bending, movements strictly related to the sagittal plane. It's then possible to assume that the 2-D system lies on the sagittal plane. From now on all the motion, the forces, and the torques will be considered lying on the sagittal plane, taking the vertical axis z (*fig.29*), perpendicular to the ground, as reference axis. For simplicity it is possible to think that this axis lies on a plane in which both human hip joints also lie, which is coherent with the 2-D schematization.

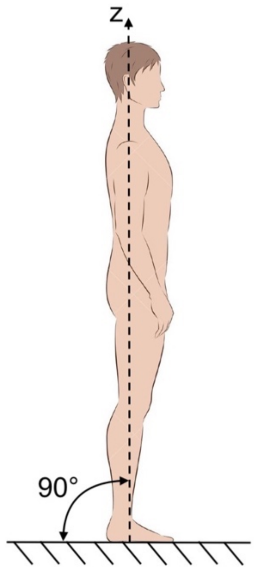


*Figure 29. Reference Axis z*

Starting from the 2-dimensional configuration in *fig.29* it's possible to define one of the main variables of the problem, that is the angle θ (*fig.30*), thought as the angle between the vertical axis and the trunk, achieved by a trunk rotation around the hip. The trunk line is assumed as the interference between the sagittal plane and the plane passing both through the hip and the shoulders of the user. The positive direction of this angle is considered in case of hip flexion, with the trunk forward. Nevertheless, the human trunk does not maintain a straight configuration during the flexion/extension movement. In this first calculation is however possible to consider the trunk always straight, for simplicity.

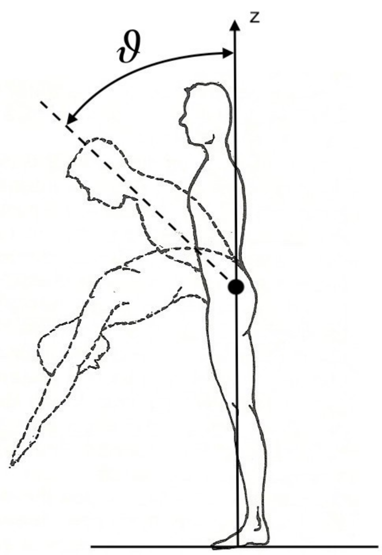


*Figure 30. Angle $\theta$ Definition*

As a first approximation is possible to think both the human legs always in vertical position, but in practice this is only one of the several possible configurations, due to the gait cycle, the case of squatting, etc. It's then important going to identify also the angle between the trunk and the thighs, the angle $\alpha$ (*fig.31*). The angle $\beta$ will correspond to the angle between the vertical and the thigh axis.

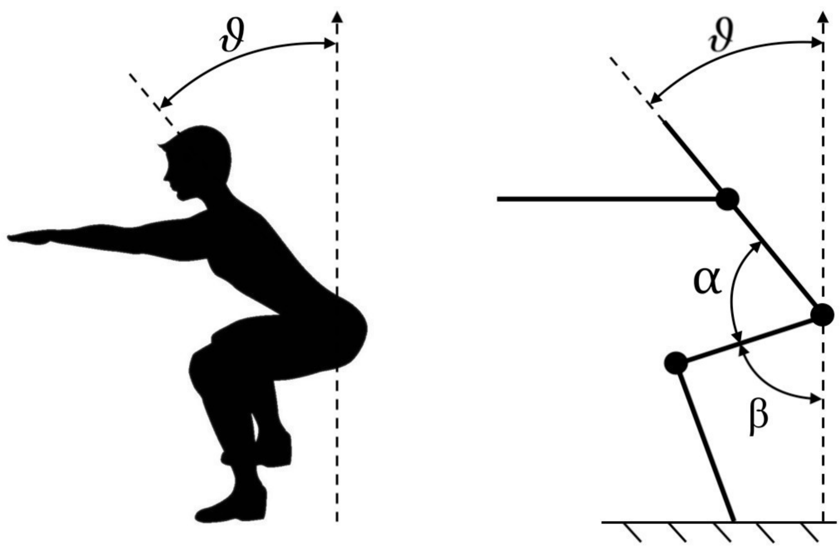


*Figure 31. Human Body Angles*

These angles correspond to the human body angles, but in the first measure it's possible to consider the exoskeleton fixed with the user, and the human body angles correspondent to the exoskeleton links angles.
Starting to think about a future exoskeleton sensorization, is possible to assert that the angle $\theta$ will be detected by an accelerometer positioned as close as possible to the pad in which the force is applied to the upper body (realistically on the chest or on the shoulders). An accelerometer is able to return an angle taking as reference the vertical axis, and it's important locating it nearby the reaction forces because that is the point in which the exoskeleton interacts with the user upper body. The angle $\alpha/\beta$ will be detected by a sensor (a potentiometer or an encoder) positioned on the hip, returning the absolute angular displacement of the thigh.

## 2.2 Anatomical Data Calculation

From the regulation ISO/TR 7250-2:2010 [79], which contains statistical summaries of basic human body measurements for technological design, is possible to extrapolate data about human body mass and human body height. Considering that the exoskeleton has to be worn by the majority of the people, the reference subject is now arbitrarily chosen as the 99 percentile Italian man. The obtained data relative to height and mass are the following:

$H = 1.883\ m$

$M = 103\ kg$

These data may be used to calculate partial body masses and lengths by means of coefficients (*fig.32,33)* found in literature [80], just multiplying them by the total mass or height.

| segment | segment mass/ total body mass $m_b$ |
|---|---|
| hand | 0.006 |
| forearm | 0.016 |
| upper arm | 0.028 |
| forearm and hand | 0.022 |
| total arm | 0.050 |
| foot | 0.0145 |
| lower leg (calf) | 0.0465 |
| upper leg (thigh) | 0.100 |
| foot and lower leg | 0.061 |
| total leg | 0.161 |
| head and neck | 0.081 |
| trunk | 0.497 |

*Figure 32. Human Body Masses Coefficients [80]*

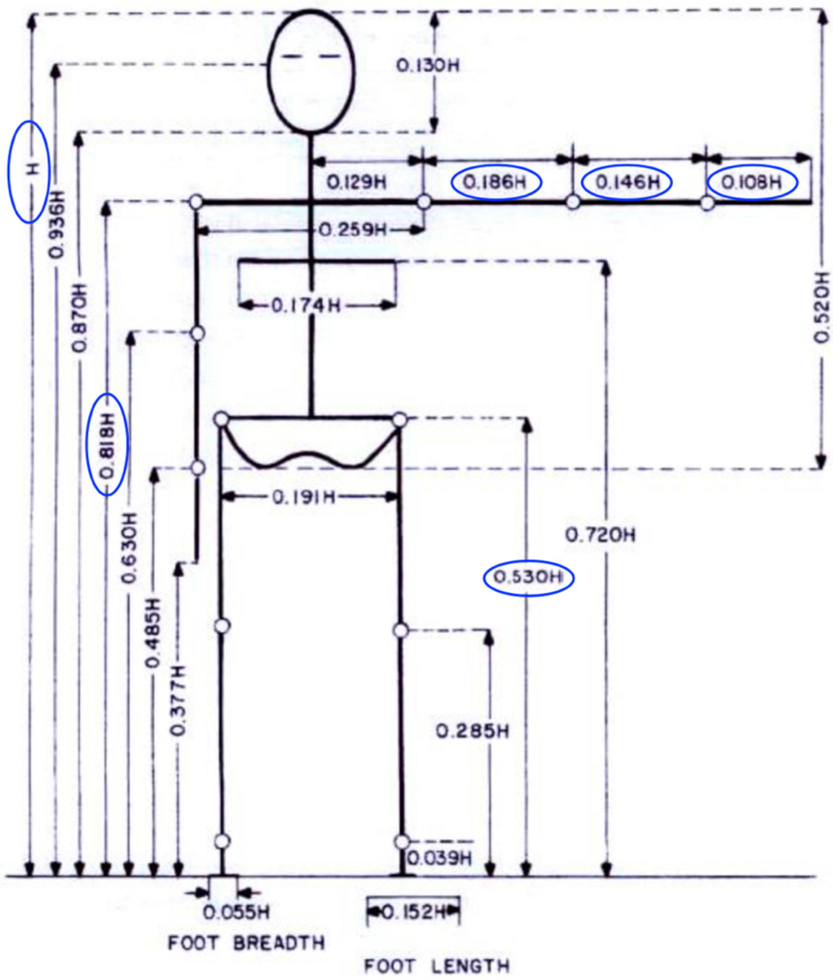


*Figure 33. Human Body Lengths Coefficients [80]*

With reference to *fig.34* and *fig.35* for the nomenclature is now possible to calculate masses and lengths of the different anatomical portions.

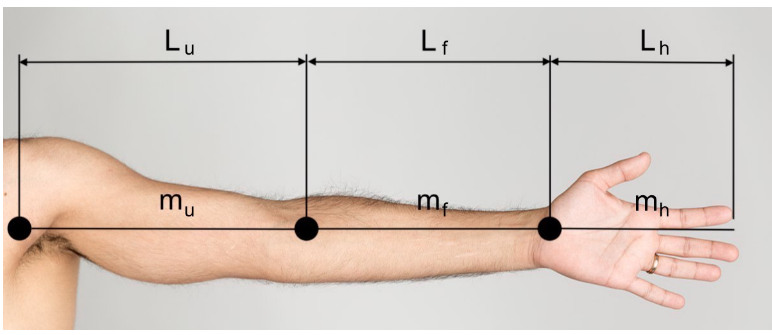


*Figure 34. Arm Scheme*

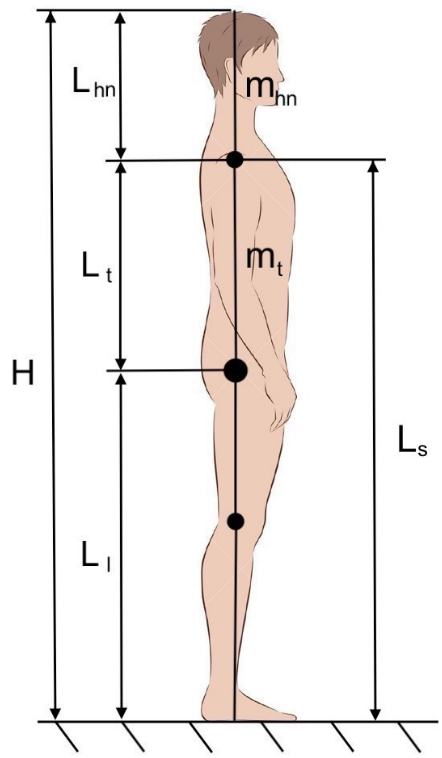


*Figure 35. Legs, Trunk, Neck and Head Scheme*

$m_u = 0.028 \cdot M = 2.884\ kg$ (upper arm mass)

$L_u = 0.186 \cdot H = 0.3502\ m$ (upper arm length)

$m_f = 0.016 \cdot M = 1.648\ kg$ (forearm mass)

$L_f = 0.146 \cdot H = 0.2749\ m$ (forearm length)

$m_h = 0.006 \cdot M = 0.618\ kg$ (hand mass)

$L_h = 0.108 \cdot H = 0.2034\ m$ (hand length)

$L_l = 0.530 \cdot H = 0.9980\ m$ (leg length)

$L_s = 0.818 \cdot H = 1.5403\ m$ (shoulder height)

$m_t = 0.497 \cdot M = 51.191\ kg$ (trunk mass)

$L_t = L_s - L_l = 0.5423\ m$ (trunk length)

$m_{hn} = 0.081 \cdot M = 8.343\ kg$ (head and neck mass)

$L_{hn} = H - L_s = 0.3427\ m$ (head and neck mass)

$m_a = m_u + m_f + m_h = 5.150\ kg$ (arm mass)

$m_{sup} = m_t + m_{hn} + 2 \cdot m_a = 69.834\ kg$ (trunk, arms, neck and head mass)

## 2.3 Center of Mass Determination

In order to proceed with the calculation of the hip torque it's necessary to determine the points in which the weight forces of each body portion are applied. The following hypotheses will be assumed:

- Homogeneous masses in the considered body segments;
- Mass of the exoskeleton still unknown and then neglected;
- Longitudinal axis of upper arm, forearm and hand always collinear;
- Parallel arms;
- Parallel legs;
- Longitudinal axis of trunk, neck and head always collinear.

By means of these assumptions it is possible to determine the position of the center of mass of the different anatomical portions, thinking the weight forces as concentrated forces applied in the midpoint of the above-mentioned portions, on the same axis of them.

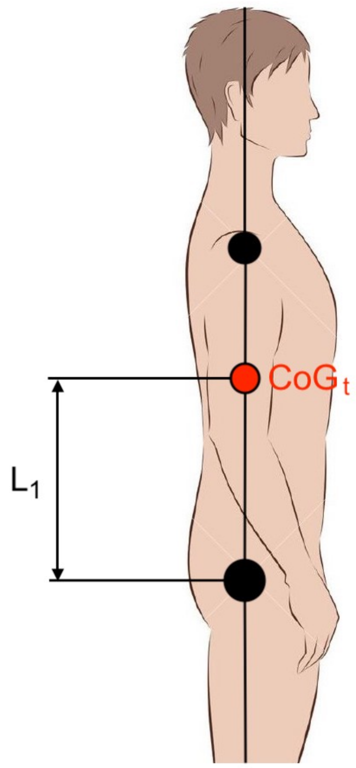


*Figure 36. Position of Trunk, Neck and Head Center of Mass*

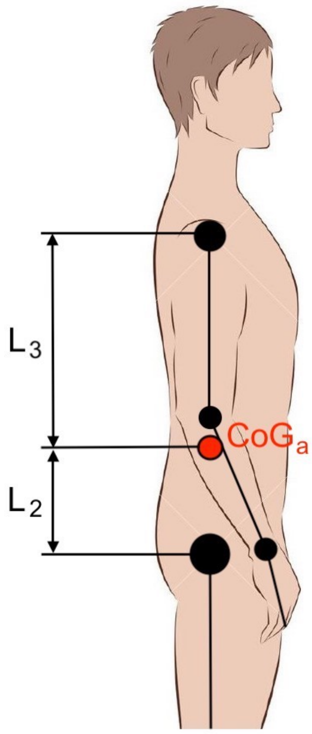


*Figure 37. Position of the Arm Center of Mass*

With reference to *fig.36* and *fig.37*, the target is now calculating the position of $CoG_t$ and $CoG_a$ respectively. The anatomical distances of the centers of mass may be calculated by means of the well-known formula of the center of mass for homogeneous bodies.
The distance $L_1$ (*fig.36*) between hip and center of mass of trunk, neck and head $CoG_t$ is:

$$L_1 = \frac{m_t \cdot \frac{L_t}{2} + m_{hn} \cdot \left(L_t + \frac{L_{hn}}{2}\right)}{m_t + m_{hn}} = 0.3332\, m \tag{1}$$

The distance $L_3$ (*fig.37*) between shoulder and center of mass of the arm $CoG_a$ is:

$$L_3 = \frac{m_u \cdot \frac{L_u}{2} + m_f \cdot \left(L_u + \frac{L_f}{2}\right) + m_h \cdot \left(L_u + L_f + \frac{L_h}{2}\right)}{m_u + m_f + m_h} = 0.3414\, m \tag{2}$$

By means of the previous results is possible to calculate the distance $L_2$ (*fig.37*) between hip and center of mass of the arm $CoG_a$ through a simple subtraction:

$$L_2 = L_t - L_3 = 0.2010\ m \tag{3}$$

Now all the data for the hip torque calculation in the set conditions were found.

## 2.4 Free body Diagram and Hip Torque Calculation

Now all the data necessary for the calculation of the torque to provide at the hip to maintain the static equilibrium of the upper body were found. In fact, in this section only the static case will be considered, neglecting all the inertia effects, besides exoskeleton weight, articulation friction, muscular forces and hip joint center-torque misalignments.
Nevertheless, the number of possible configurations is potentially infinite. Two different configurations were chosen and studied, considering them related to the two extreme opposite situations in a working environment, and attributable to the best and the worst case, respectively. In both cases the legs were considered as vertical, and the arms straight and parallel to each other.

- Configuration 1: trunk tilted forward and arms alongside the bust and parallel to it (*fig.38*);
- Configuration 2: trunk tilted forward and arms forward, always horizontal (*fig.39*).

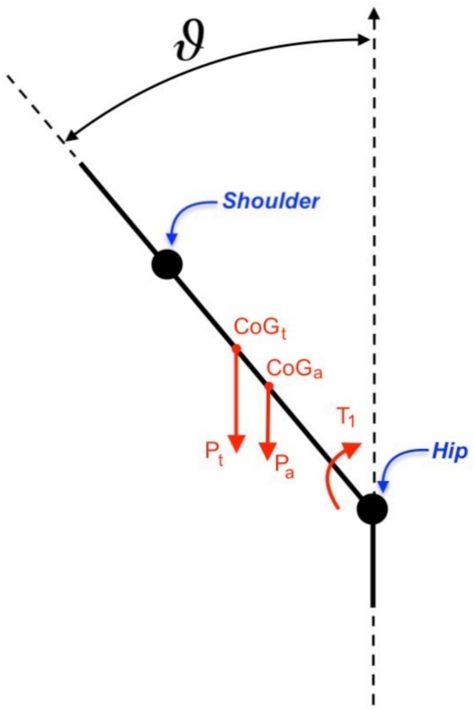


*Figure 38. Configuration 1*

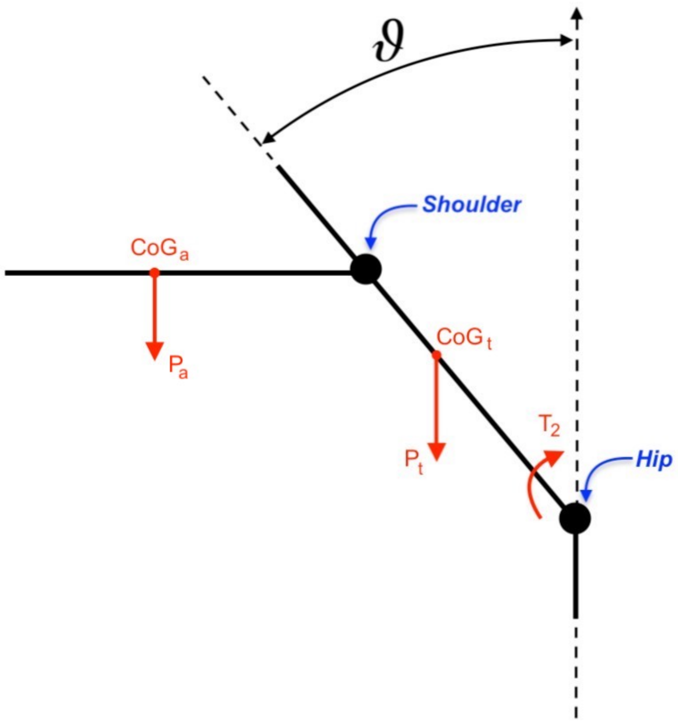


*Figure 39. Configuration 2*

The weight forces $P_t$ (weight force of trunk, neck and head) and $P_a$ (weight force of the two arms) depicted in *fig.38* and *fig.39* are defined as follow:

$$P_t = (m_t + m_{hn}) \cdot g = 584.029\ N$$
$$P_a = 2 \cdot m_a \cdot g = 101.043\ N \tag{4}$$

It's now possible to calculate the hip torque T, as a function of the angle θ, for both configurations, just imposing the static equilibrium of the rotation around the hip, in order to neglect the reaction forces of the hip itself.
The obtained torque functions are:

$$T_1(\theta) = (P_t \cdot L_1 + P_a \cdot L_2) \cdot \sin\theta \tag{5}$$

$$T_2(\theta) = P_t \cdot L_1 \cdot \sin\theta + P_a \cdot (L_3 + L_t \cdot \sin\theta) \tag{6}$$

The evolution of the hip torques as a function of the angle θ in both configurations is shown in *fig.40*. Both plots have the evolution of a quarter period sine wave.

As it's possible to see from equations 5 and 6, it's clear that the maximum torque is achieved for an angle θ equal to π/2 rad for both configurations. Nevertheless, that angle has not a physical meaning, because is almost impossible to reach from an anatomical point of view, especially in a working environment. An angle, defined as "working angle", was chosen as reference, considering it the limit condition for a user in a working environment. It's defined as $\theta_W=\pi/4$ rad.

The resulting total working torques are the following:

$T_{1,w} = T_1(\theta_w) = 151.94\ Nm$

$T_{2,w} = T_2(\theta_w) = 210.82\ Nm$

These torques may also be split into two halves, corresponding on left and right side of the hip.

In addition, it's possible to note that for a null value of θ in the first case (*eq.5*), the value of $T_1$ is null too, but $T_2$ assumes a non-zero value, due to the arms weight:

$T_{2,0} = T_2(0) = 34{,}49\ Nm$

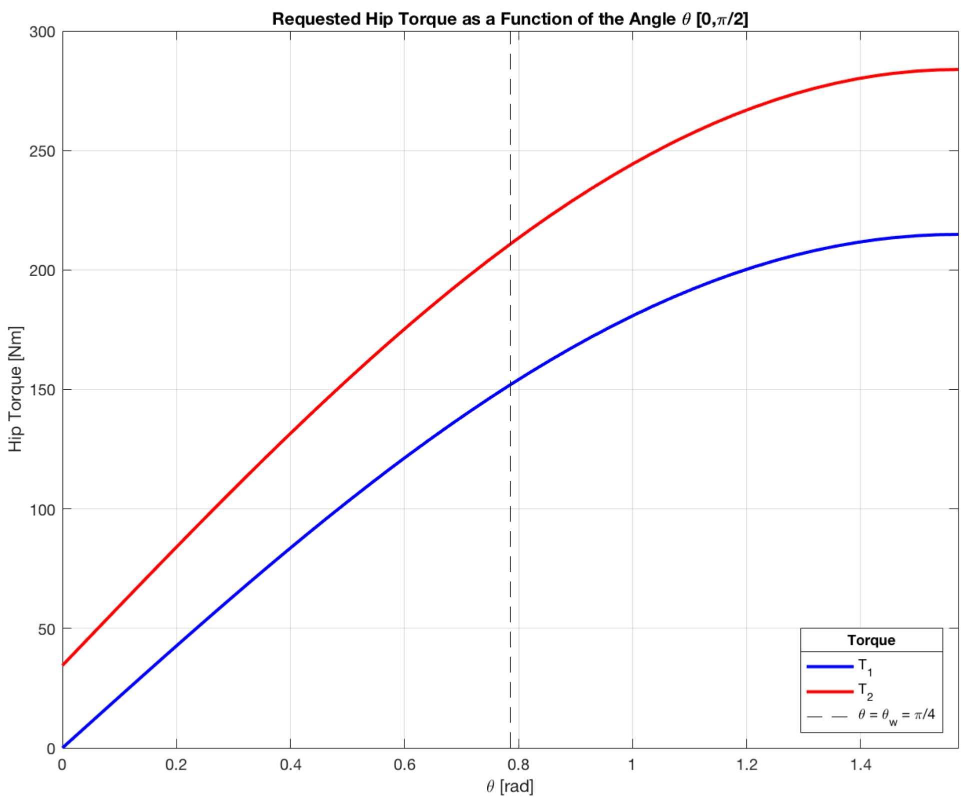


*Figure 40. Hip Torques in Static Conditions*

# Chapter 3

# Concept Design

## 3.1 Introduction to the Concept Solutions

In this chapter two concept solutions will be introduced. The aim of the following paragraphs is providing a set of information about the elements composing each proposed solution, in order to understand the idea behind these concepts, their working principles and their pros and cons, in order have the key-elements for choosing a solution to develop. These solutions were studied on the base of found literature, considering different aspects of several robots, among which the power supply, the actuation type, the materials, the links configuration, the degrees of freedom, the sensorization, the control system, the hip joint mechanism and the motion transmission mode.
Their detailed specifications will be studied in the following chapters.
The main robots considered were the BLEEX [14-15], for its interesting C-Frame, the HAL Lumbar Support [28-31] for its compactness, the ActiveLink AWN-03B [68] for its

working modes, the IHMC Mobility Assist Exoskeleton [32] for its control system, the APO [41-43] for its SEA, and the Innophys Muscle Suit [44-49] for the use of PMAs.

## 3.2 Characteristics Shared by Both Solutions

Before introducing the two proposed concept solutions, in this paragraph will be made an examination of the design characteristics that both solutions have in common, in order to avoid repetitions. Some of these characteristics will probably have a different implementation in practice, but they can anyway be considered as common characteristics as they're based on the same principle. For some characteristics will not be provided detailed information, due to the fact that the focus of the thesis is always the hip joint.

### 3.2.1 Materials

The choice of the materials is crucial for the exoskeleton links design. They must have good mechanical properties, being resistant enough to endure to the applied bending forces, but also lightweight to avoid an excessive load for the user, and consequent discomfort. The ultimate version of the exoskeleton frame may then be composed by aluminum beams and surrounded by carbon fiber to make it adaptable to the different anatomical portions, solution seen in different robots found in literature. The choice of the materials can be considered common to both concepts, even if the links configuration will necessarily be different, depending on the chosen solution.

### 3.2.2 Contact Surfaces

This characteristic is directly connected to the chosen materials. In fact, in the contact zones in which the forces are applied, a soft material is needed at the pHRI between robot link and user, in order to avoid discomfort for the latter. In addition, the contact surfaces must be as wide as possible, so that decreasing the pression being equal the applied force. The reaction forces are expected to be applied on both sides on the thigh, above the knee level, and on the chest, below the shoulder level. All the other contact surfaces, where only negligible forces are applied, have to be as small as possible, to avoid an excessive perspiration of the subject, resulting in discomfort. A particular attention for the back link of the exoskeleton must be made for this reason. Moreover, especially in the surfaces where the forces are applied, the contact between exoskeleton and user must be held, in order to avoid slippage, and consequent irritations and unintended misalignments, that will bring to a mismatch between expected and actual forces.

### 3.2.3 Size Adjustments

A set of links' length size adjustments must be provided to the exoskeleton, in order to adapt it to a range of people as wide as possible. The main regulations needed (*fig.41*) are the shoulder width, the back length, the hip width, the upper leg length and the thigh width. Some regulations may be obtained by means of rigid couplings, with discrete or continuous adjustments, besides other regulations, such as the thigh width one, may be achieved by means of soft cuffs.

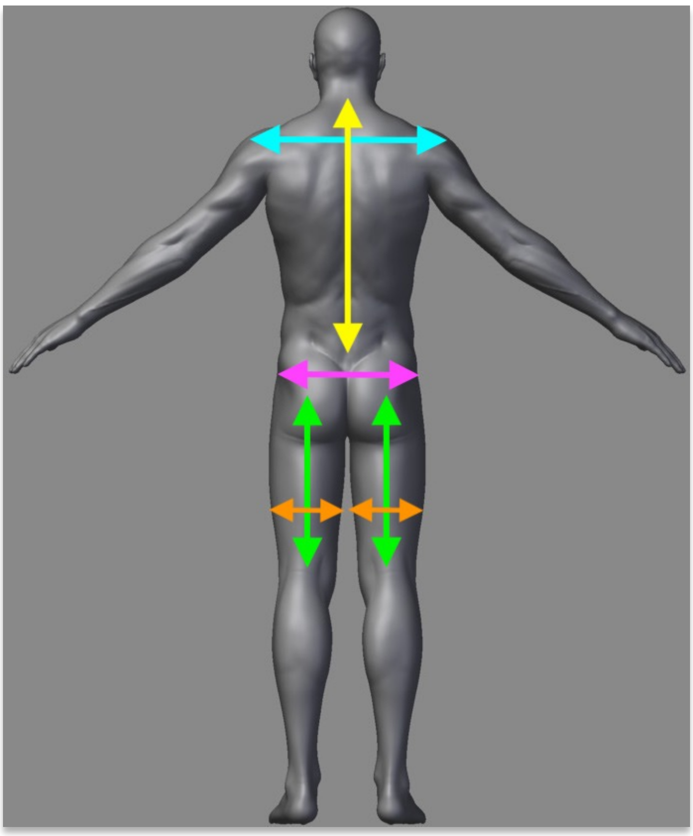

*Figure 41. Set of Exoskeleton Adjustments*

### 3.2.4 Degrees of Freedom

The exoskeleton must be provided of different degrees of freedom to allow not only the motion related to the actuation unit, but also other movements. As already discussed, the exoskeleton won't have to be an obstacle for the user, but it has to be as transparent as possible, especially when the actuation is not needed, for example during the gait cycle.
The hip flexion/extension movement will correspond to the only active DoF and will be positioned in correspondence of the hip joint center, on both hip sides. All the other DoFs are assumed to be passive, without compliant elements.
The hip abduction/adduction may be provided in different ways, as found in literature, but the most appropriate for the studied case corresponds to a simple rotational joint on the thigh side, allowing the rotation on the frontal plane on both hip sides.
Even though the internal/external rotation of the leg is not compulsory to be provided by a specific joint, due to the fact that the knee is assumed as not constrained and then this rotation is allowed, the internal/external rotation of the hip must be allowed trough a single rotational joint on the coronal plane, realistically positioned on the back frame of the exoskeleton.
Another DoF is needed between the thigh frames and the thigh contact shells. A spherical joint, for example, will guarantee the perpendicularity between the applied force and the thigh contact surfaces. This is required to adapt the shell to different thigh shapes at different hip joint angles.

### 3.2.5 Control System, Sensorization and Manual Inputs

The actuators represent the plant of the actuation system, and they are described by an appropriate transfer function which indicates the relation between inputs and outputs. They have to be controlled through a suitable control system, responding to the inputs given by the environment, either feedback or reference signals, through sensors and manual switches/buttons.
The sensors and other inputs needed by the exoskeleton are the following:

- An accelerometer, positioned on the back frame of the exoskeleton as close as possible to the chest pad, able to detect the angle between the torso and the vertical axis (angle θ in *fig.31*), useful to have the absolute initial condition of the trunk;

- A potentiometer or an encoder for each side able to detect the relative angle between the thigh and the back (angle a in *fig.31*), useful both to have the initial condition of the leg and to have a feedback of the trunk displacement;
- A sensor for each actuator, whose type depends on the actuation type, which detects the actual state of the actuator, such as angle, displacement or internal pression, needed by the actuation control unit;
- An absolute encoder able to detect the deformation of a compliant element, through which is possible to determine the actual provided torque T, transforming the torque control problem into a position control problem;
- An ON/OFF manual switch, able to power on and power off the system;
- A couple of plus/minus manual buttons, which will introduce a different gain in the control system, to modify the output torque and adapt the exoskeleton to users with different weight;
- A three states manual switch, to allow the user to select the mode of operation of the device.

It's now necessary to examine in depth the last point. Indeed, the exoskeleton will have three operating modes.

The first and most trivial is the "free mode". This operating mode is related to the state in which the user is walking, the exoskeleton does not assist the wearer and the actuators don't provide any torque. In this situation the motion of the legs is decoupled with respect to the motion of the back, leaving to the user the possibility to perform the gait cycle. All the sensors will anyway continue to collect data.

The second operating mode is the "stooping mode", needed when the user needs to hold a certain posture. Here the exoskeleton, at the beginning of the operation, will register the initial torso angle $\theta$, also called $\theta_0$, and will keep it as a constant reference. The aim is to maintain the static equilibrium of the upper body of the user until this one is the current operating mode. To obtain this result the legs/back motion will be coupled, and the actuator will provide a torque able to partially hold the human upper body load, taking as feedback the angle $\theta$, here calculated as a function of the hip angles (for reasons that will be explained in the future chapters), in order to maintain it constant and equal to $\theta_0$. In this way the actuator works as a mechanical block, and the control is essentially a position control with a constant reference.

The third operating mode is called "bending mode". In this last functioning mode, the exoskeleton will help the user to reach the erect position, helping him in the uprising phase, by providing a suitable torque. The torque must then be controlled, receiving the feedback through the encoders, position must be controlled as well, in order to achieve the desired velocities and accelerations. The feedback will be the angle $\alpha/\beta$, more precise than $\theta$ in dynamic conditions, but also the latter must be kept in consideration, to be sure to don't surpass the null value of $\theta$ for safety reasons. Another feedback is represented by the state of the actuator, needed by the actuator drivers.

This discrete control system has the advantage to activate the actuators only when needed, allowing a lower energy consumption.

All the buttons and switches must be placed in a position easy to reach by the user's hands, but at the same time difficult to activate unwantedly. A good positioning could be the hip side. The control unit may be external to the exoskeleton, if the control runs either on a PC with a platform such as MATLAB/Simulink or on a remote PLC, or integrated to the exoskeleton, if the control is performed on an embedded microprocessor or on a micro PLC.

## 3.3 Solution #1

This first solution takes inspiration from the actuation system of the APO [41-43]. It considers an electric actuation, taking advantage of a SEA system.

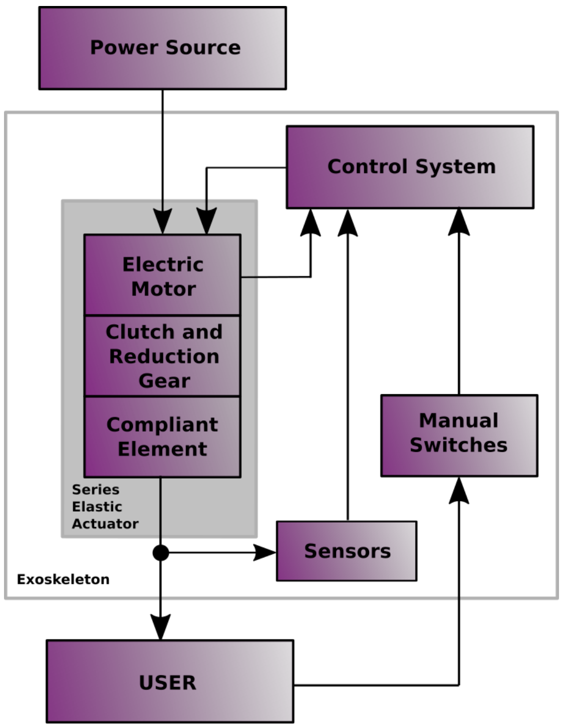


*Figure 42. Conceptual Scheme of Solution #1*

As shown in *fig.42*, an external power supply provides electric energy to the system, with an actuation unit composed by an electric motor, a clutch, a reduction gear and a compliant element. It is controlled by a control system which interacts both with the sensors implemented in the system and the user interface.

### 3.3.1 Series Elastic Actuators

The core of this actuation system is the addition of a compliant element in series with the power train, reducing the interface stiffness between actuator and load. As already said, this system is commonly known as Series Elastic Actuator [8, 81-84]. This allows to obtain a lower mechanical impedance, feature characterizing the so-called yielding systems. This property is crucial for a wearable robot to have a reduction of the peak forces, due to a low-pass filter effect on high frequency forces and shock loads, quite common in the studied devices.

The first component of the SEA will be an electric motor, in first assumption a brushless DC electric motor, clamped at one end to the hip/trunk frame. This motor could have an embedded incremental encoder, to have an indication of the motor status time-by-time. These motors have a very high efficiency, a low environment impact and a high reliability, then their use is particularly advisable for this purpose. Nevertheless, their power strongly depends on their dimension, and then to their weight, which will ever be limited. A suitable alternative to this motor will be discussed later on.

The output of the electric motor will be coupled with a device performing the motion decoupling of the system, compulsory when working in free mode. This element will be an electromagnetically actuated single disc clutch, chosen for the absence of backlash, for the high transmittable torque and for being perfect for a dry use. This device can transmit high torques with low losses, due to the absence of slippage except during the clutch activation. Furthermore, no lubrification is required. The only trade-off is the relatively high weight of this device.

The output of the clutch is coupled with a harmonic drive (HD), which will modify the velocity/torque values and will invert the rotating direction. This component was chosen for its high gear reduction ratio, especially considering the impressive compactness of these devices. In this way is also avoided the backlash problem common to the other gear systems, and nearly zero in a HD. These components are very lightweight, and they have

high torque capability, even though their introduction lowers the overall efficiency of the system.
The harmonic drive output is then connected to a compliant element, a torsional spring with highly linear characteristic without presenting hysteretic behavior, corresponding to the final element of the SEA, to which the load will be connected.
An actuation system composed as previously exposed has a good efficiency, due to a lower reflected inertia and to the potential energy stored in the torsional spring. From the control point of view, this system may easily achieve the stability, also considering that the force/torque control problem can be turned into a position/angle control problem, much easier than the previous one. As a trade-off, this system has a weight much more important than a simple electric motor directly connected to the load, characteristic to take in to account for a wearable robot design. Moreover, reducing actuator-load interface stiffness also lowers zero motion force bandwidth.

### 3.3.2 Power Supply

This device will be supplied by an external electrical power line connected to the exoskeleton through a cable. This choice was made considering the working destination of the device, that is a factory, in which is not required an extreme portability to the user in the work shift, and it’s easy to arrange a supply from the many power sources of the structure. This solution was considered the best one also due to its simplicity, in fact will not be necessary dimensioning a battery pack, that would provide an infinite mobility, but a higher weight, an increased incumbrance and a limited autonomy. With the adopted solution the user will not have an extra weight due to the power supply but will also have a potentially infinite autonomy, and the limited mobility is justified by the working conditions, making this the most suitable choice.

### 3.3.3 3D Concept Model

A preliminary 3D model of the left hip side of this first solution was created in order to clarify the effective working principle behind the concept idea. It’s necessary to notify that this is not a detailed model, just a concept useful to show the components positioning, and their relative interaction.

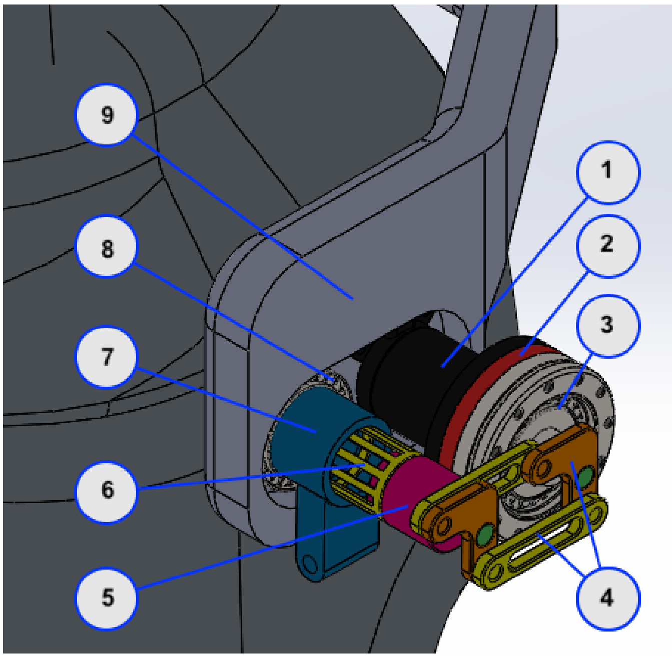

*Figure 43. Numered List of the Solution #1 Components*

With reference to *fig.43*, the numbered list of the elements composing the system is reported in the following table:

| ***Element Number*** | ***Element Name*** |
|---|---|
| 1 | Electric Motor |
| 2 | Single Disc Clutch |
| 3 | Harmonic Drive |
| 4 | Four-Bar Linkage |
| 5 | Spacer |
| 6 | Torsional Spring |
| 7 | Thigh Joint |
| 8 | Bearing |
| 9 | Trunk frame |

*Table 1. Numbered List of the Solution #1 Concept Model*

The system depicted in *fig.43-45* is, as already enunciated, just a concept with approximated dimensions and positioning. For example, the position of the single disc clutch [*elem.2*] and of the harmonic drive [*elem.3*] in the final system will be evaluated, considering a possible inversion depending on the actual components characteristics, and the shapes of the elements, such as the torsional spring [*elem.6*], are approximated and they can be considered as black-boxes.

Consider the system in an operating mode different from the "free mode", with the clutch activated. The brushless DC motor [*elem.1*] is clamped at one end to the trunk frame [*elem.9*], providing the desired torque and developing the resulting reaction force to the chest through the back link. The output of the motor is connected to the single disc clutch [*elem.2*], and to a harmonic drive reduction gear [*elem.3*], with a suitable reduction ratio.

As already seen in the case of the APO, the series elastic actuator was split into two branches for saving lateral encumbrance, and coupled by means of a modified version of the four-bar linkage [*elem.4*].

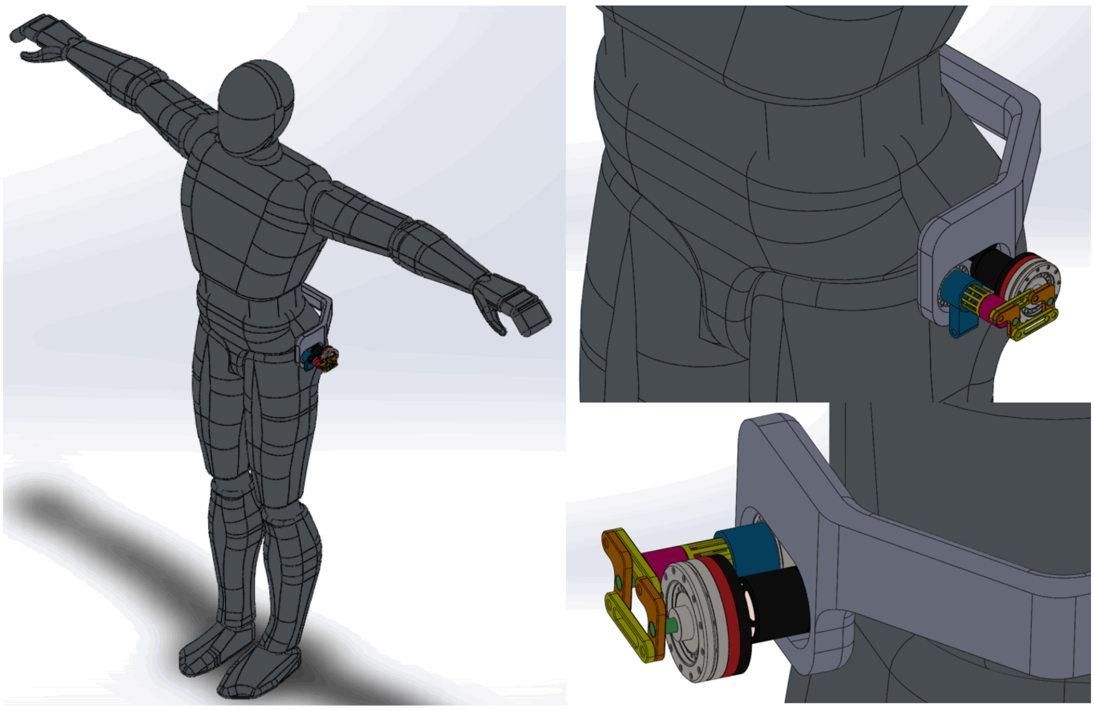

*Figure 44. Axonometric Views of the Solution #1 Concept Model*

Two main modifications were made to the four-bar linkage. The upper connecting rod (upper yellow element) was put behind the two crank elements (orange elements), to avoid the interference with the lower connecting rod when the cranks are rotating. The crank themselves were modified, giving them a "reversed L shape". These modifications allow to extend the range of motion up to values close to the human ROM values, to have an exoskeleton as transparent as possible.

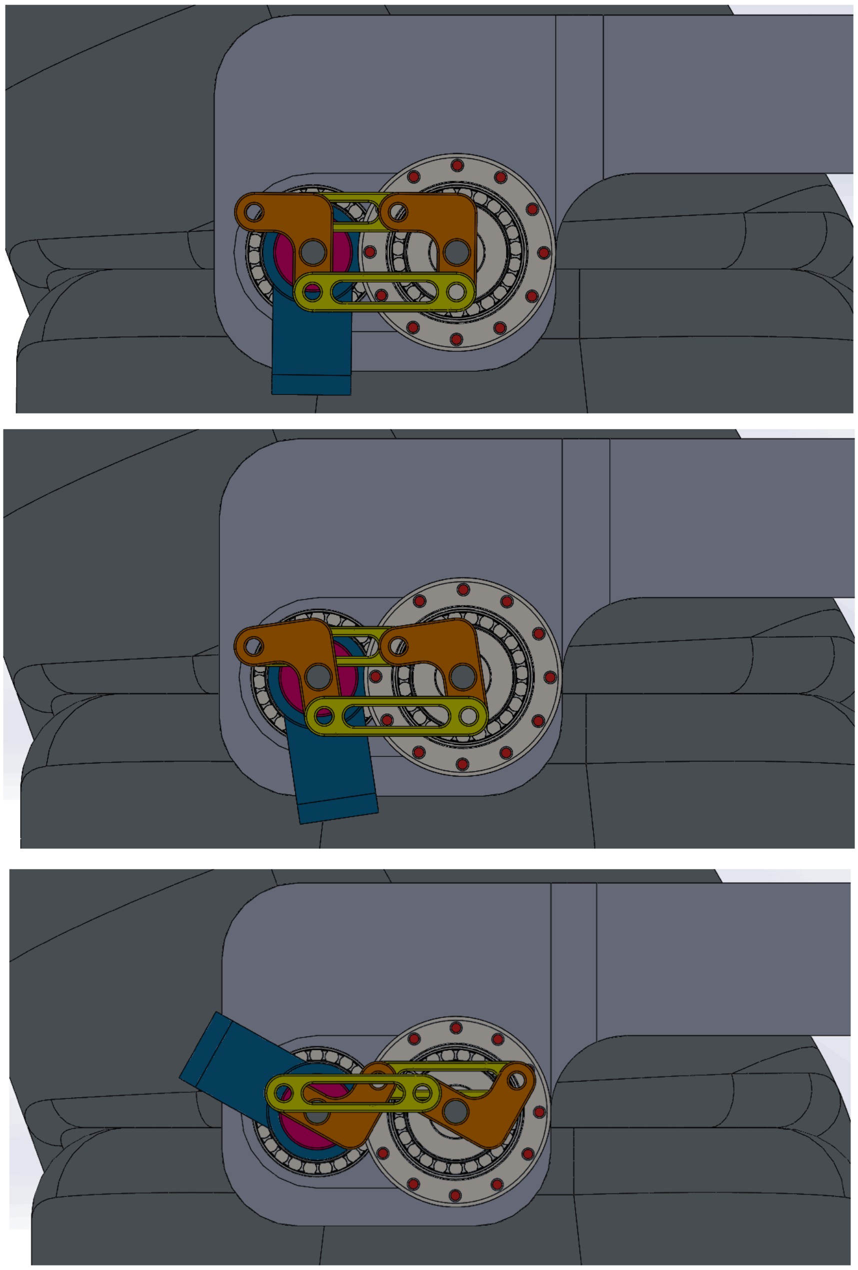

*Figure 45. Vertical Position, Maximum Extension Condition and Maximum Flexion Condition*

With the current configuration a wide ROM was achieved [fig.45], with a maximum extension equal to 15° and a maximum flexion equal to 120°. It's however possible change these values by adjusting the four-bar linkage geometry, because the motion limit depends on the interference between the upper connecting rod and the two branch shafts. In the ultimate model will be expected some angular limiters to avoid this contact.

Neglecting the friction, the power is transmitted without losses between the two branches by means of the rigid four-bar linkage. The torsional spring [*elem.6*] is then deformed proportionally to the provided torque and inversely proportional to its stiffness. The torque

is then transmitted to the thigh joint [*elem.7*], developing a reacting force on the thigh by means of the thigh link, not depicted yet.
A bearing [*elem.8*] connects the frame and the thigh joint, to allow the free movement between them.

### 3.3.4 Solution #1 Conclusions

The first proposed solution allows to achieve a very wide range of motion with a compact solution, having the whole actuation unit on the hip side. It follows that the back encumbrance is reduced, letting to the user also the possibility to seat wearing the exoskeleton. However, this yields to an increased lateral encumbrance, and the consequent difficulty to perform the so-called "arm swing" while walking, despite the two shafts subdivision of the SEA.
As already discussed, the system will be easy to control, allowing to achieve stability and robustness without particular issues.
It's important to notice that, due to the expected components, the cost of this system will be relatively high, so that its weight.
The geometry of the four-bar linkage will be later modified, passing from a "reversed L shape" of the cranks to a "Z shape", to enhance the functioning of the system.

## 3.4 Solution #2

The second proposed solution considers the work made by the Innophys [44-49] on their Muscle Suit, trying to adapt the system for the case of study. Indeed, the core of this solution is the employment of the McKibben artificial muscles.
As shown in *fig.46*, an external power supply provides pneumatic energy to the system, with an actuation unit composed by an air flow control unit, artificial muscles actuators and a pulley system for the power transmission. The motion decoupling considers the employment of brakes. It is controlled by a control system which interacts both with the sensors implemented in the system and the user interface.

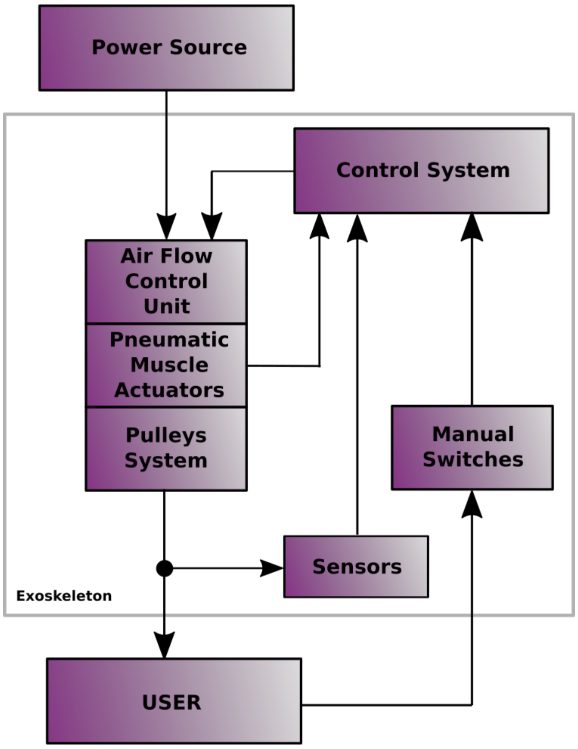


*Figure 46. Conceptual Scheme of Solution #2*

### 3.4.1 Pneumatic Muscles Actuation

A still not determined number of pneumatic muscle actuators will be used for the actuation of each side of the exoskeleton. They will be positioned on the back of the exoskeleton. Their positioning on the back of the thigh was also hypothesized, to create a counter force and increasing the hip torque, but this chance was discarded, because it would have eliminated the possibility to seat for the user, capability that was decided to maintain. Nevertheless, seating will be more difficult than in the previous case, because the back encumbrance will be much more significative. The McKibben artificial muscles will be clamped at one end to a structure fixed with the trunk frame of the exoskeleton. On the same end will be positioned an air flow control unit, commanded by the control system, that will manage the air flew into the pneumatic muscle, its inlet pressure, and then the provided force due to its contraction. The pneumatic muscles will be surrounded by a cover, to avoid undesired contacts, that could damage the actuators or hurt user and other people in the surroundings. McKibben actuators are a lightweight, flexible and biomimetic solution, capable to produce a high force with a good mechanical efficiency. Moreover, at low pressures, they have a compliant behavior. Nevertheless, they have a highly nonlinear

characteristic, making them difficult to control properly. In addition, they may be quite bulky, and can produce contractive force only, behavior similar to the human muscles but that can be considered as a design limitation.
The lower extremity of the McKibben actuator will be coupled with a steel wire cable, that will transmit the force to the hip through a grooved pulleys system, converting it into a torque. The grooved pulleys are free to rotate around an axis perpendicular to a trunk frame surface, where their shafts are fixed. This transmission system is flexible, simple, lightweight and cheap, but it may present losses due to friction between pulleys and frame, and between cable and pulleys. Another problem to consider is the possible cable escape from the grooves of the pulleys. It happens if the cable is not kept tightened, if the grooves of two successive pulleys does not lie on the same plane, or if the cable axis doe not correspond to the intersection line between the planes of the grooves of two successive not-coplanar pulleys.
The motion decoupling is accomplished putting a grooved pulley on a prismatic slider. The leg motion will make the pulley move, keeping the cable tightened with a helical spring, without pulling the pneumatic muscle. When needed, the leg-trunk motion will be coupled again with a brake on the slider, that will stop the pulley, allowing the power transmission to the hip-leg joint segment.

### 3.4.2 Power Supply

As in the solution #1 case, exposed in 3.3.2, the power supply of the device will be provided externally, with a flexible tube providing the compressed air from an outer compressor to the actuators' air flow control unit. As though the previous case an alternative would be including the power supply into the exoskeleton, here with a compressed air reservoir. The latter solution would significantly increase the device weight, but would give to the user an infinite mobility, however limited by a determined autonomy. An infinite autonomy and a lower weight are characteristic that have driven the choice to the external supply, accepting the limited mobility draw-back.

### 3.4.3 3D Concept Model

A 3D concept prototype was designed also for this second solution, with the same assumption made on 3.3.3.

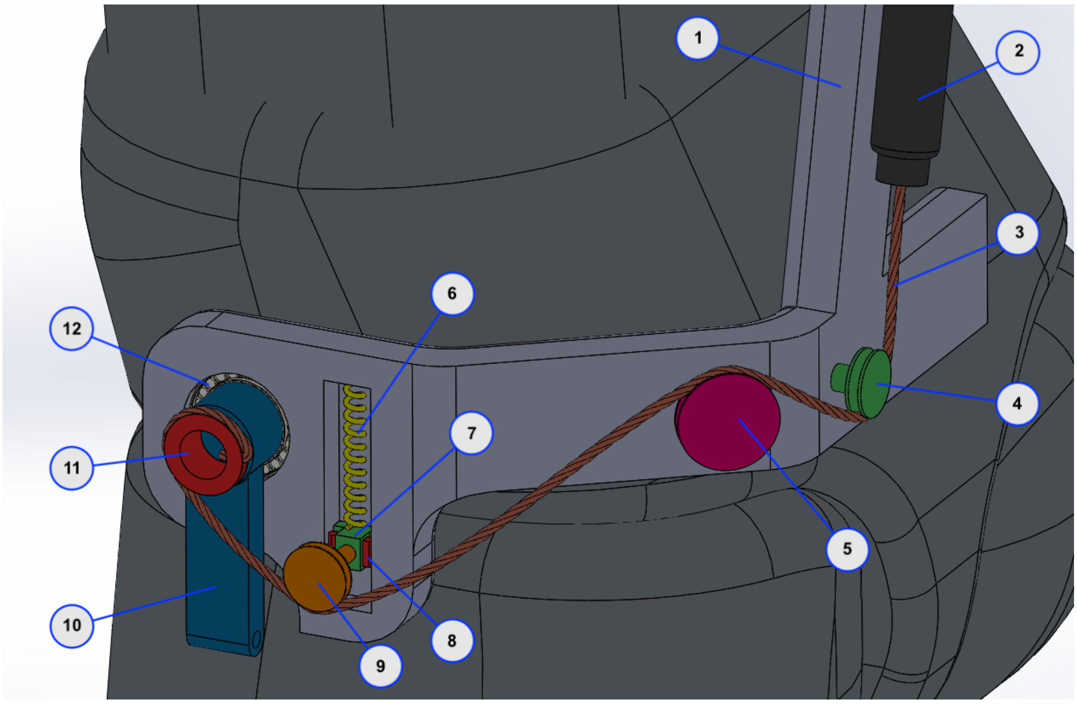


*Figure 47. Numbered List of the Solution #2 Components*

With reference to *fig.47*, the numbered list of the elements composing the solution #2 system is the following table:

| ***Element Number*** | ***Element Name*** |
|---|---|
| 1 | Trunk Frame |
| 2 | McKibben Artificial Muscle |
| 3 | Steel Wire Cable |
| 4 | Back Pulley |
| 5 | Side Pulley |
| 6 | Helical Compression Spring |
| 7 | Prismatic Slider |
| 8 | Drum Brake |

| | |
|---|---|
| 9 | Moving Pulley |
| 10 | Thigh Joint |
| 11 | Hip Pulley |
| 12 | Bearing |

*Table 2. Numbered List of the Solution #2 Concept Model*

Analogously to the previous case, this is a simplified model designed to explain the working principle. The left side only was modeled, just one pneumatic muscle actuator per side was considered, all the pulleys were modeled as a single body, coupling elements, air control unit and sensors were neglected.

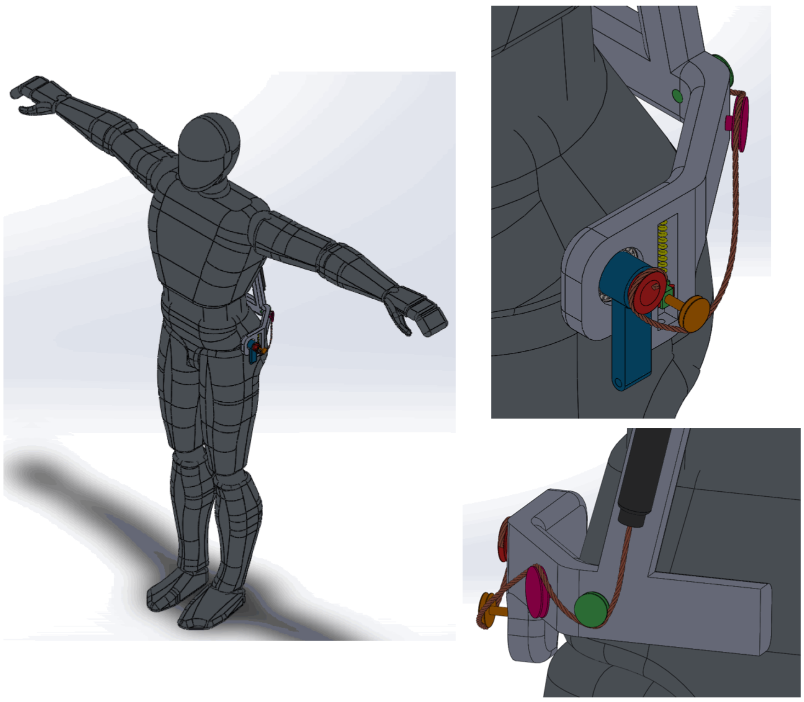

*Figure 48. Axonometric Views of the Solution #2 Concept Model*

Consider now the system depicted in *fig.47-49* working in "free mode" and the user walking. During the gait cycle the thigh joint [*elem.10*] will rotate following the leg movement, being coupled with it. At the same time, the hip pulley [*elem.11*], fixed with the hip-leg segment, will rotate synchronously, pulling and relaxing the steel wire cable [*elem.3*]. The slider [*elem.7*] is now free to move on the prismatic guide, and the contact between the cable and the moving pulley [*elem.9*] is guaranteed by the spring action on the slider. The leg motion during the gait cycle will cause the upward/downward motion of the pulley on the slider by means of the cable action, without interacting with the McKibben actuator. An equivalent situation occurs when the user is bending forward, keeping the legs in vertical position, and pulling and relaxing the cable by means of the PMAs.

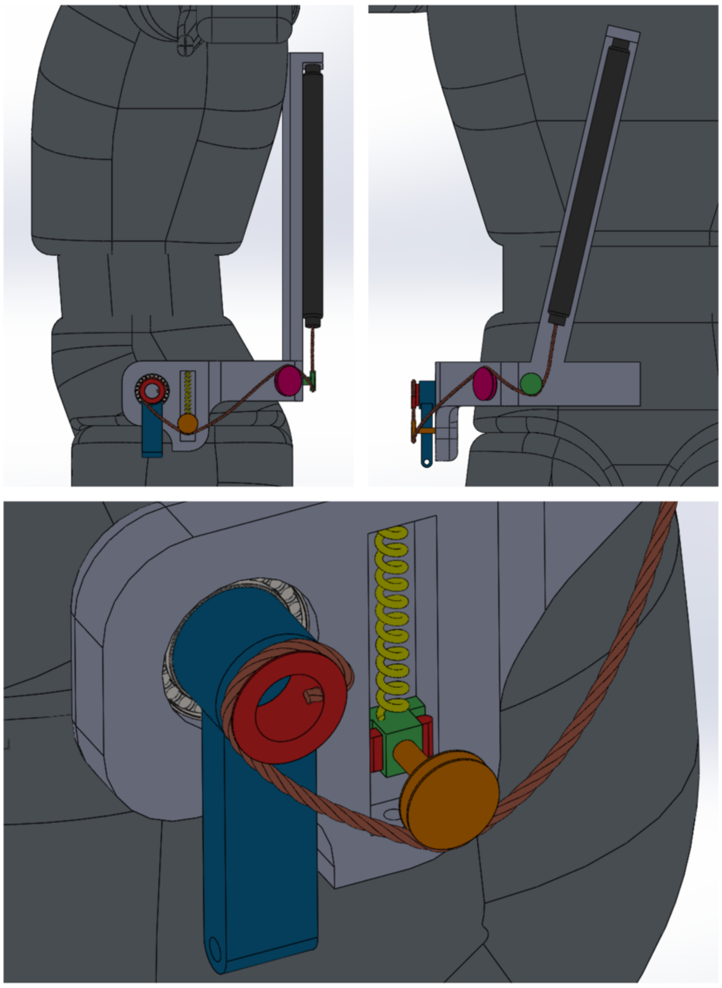

*Figure 49. Left, Back and Detailed View of the Solution #2 Concept Model*

Consider now the device working no more in "free mode". When needed the air flow control unit will let flow air into the McKibben artificial muscle [*elem.2*], pressurizing it. The PMA contraction will bring to a reduction of its length, and to a consequent pulling force directly transmitted to the steel wire cable. The cable will pass through the grooves of the back [*elem.4*] and side [*elem.5*] pulleys that will guide it, changing its orientation till arriving to the moving pulley. Now the cable action will not move upward this pulley, because at the same time when the pneumatic muscle start pressurizing, the drum brake [*elem.8*] on the slider will activate, blocking the slider itself into the prismatic guide, and so the pulley. The steel wire rope will pass through the orange pulley groove without moving the pulley itself but acting on the final hip pulley [*elem.11*], being the cable fixed with it. A hip torque will be generated, proportional to the McKibben pulling force and to the hip pulley radius, neglecting the losses. The same torque will propagate to the thigh joint and then to the leg link, generating the thigh reaction force. As already said, the other reaction force will be applied on the chest by means of the back link.

### 3.4.4 Solution #2 conclusions

This second proposed solution results really simple from a mechanical point of view, with cheap, lightweight and mechanically simple components. The lateral encumbrance is reduced to its lowest, to the detriment of the back encumbrance due to the presence of the pneumatic muscle unit. The McKibben actuators also provoke the main issue of this solution: indeed, they are characterized by a nonlinear behavior, so they are difficult to control.

It's easy to foresee that the range of motion of motion of the user in the sagittal plane, wearing an exoskeleton designed as explained, strongly depends on the prismatic guide length: the longer the prismatic guide, the wider the ROM. Besides, in this second solution is more difficult to achieve wide range of motions as in the first one, because an excessively long guide will cause complaint to the waist and to the thigh side of the user, obstructing various movements.

Another remarkable draw-back of this solution is the possible cable escape from the pulley grooves. This can be caused by external forces, by rapid movements, either of the user or of the PMA, and by a bad relative positioning of two successive pulleys. To overcome this problem, it's possible to employ a counter-pulley to pass the cable without escaping, besides studying a better positioning of the pulleys and of the actuators. This will cause an increase of the friction losses, and so an undesired effect on the system efficiency.

# Chapter 4

# Actuation Unit Definition

## 4.1 Adopted Solution

Considering the previously exposed solutions, only one of them was chosen and will be considered from now on. The chosen one is the solution #1, contemplating the use of a series elastic actuator system composed by an electric motor, a clutch, a harmonic drive, a four-bar linkage and a torsional spring, which meanings inside the actuation system were already explained. In the following paragraphs will be shown the realized study on each component, going to choose from a shortlist of different companies each element from their catalogue, in order to have an idea about the dimension and the weight of the actuation unit. These components will be going to define the actual hip joint actuation, and their data will be used for the calculations and the evaluations, independently from the components that will be employed in practice.
Nevertheless, before designing the components, the kinematic behavior in bending mode and the design torque must be discussed, in order to have a design target to reach.

## 4.2 Desired Motion Planning in Bending Mode

As already exposed, the aim of the exoskeleton when working in the so-called "bending mode" is providing a torque with a non-zero rotating speed, able assist the human upper body during the uprising phase, until reaching the vertical position. The motion of the hip joint is controlled by the control system, which has to impose a smooth and continuous motion, with limited velocities and accelerations compatible with the limited torques that the actuators are capable to provide, without going beyond the position related to the null θ angle.

An ideal velocity profile was designed, hypothesizing a trapezoidal 2-1-2 speed profile, with a first section with constant acceleration, a second part with constant speed and a third part with constant deceleration. This velocity profile, very common in robotics, was chosen for its simplicity. The maximum output speed was designated to be 7.5 rpm, equivalent to the speed related to the constant speed section. This value was chosen considering the average human uprising speed and relating it as the maximum comfortable value. It can be considered a sort of limit value and it's required to don't cross it.

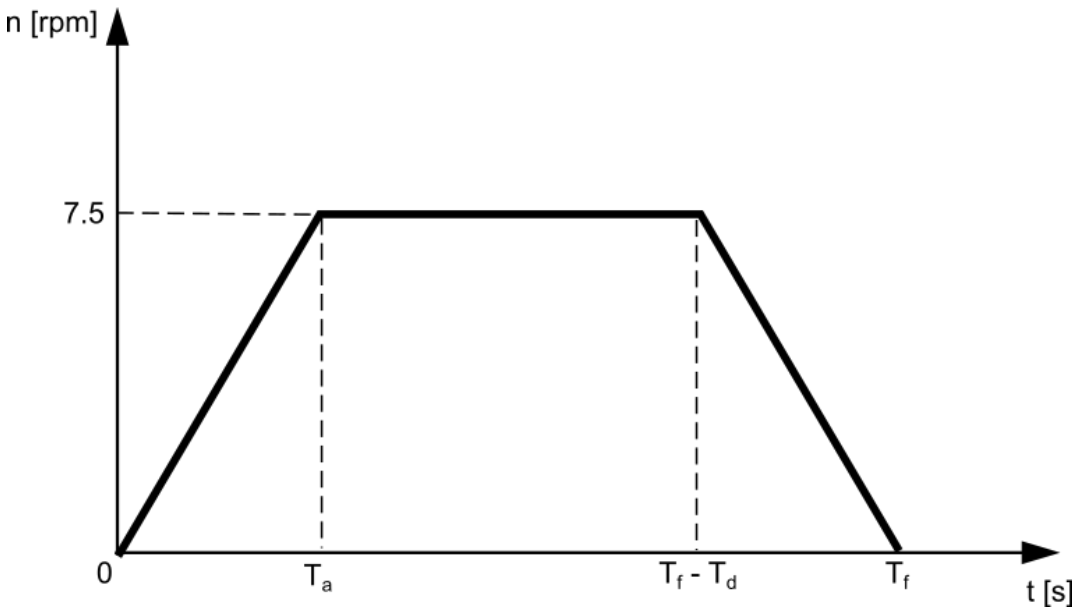


*Figure 50. Example of Ideal 2-1-2 Trapezoidal Rotating Velocity Profile for the Hip Joint in Bending Mode*

## 4.3 Design Torque Definition

To estimate the torque that the actuation unit has to provide it's necessary to define the conditions in which the designed robot has to operate. This is made to estimate a so-called design torque, a nominal torque needed for the components dimensioning and choosing.
The resistant hip torque, due to the weight of the human upper body, was already studied in the previous chapters. Nevertheless, it's necessary to add the exoskeleton weight to the human weight, because even the robot itself will create an additive undesired hip torque. The obvious problem is that now results impossible to know precisely the weight of the exoskeleton that will be designed, and where its own CoG is located. To bypass the issue related to the exoskeleton weight an investigation was performed about the exoskeletons considered similar to the one designed in this paper, considering the function and the actuation system of each robot, with the aim of obtaining an estimated average mass. Eight robots were considered (*tab.3*).

| **Company** | **Product** | **Function** | **Actuation** | **Mass [kg]** |
|---|---|---|---|---|
| S.S. Sant'Anna Pisa | APO | Gait support | BLDC (SEA) | 4.2 |
| Innophys | Muscle Suit | Back Support | McKibben PMA | 5.5 |
| StrongArm Tech | V22 Ergosk. | Back Support | Passive | 1.8 |
| ActiveLink | AWN-03 | Back Support | AC Electric Motor | 6.0 |
| SuitX | backX | Back Support | Passive | 3.4 |
| StrongArm Tech | FLx Ergosk. | Back Support | Passive | 1.0 |
| Cyberdyne | HAL L.S. | Lumbar Support | BLDC | 3.0 |
| Laevo V2 | V2 | Back Support | Passive | 2.3 |

*Table 3.Weight of the Reference Exoskeletons*

The estimated average mass, to add to the back load, results to be $M_{exo,avg} = 3.4\ kg$.

It's useful to notice that most of the considered exoskeletons are passive, without a real actuation system, and then are slightly lighter than the one designed in this paper, especially considering the chosen hip joint actuator, surely heavier than most of the other ones. For a conservative design, the weight force of the exoskeleton was considered as applied all in one point, the trunk center of gravity. This is a strongly conservative assumption, because even if the actual exoskeleton mass will be higher, its weight will be concentrated mostly on the hip, without the possibility to produce a hip torque due to the weight itself.

Now all the elements needed for the design torque definition are given, everything else is chosen arbitrarily.

The total design torque is defined as the hip torque needed to hold the static equilibrium with the weight correspondent to the 70% of the weight of the upper body (trunk, neck, head and arms) of a 99 percentile Italian man, with both arms through the trunk and the exoskeleton worn. The "70%" was arbitrarily chosen considering a minimum of a 30% of the weight always held by the user's muscles.

The design point is defined as the design torque correspondent to the maximum bending angle (design angle) for which the static equilibrium is desired, equal to π/4 rad.

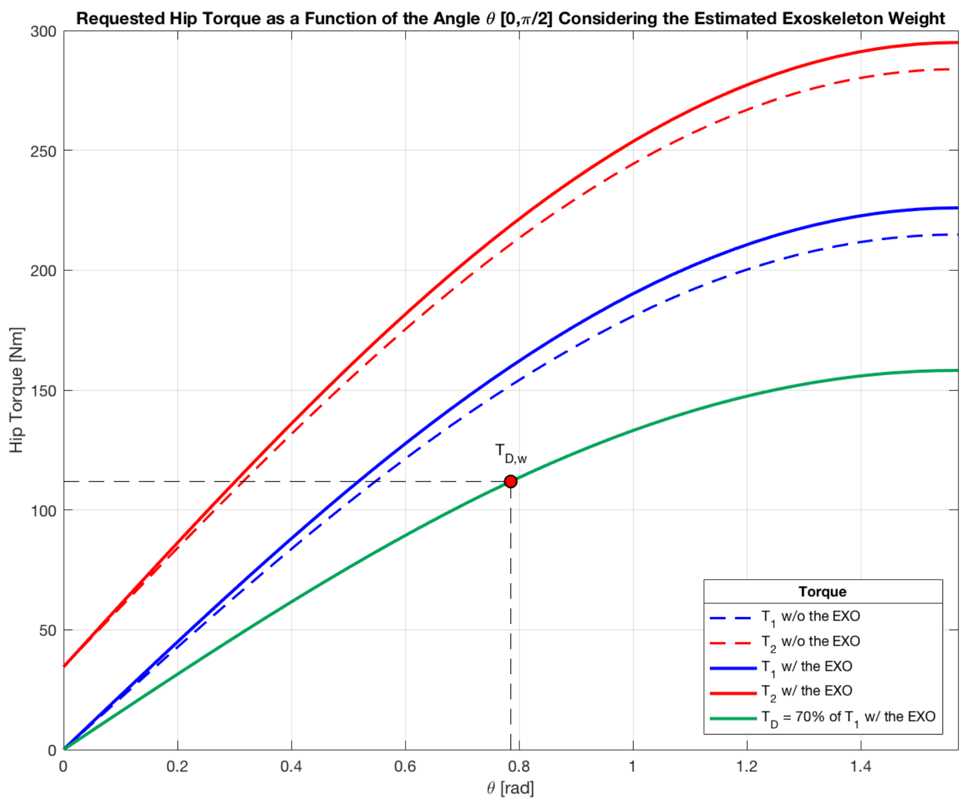


*Figure 51. Design Torque Definition*

The total design torque in the design angle is equal to $T_{D,TOT,w} = 110\ Nm$. This torque has to be divided by the two hip sides, halving the value. Each hip joint actuation unit must then be able to provide up to $T_D = 55\ Nm$, value of the design torque of each actuation unit.

## 4.4 Reaction forces on the User

By knowing the hip design torque $T_{D,TOT}(\vartheta)$ is possible to study the reaction forces applied to the load. An assumption has to be made: the only contact zones in which the user and the robot interact are supposed to be on the chest and on the thighs, with one contact zone per side. This is a hypothesis made on the base of similar robots found in literature and it's possible that it will change in advanced design phases, depending on the exoskeleton design. All the other contact zones (e.g. on the pelvis and the back) will be neglected, hypothesizing that these forces will be much smaller than the previously considered ones.
The actual contact point is not known yet, then will be assumed to be at a distance equal to $L_{AP} = 0.1\ m$ (*fig.52*) from the shoulders or from the knees. This value was arbitrarily chosen, considering it as a suitable value.

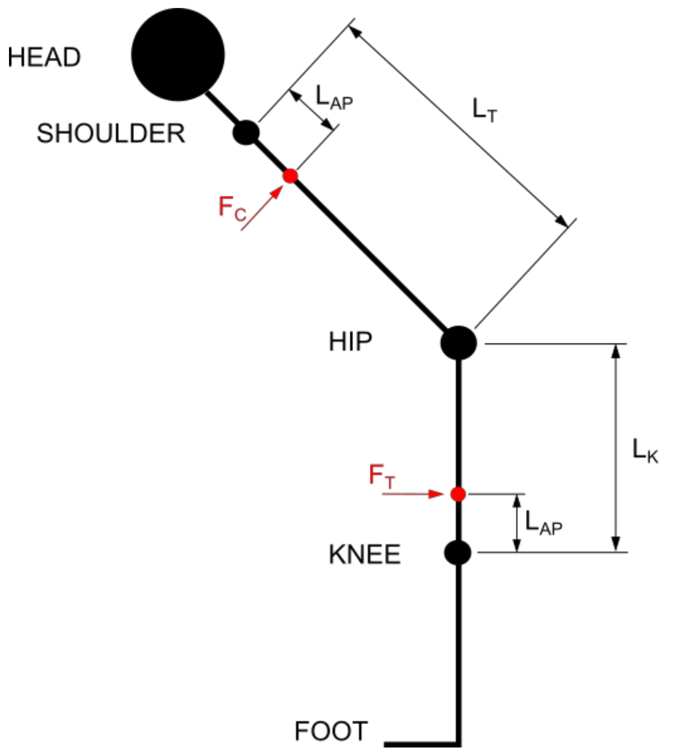


*Figure 52. Application Points of Chest/Thigh Reaction Forces*

By knowing the height of a 99 percentile Italian man H and the body segment coefficients reported in *fig.33*, is possible to obtain the partial length of trunk and thigh.

$L_T = (0.818 - 0.530)H = 0.5423\ m$

$L_K = (0.530 - 0.285)H = 0.4613\ m$

By means of these data the reaction forces can be easily obtained imposing the static equilibrium.

$$F_C(\vartheta) = \frac{T_{D,TOT}(\vartheta)}{2(L_T - L_{AP})} \tag{6}$$

$$F_T(\vartheta) = \frac{T_{D,TOT}(\vartheta)}{2(L_K - L_{AP})} \tag{7}$$

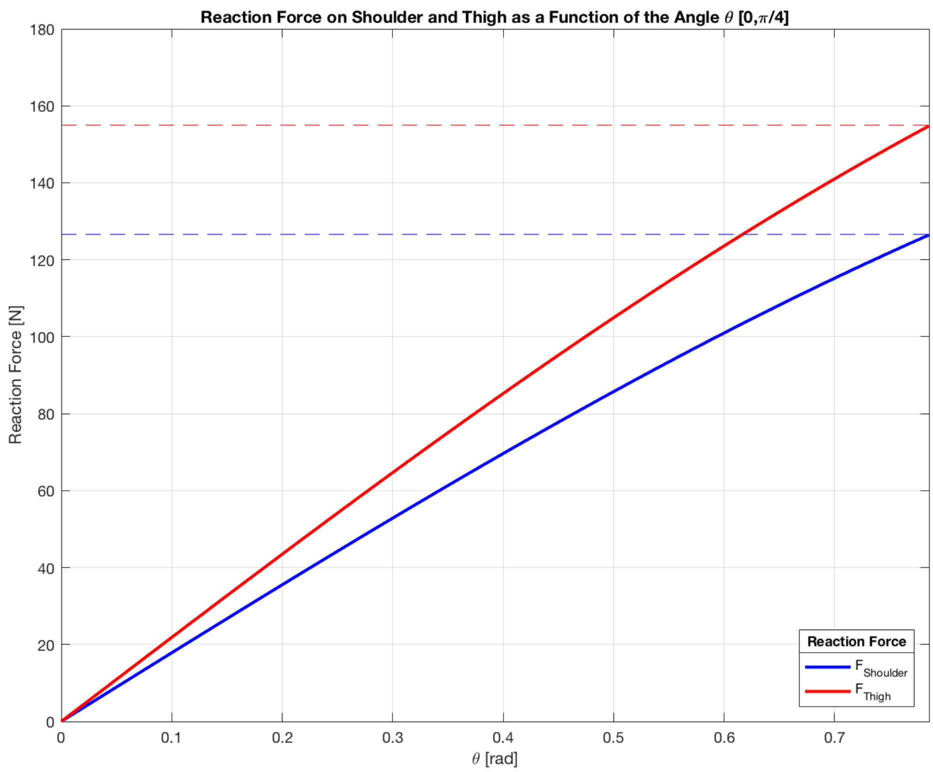


*Figure 53. Chest and Thigh Reaction Forces Behavior*

The plot of the reaction forces is reported in *fig.53*, in a bending range [0,π/4] rad.

The maximum forces are reached when θ=π/4, and their values are:

$F_{C,max} = 127N$

$F_{T,max} = 155\ N$

It's now necessary to understand if these forces produce a pressure capable to cause discomfort or even pain to the human. The force taken as reference will be $F_T$, the greatest between them, but to obtain a pressure is necessary to know the surface in which the force itself is applied. Unfortunately, the contact area is not known yet, so it's needed to estimate a suitable thigh-robot contact surface. A small 0.1x0.1 m square was hypothesized, equal to an area of $S=0.01m^2$. This surface is hypothesized to have a value smaller than the actual one, or almost similar. If it will really be smaller it will produce a bigger pressure, good for this estimation.
The estimated maximum pressure is then $P = F_T/S = 15500\ Pa = 0.155\ bar$. For what was found in literature, this value is abundantly below the pain threshold for healthy individuals, that is around 2.2 bar, so it's possible to consider the human-robot interaction as a comfortable interaction [85-86], not dangerous for the user. The interaction may be even more comfortable by a suitable design of the contact zone, with soft and wider surfaces, and predisposing a passive DoF that will assure the perpendicularity of the force with the thigh, avoiding slippage and then abrasions to the user's skin.

## 4.5 Selection of the Components

In this paragraph it's shown the outcome of a selection work about the components included into the hip joint actuation unit, taking into account the desired output torques and speeds, the weight and the dimensions. The choice of these elements was made directly from the companies' catalogues, in order to have real data to use in the future works.

### 4.5.1 Electric Motor

The first choice for the electric motor is a brushless DC motor. In the brushless motor the magnetic field is generated by permanent magnets located on the rotor, producing an electro-motive force on the windings of the stator. These motors offer several advantages over the classic brushed DC motors: high efficiency, high reliability, high torque/weight ratio, lower noise and longer lifetime because there is no erosion due to the brushes.
The chosen motor is the Maxon Motor© EC frameless 90 flat [87], a 160W motor capable to produce a nominal torque of 0.477 Nm, whose main characteristics are reported in *fig.54*.

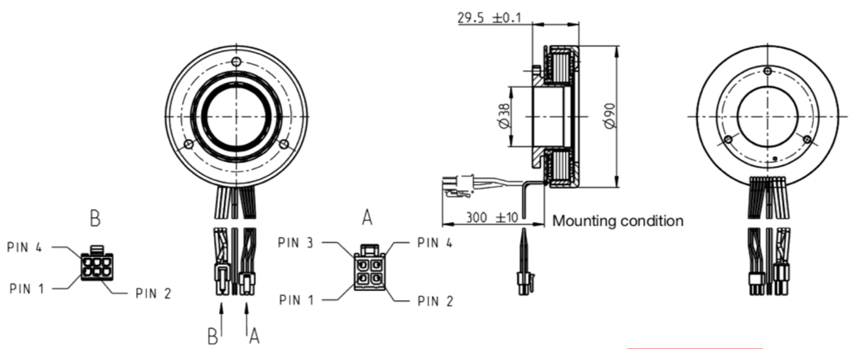


| | | | with Hall sensors 588847 |
|---|---|---|---|
| **Motor Data** | | | |
| | **Values at nominal voltage** | | |
| 1 | Nominal voltage | V | 12 |
| 2 | No load speed | rpm | 3150 |
| 3 | No load current | mA | 1310 |
| 4 | Nominal speed | rpm | 2610 |
| 5 | Nominal torque (max. continuous torque) | mNm | 477 |
| 6 | Nominal current (max. continuous current) | A | 13.1 |
| 7 | Stall torque | mNm | 5980 |
| 8 | Stall current | A | 168 |
| 9 | Max. efficiency | % | 83.3 |
| | **Characteristics** | | |
| 10 | Terminal resistance phase to phase | Ω | 0.0715 |
| 11 | Terminal inductance phase to phase | mH | 0.0644 |
| 12 | Torque constant | mNm/A | 35.6 |
| 13 | Speed constant | rpm/V | 268 |
| 14 | Speed/torque gradient | rpm/mNm | 0.538 |
| 15 | Mechanical time constant | ms | 20 |
| 16 | Rotor inertia | gcm² | 3398 |

*Figure 54. Brushless DC Motor Datasheet [87]*

The reported value doesn't consider the presence of the harmonic drive in the system, whose effects will be highlighted later on.

This is a powerful but lightweight motor, with an extremely reduced longitudinal dimension.

The ideal motor torque-speed characteristic at nominal voltage was created starting from the data taken from the datasheet, neglecting ripple, cogging, tolerances, thermal influences and mechanical and electrical losses. The ideal characteristic (*fig.55*) was achieved by the typical equation:

$$T(\omega) = T_S\left(1 - \frac{\omega}{\omega_0}\right) \tag{8}$$

Where $T_S$ is the stall torque, that is the torque with the locked rotor when supplied at nominal voltage, and $\omega_0$ is the no load speed. The nominal torque, corresponding to the maximum torque available when the motor is continuously working, and the nominal speed were also considered.

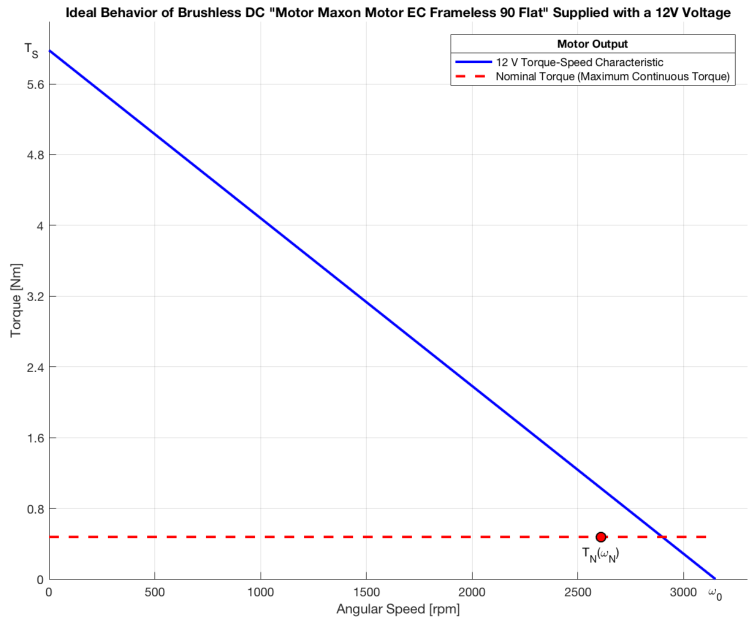


*Figure 55. Ideal Characteristic of the Brushless DC Motor*

The motor characteristics translate through parallel lines when changing the voltage: the higher the voltage, the higher the motor output torque. By changing the current, maintaining the same input voltage, it's possible to change the working point on the characteristic line. The efficiency [88], describing the ratio between output mechanical power and input electric power, is described by the following equation:

$$\eta = \frac{\omega \cdot (T - T_f)}{V \cdot I} \tag{9}$$

Where $T_f$ is the resistant torque of the motor due to friction effect, V is the voltage and I is the current.

It's possible to see that, considering the proportionality between torque and current ($T=k_m I$ with $k_m$ torque constant available from the datasheet), the efficiency increases linearly when increasing the speed.

The motor was chosen considering the speed and the torques applied to the load, taking into account the presence of the harmonic drive that will modify the output values. The mainly considered value was the nominal torque, that is the maximum value for which the motor can work continuously.

### 4.5.2 Clutch

The clutch is required in the system to couple and decouple the relative motion between legs and trunk, when passing from the free mode, in which the clutch is disengaged, to the stooping or bending mode, in which the clutch is engaged, and input and output are synchronous.

The clutch receives as input the motor output speed and torque through a shaft element and gives as output the very same speed and torque when engaged, considering no slippage. This will be the harmonic drive input. The clutch engagement will normally take place at standstill but may also happen with a speed difference.

The chosen clutch is the Warner Electric© SMF VAR 00 size 10 [89], an electro-magnetic single disc clutch with a single friction face activated by power on. This clutch has all the needed requirements, because no lubrification is required, it has no backlash, it has a high maximum transmissible torque, and there is no residual torque when disengaged, important when working in free mode to avoid interfering with the gait cycle. The heat dissipation of the clutch can’t be considered an issue, due to the few cycles per hour that the hip joint must fulfill.

The main disadvantage of this component is its high weight but is a necessary compromise for a component needed for the correct working of the system. In fact, it has a mass of 0.5 kg, a high value considering its small dimensions, especially if compared with the weight of the other components of the hip joint actuation unit.

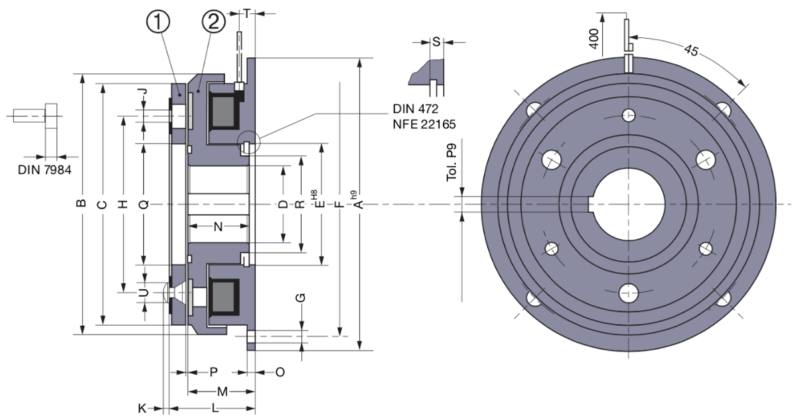


| Sizes | | | 10 |
|---|---|---|---|
| Nom. Torque | | [Nm] | 7 |
| Max. Speed | | [$\text{min}^{-1}$] | 8000 |
| Power | P20[U=12/24/103,5V] | [W] | 12,5 |
| | A | | 80 |
| | B | | 68 |
| | C | | 63 |
| | D min | | 10H8 |
| | D Std | | 10/15/17 |
| | D max | | 17H8 |
| | E | | 35 |
| | F | | 72 |
| | G For screw | | 4xM4 |
| | H | | 46 |
| | J (1) For screw | | 3xM3 |

| | | | |
|---|---|---|---|
| | K | | 1,5 |
| | L | | 28 |
| | M | | 24 |
| | N | | 22 |
| | O | | 2 |
| | P | | 0,2 |
| | Q | | 35 |
| | R | | 23 |
| | S | | 3,5 |
| | T | | 5,6 |
| | U | | 6 |
| Inertia | 1 | [$kgm^2$] | 0,00004 |
| Inertia | 2 | [$kgm^2$] | 0,00011 |
| Weight | | [kg] | 0,5 |
| Connection | | | Leads |

*Figure 56. Electro-Magnetic Single Disc Clutch Datasheet [89]*

For choosing the clutch the design torque of the actuation unit was considered, conveniently divided by the HD transmission ratio (not presented yet), applying a safety factor at least equal to three, and comparing the value with the nominal torque of the clutch equal to 7 Nm: the clutch will be located between electric motor and HD to satisfy its nominal torque requirement.

It’s important to highlight that in the simulations of the following chapters, the clutch will be neglected when disengaged, considering the disengagement as an open circuit, and only its inertia will be considered when engaged.

### 4.5.3 Reduction Gear

The harmonic drive is a necessary component to avoid having a motor with dimensions and weight bigger than needed. It will modify the input torque/speed value and direction depending on a factor related to its own transmission ratio and the mounting arrangement. The transmission ratio depends on the number of teeth of the gear, the arrangement depends

on which of the three elements of the HD are used as fixed element, input element and output element. For the examined case the motion inversion is required.
The chosen harmonic drive is the Harmonic Drive© CPL-20A-120-2A [90], characterized by a very lightweight design, a low moment of inertia (MOI) and a transmission ratio i=120, with a repeatable peak torque of 87 Nm.

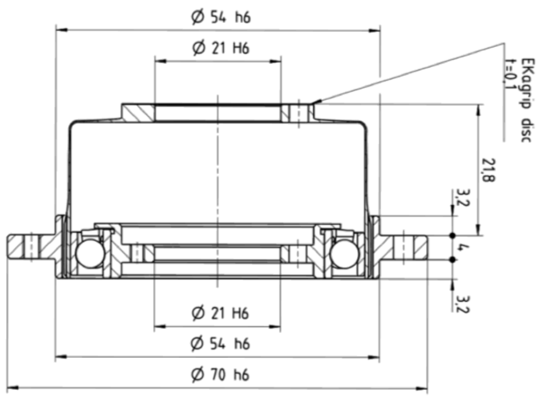


| | Unit | CPL-20-2A | | | | | |
|---|---|---|---|---|---|---|---|
| Ratio | i [] | 30 | 50 | 80 | 100 | 120 | 160 |
| Repeatable peak torque | $T_R$ [Nm] | 27 | 56 | 74 | 82 | 87 | 92 |
| Average torque | $T_A$ [Nm] | 20 | 34 | 47 | 49 | 49 | 49 |
| Rated torque | $T_N$ [Nm] | 15 | 25 | 34 | 40 | 40 | 40 |
| Momentary peak torque | $T_M$ [Nm] | 50 | 98 | 127 | 147 | 147 | 147 |
| Maximum input speed (oil lubrication) | $n_{in\,(max)}$ [rpm] | 10000 | | | | | |
| Maximum input speed (grease lubrication) | $n_{in\,(max)}$ [rpm] | 6500 | | | | | |
| Average input speed (oil lubrication) | $n_{av\,(max)}$ [rpm] | 6500 | | | | | |
| Average input speed (grease lubrication) | $n_{av\,(max)}$ [rpm] | 3500 | | | | | |
| Moment of inertia | $J_{in}$ [x$10^{-4}$ kgm$^2$] | 0.112 | | | | | |
| Weight | m [kg] | 0.14 | | | | | |

*Figure 57. Harmonic Drive Datasheet [90]*

Considering the average torque in which each hip joint will operate as half the value of the maximum available torque, then $T_{av}$=27.5 Nm. For a good dimensioning the actual average torque $T_{av}$ must be lower than the maximum average torque $T_A$ in the HD datasheet (fig.57); is easy to verify that this condition is respected. The conditions about the maximum input and output speed and the maximum torque are analogously respected.
The efficiency of the harmonic drive may be achieved by using the efficiency graphs. Firstly, is required to calculate the torque factor V, depending on average torque and nominal torque.

$$V = \frac{T_{av}}{T_N} = 0.563 \tag{10}$$

The torque factor V allows to obtain the factor K, required to achieve the load efficiency. The factor K results to be around 0.92 from the graph in *fig.58*. The efficiency depends on the rotating speed and the lubrification type of the harmonic drive, being a variable efficiency. Considering the lowest rotating speed, a temperature of 25°C and a greased gear, the efficiency results to be η=0.84 by the graph in *fig.59*. This efficiency must be multiplicated by the factor K to achieve the load efficiency.

$$\eta_L = \eta \cdot K = 0.77 \tag{11}$$

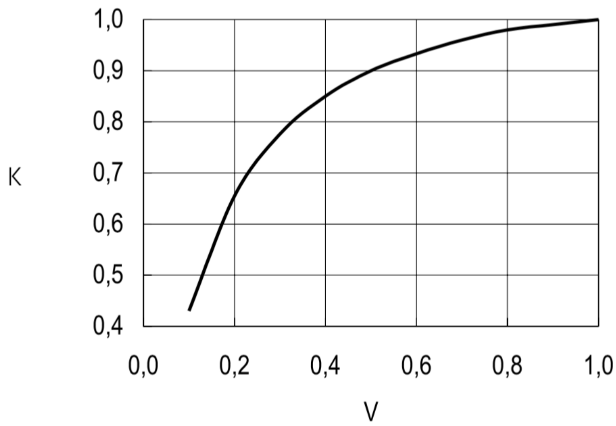


*Figure 58. Factor K Graph [90]*

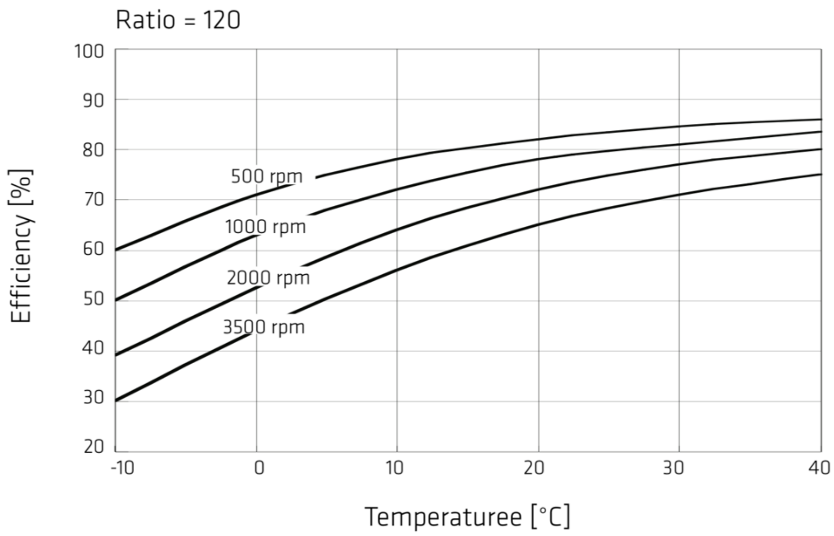


*Figure 59. Harmonic Drive Efficiency Graph [90]*

By means of the harmonic drive data just achieved is possible to obtain the output of the first shaft of the actuation unit, input of the four-bar linkage. The speed and torque values of the motor will be modified by the HD, and these values will be transmitted to the back link on one side, and to the four-bar linkage, to the leg shaft (without losses neglecting the friction), to the torsional spring and then to the thigh link.
Speed and torque are transmitted as follows:

$$\omega = \frac{\omega_{mot}}{i} \tag{12}$$

$$T = \eta_L \cdot T_{mot} \cdot i \tag{13}$$

As it's possible to see, the harmonic drive efficiency only affects the output torque, not the speed.
By means of these considerations it's now possible to plot the output of the harmonic drive giving the brushless DC motor speed/torque characteristic as input (*fig.60*). The nominal output torque becomes $T_{N,out}$=45 Nm, a bit lower than the maximum design torque needed when stooping, and the maximum torque available for a short time for the maximum desired output speed (n=7.5 rpm) is $T_{max}$=400 Nm, much higher than needed. The latter value is greater than the value tolerable by the harmonic drive, which is lower also than the maximum acceptable value of the clutch. The maximum available torque for short times is then equal to the repeatable peak torque of the harmonic drive, that is $T_{max}$=87 Nm.

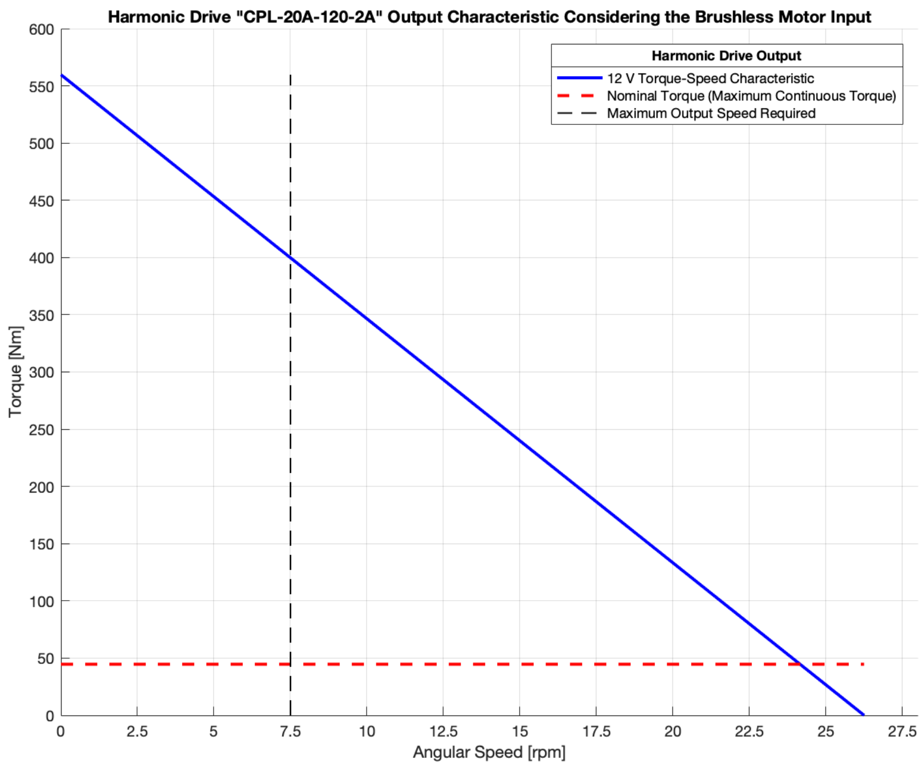


*Figure 60. Harmonic Drive Output Characteristic*

### 4.5.4 Torsional Spring

Moving onto the leg shaft of the actuation unit, the main element of this part is the torsional spring. The dimensioning of this element was performed considering its maximum deformation that it's possible to achieve when the design torque is applied. This value was arbitrarily chosen, for a maximum deformation of $\theta_{def,max}=15°=\pi/12$ rad. Applying the design torque $T_d=55$ Nm follows that the torsional spring stiffness must be around $k_S=200$ Nm/rad.

Unfortunately, springs with similar a stiffness and a design suitable for this project are not available in the companies' catalogues. A custom designed spring is then needed to implement the spring in a real system. The torsional spring characteristic must be as linear as possible because its deformation will be measured in order to achieve the applied torque, transforming the torque control in a position (i.e. deformation) control.

This design part falls outside the thesis topic, then from now on the torsional spring will be considered as a virtual element clamped on the leg on one side, with a perfectly linear characteristic and a stiffness of 200 Nm/rad.

### 4.5.5 A Suitable Alternative Motor

Considering the operating modes of the exoskeleton it's easy to notice that most of the required operation are performed with the motor rotating at very low speeds, or even at null speed and high torque in stooping mode. This operating behavior, even if compatible with the brushless DC motor functioning, brings with it some issues for the motor itself. In fact, when working in stooping mode, the motor is required to provide a constant torque with the locked rotor: the so-called stall torque. In this situation the current flows always in the same coil of the brushless DC motor, producing an overheating due to Joule effect and, if prolonged in time, cause damages to the brushless motor windings.
It's then important proposing a suitable alternative for the electric motor element to avoid this problem. The most appropriate solution is the stepper motor, a discrete step-by-step motor widely used in robotics. The stepper motor is a synchronous motor working in pulsed direct current without brushes, controlled by a stepper motor drive, which rotation is divided in a finite number of steps depending on the number of teeth.
The stepper motor is a cheap, quiet, strong and very precise motor, perfect for working locked, with a null rotor velocity providing its holding torque without oscillations around the equilibrium position. The main disadvantages of these motors are their dimensions, bigger than the brushless DC motor ones, in addition to their jerk working behavior and their attitude to produce vibrations. These last issues are attenuated by the presence of the harmonic drive that, having a high transmission ratio, will transform the motor movement in a smooth and almost undisturbed movement, which can be considered as continuous. Furthermore, these motors have a low maximum speed, but for the project task they are not asked to rotate at high speeds. The real main trouble of the stepper motors is that, after only a few minutes of working, they produce a lot of heat. A system of thermal insulation must then be provided or, in alternative, a cooling system, to avoid undesired interactions with the user.
The chosen stepper motor is the Schneider Electric© Nema M-1719-1.5 [91], a two-phases stepper motor with a holding torque of $T_H$=0.53 Nm (*fig.62*), that will produce a harmonic drive output up to $T_{H,out}$=49 Nm, considering the harmonic drive efficiency. It has a total of 200 teeth and so a step angle of 1.8°. With the harmonic drive each step becomes equal to 0.015°, and it demonstrate that the movement may be considered as continuous without losing precision. This motor has a longitudinal dimension much more important than the previously considered brushless motor, being long 43 mm (*fig.61*), but this is an acceptable trade-off for the component properties.

The stepper motor torque behavior when the rotating speed rises is nonlinear, and it's depicted in *fig.63*.

**Motor types**

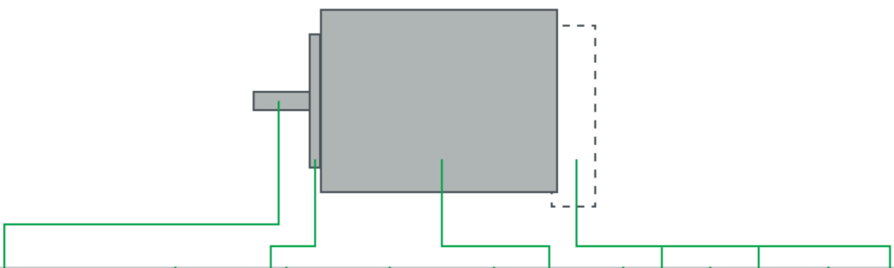

| Shaft version | | | Centering collar | | Flange size | | Lengths without shaft | | Winding | Motor connection | Optional rear shaft *(1)* | Optional encoder |
|---|---|---|---|---|---|---|---|---|---|---|---|---|
| **M-14•** | inches | mm | inches | mm | inches | mm | inches | mm | | | | |
| Round shaft with single flat feature | Ø 0.197 | Ø 5.0 | Ø 0.866 | Ø 22 | 1.39 | 35.3 | 1.02 | 26 | 2-phase full coil for bi-polar operation | 4 flying leads | Round shaft | Single-end or differential |
| **M-17•** | | | | | | | | | | | | |
| Round shaft with single flat feature | Ø 0.197 | Ø 5.0 | Ø 0.866 | Ø 22 | 1.67 | 42.3 | 1.34<br>1.57<br>1.89 | 34<br>40<br>48 | 2-phase full coil for bi-polar operation | 4 flying leads | Flat feature extending to rear end bell | Single-end or differential |
| **M-22•** | | | | | | | | | | | | |
| Round shaft with single flat feature | Ø 0.25 | Ø 6.35 | Ø 1.50 | Ø 38 | 2.22 | 56.4 | 1.77<br>2.13<br>2.99 | 45<br>54<br>76 | 2-phase full coil for bi-polar operation | 4 flying leads | Flat feature extending to rear end bell *(2)* | Single-end or differential |
| **M-34•** | | | | | | | | | | | | |
| Round shaft with single flat feature | Ø 0.554 | Ø 14.0 | Ø 2.874 | Ø 73 | 3.386 | 86.0 | 2.48<br>3.15<br>4.72 | 63<br>80<br>120 | 2-phase full coil for bi-polar operation | 4 flying leads | Flat feature on round shaft | Single-end or differential |

*(1) Optional rear shaft available except for NEMA23 2.4amp motors.*
*(2) Optional rear shaft on NEMA23 6.0amp motors is round without a flat feature.*

*Figure 61. Stepper Motor Dimensional Datasheet [91]*

| **NEMA17** | | **M-1713-1.5•** | **M-1715-1.5•** | **M-1719-1.5•** |
|---|---|---|---|---|
| **Stack length** | | single | double | triple |
| **Phase current** | **amps** | 1.5 | 1.5 | 1.5 |
| **Holding torque** | **oz-in** | 32 | 60 | 75 |
| | **N-cm** | 23 | 42 | 53 |
| **Rotor inertia** | **oz-in-sec²** | 0.000538 | 0.0008037 | 0.0011562 |
| | **kg-cm²** | 0.038 | 0.057 | 0.082 |
| **Phase inductance** | **mH** | 2.1 | 5.0 | 3.85 |
| **Phase resistance** | **Ω** | 1.3 | 2.1 | 2.0 |
| **Weight** | oz | 7.4 | 8.1 | 12.7 |
| | grams | 210 | 230 | 360 |

*Figure 62. Stepper Motor Mechanical and Electrical Datasheet [91]*

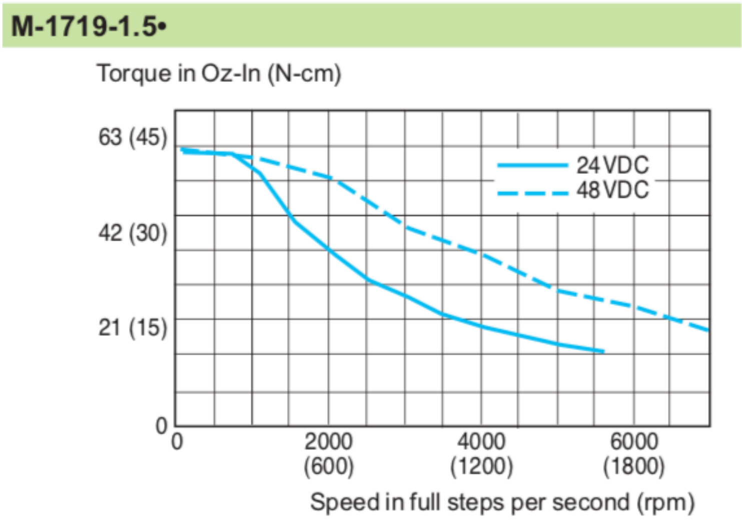


*Figure 63. Stepper Motor Torque Characteristic [91]*

# Chapter 5

# "Passive Mode" Analysis

## 5.1 Kinematics Introduction

In this chapter the kinematic behavior of the four-bar linkage will be studied. Particular attention will be paid when the wearable robot is working in the previously defined "free mode", with the clutch is disengaged and the leg motion is decoupled by the trunk motion, when performing the gait cycle. It means that the only input provided to the hip joint system is the angular velocity imposed by the leg. The trunk was considered always vertical, for simplicity.

To perform the study, it is then necessary to hypothesize a suitable angular speed of the leg when walking. The hip angular speed $\omega$ will be considered as the first derivative of the leg angle $\beta$ in *fig.31* and it will be obtained through the knowledge of the human walking speed.

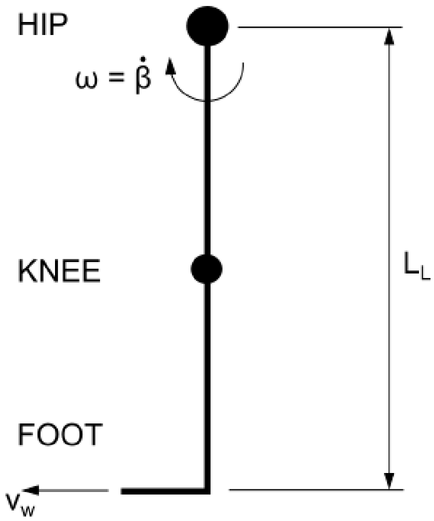


*Figure 64. Leg Kinematic Model*

Considering now both a comfortable and a maximum walking speed [92], equal to $v_{w,com} = 1.389\, {}^{m}/_{s} \simeq 5\ {}^{km}/_{h}$ and $v_{w,max} = 2.5\, {}^{m}/_{s} \simeq 9\ {}^{km}/_{h}$ respectively, for simplicity it's possible to think the walking speed as the tangential speed of the foot due to a rotational speed on the hip applied to the straight leg. For this calculation will not be considered the 99 percentile Italian man, but the average Italian man to which the walking speed data are referred. The average Italian man height is $H_{avg}$=1.75 m. From this data, and from the partial body segment coefficients reported in *fig.33* it's possible to achieve the average leg length, which is $L_{L,avg} = 0.53 \cdot H_{avg} = 0.93\ m$.

The reference hip angular speed is then easily defined as follows:

$$\omega = \dot{\beta} = \frac{v_w}{L_{L,avg}} \tag{14}$$

The comfortable and maximum hip angular speed within the gait cycle results to be, approximatively:

$\omega_{com} \simeq 1.5\ {}^{rad}/_{s}$

$\omega_{max} \simeq 2.7\ {}^{rad}/_{s}$

## 5.2 Four-Bar Linkage Kinematic Analysis

A kinematic analysis of the four-bar linkage can now be performed, giving as only input the hip angular speed ω associated to the leg motion within the gait cycle. A simplified stick model of the four-bar linkage designed in the previous chapters is reported in fig.65.

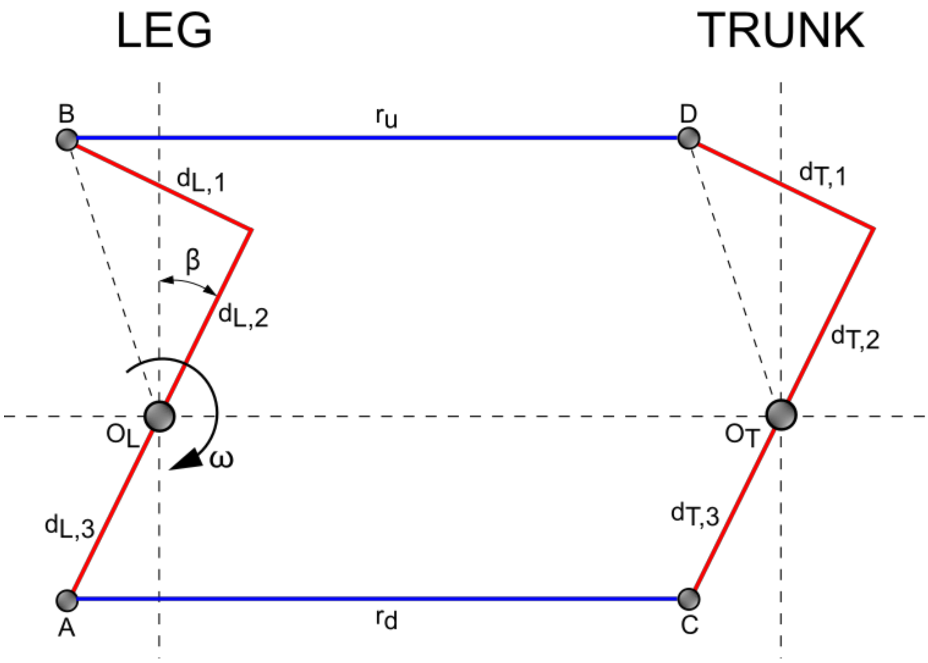


*Figure 65. Four-Bar Linkage Kinematic Model*

The considered model represents the left sided actuation unit of the exoskeleton; the right sided one is analogous but symmetric with the vertical axis. There are four elements in the system: the leg crank (associated to the actuation unit shaft containing the torsional spring and the thigh joint), the upper rod, the trunk crank (associated to the actuation unit shaft containing the motor, the clutch and the harmonic drive) and the lower rod, each one of them considered as a rigid body.

Some realistic assumptions are made about the four-bar linkage from a constructive point of view:

$\overline{O_L O_T}$ horizontal while walking

$r_u = r_d \doteq r$

$r_u = r_d \doteq r$

$d_{L,1} = d_{T,1} \doteq d_1$

$d_{L,2} = d_{T,2} \doteq d_2$

$d_{L,3} = d_{T,3} \doteq d_3$

$d_1 \perp d_2$

It follows that:

$\overline{O_L B} = \overline{O_T D} = \sqrt{{d_1}^2 + {d_2}^2}$

On the base of the previous constructive assumptions it's possible to update the previous scheme with a new simplified one, by changing the nomenclature.

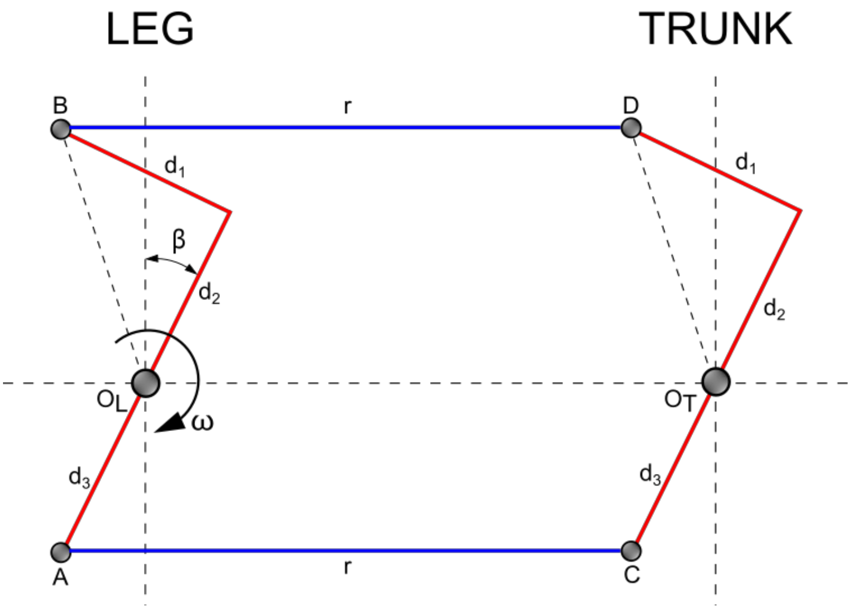


*Figure 66. Updated Four-Bar Linkage Kinematic Model*

As it's easy to see from the previous picture (*fig.66*), the input speed ω (known) is applied on the central rotational joint of the leg crank. For studying the kinematics it's necessary to isolate the leg crank element from the other ones.

By knowing the input angular speed and being conscious that the point $O_L$ is the instantaneous center of rotation (ICR) of each point of the leg crank, it's possible to determine the speed of the extremity points A and B, in which the rotational joint connecting the leg crank to the lower and upper rod respectively lie.

$$v_A = \omega \cdot d_3 \tag{15}$$

$$v_B = \omega \cdot \sqrt{{d_1}^2 + {d_2}^2} \tag{16}$$

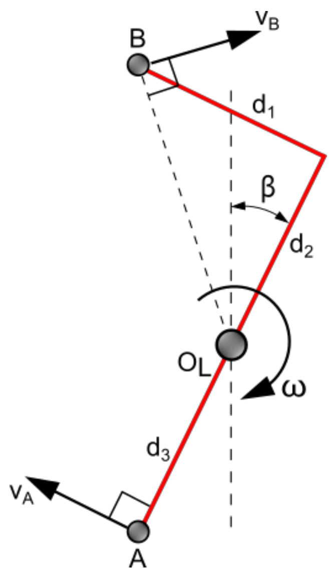


*Figure 67. Leg Crank Kinematic Model*

Being both A and B rotational joints, the speeds of the leg crank in these points will always be the very same of lower and upper rod in these same two points.
It's then possible to analyze the upper rod kinematics, starting from the already known speed $v_B$.

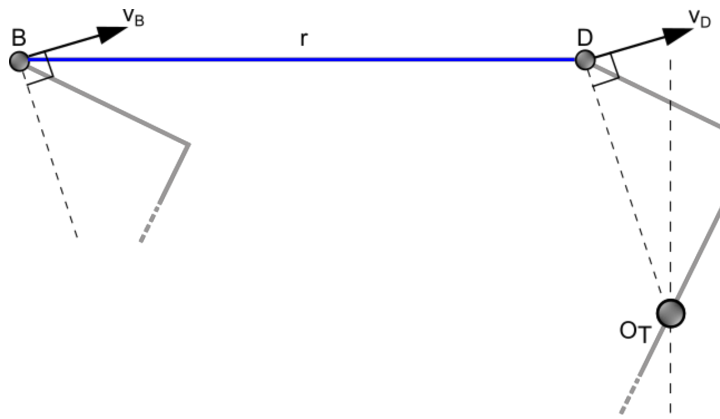


*Figure 68. Upper Rod Kinematic Model*

By means of the Galileo's theorem, it's possible to state that the speed of the point D is:

$$v_D = v_B + v_{D/B} \tag{17}$$

The speed $v_B$ is known in module and direction. The direction of $v_D$ is also known, being perpendicular with the segment $\overline{O_T D}$, as well as the direction of $v_{D/B}$ that is normal with the

rod $\overline{BD}$. But $\overline{O_T D}$ is equal to $\overline{O_L B}$ and it follows that $v_D$ is parallel with $v_B$. This means that $v_{D/B}$ is null and then, when walking, $v_D$ is equal to $v_B$ in module and direction.
This allows to assure that, while the crank motion is a pure rotation motion, the rod motion is a pure translation motion.

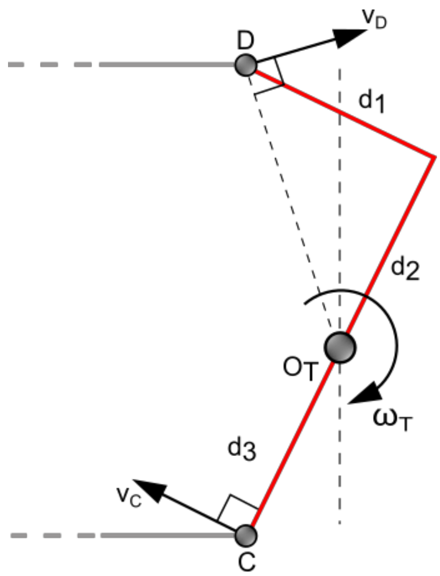


*Figure 69. Trunk Crank Kinematic Model*

The lower rod kinematic analysis is the very same of the upper one, with $v_C$ equal to $v_A$. Having $v_D$ is now possible to study the trunk crank kinematics: from this, it's easy to achieve the trunk crank rotation speed. As it was easy to suppose, the trunk crank rotation speed $\omega_T$ is equal to the leg crank one.

## 5.3 Ultimate Version of the Four-Bar Linkage

The main disadvantage of the previously studied four-bar linkage is that, when β is equal to 90° and a torque is applied to one of the two cranks, the points A and C are not capable to transmit power, but only the points B and D can. This trouble is similar to what happens in the crankshaft systems at the top/bottom dead center. A modification was applied to the four-bar linkage, transforming the "reversed L shape" of the cranks in a "Z shape" (*fig.70*). This allows to transmit torque for any β compatible with the range of motion of the four-bar linkage, decreasing the risk of damaging the cranks for an undesired overload.

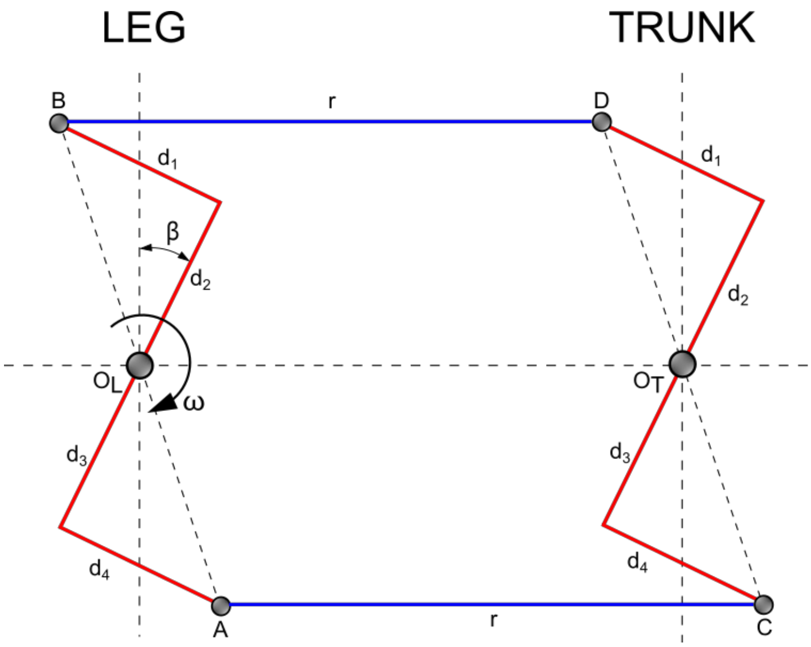


*Figure 70. Ultimate Four-Bar Linkage Kinematic Model*

The ultimate version of the four-bar linkage is pretty similar to the first one, with the addition of a lower arm in both cranks. Analyzing the kinematics of the leg crank (*fig.71*) the velocities of the points A and B can be easily obtained similarly to the previous case, assuming ω known. It's possible to notice that, if $d_1=d_4$ and $d_2=d_3$, then $\overline{O_L B} = \overline{O_L A} = s$ and then the velocities in the points A and B becomes:

$$v_A = -v_B = \omega \cdot s \tag{18}$$

Indeed, by the previous assumptions, the velocities of A and B are equal in module and opposite in directions.

The kinematics of the other elements of the four-bar linkage is absolutely comparable with the one of the first case, and it's easily verifiable that $v_D=v_B$, $v_C=v_A$ and $\omega_T=\omega$.

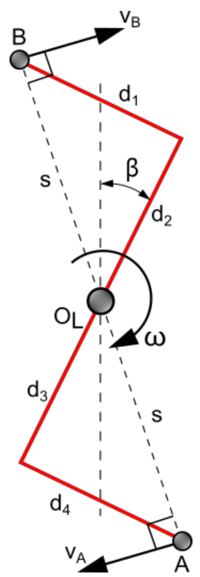


*Figure 71. Ultimate Leg Crank Kinematic Model*

A new 3D model of the four-bar linkage (*fig.72*) was designed in SolidWorks©, in the light of the last considerations and taking into account the radial encumbrance of the actual elements chosen for the system. Triangular shapes were used in the cranks to increase the stiffness of the sub-system, with holes in each component useful to decrease the weight. The thickness is small, and each element is shaped considering both the other components dimension and the desired range of motion, with a geometry created imagining a foundry production process.

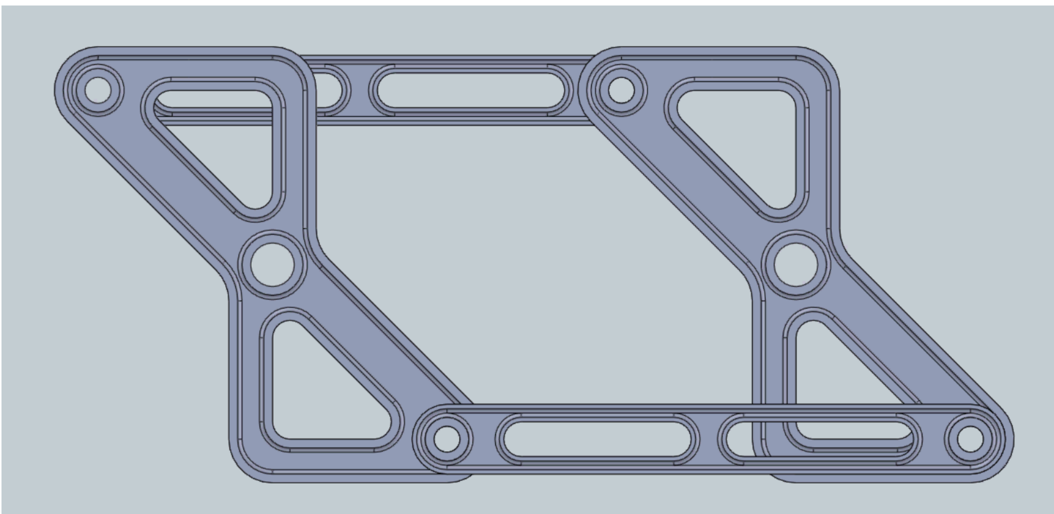

*Figure 72. Ultimate 3D Model of the Four-Bar Linkage*

The designed four-bar linkage can perform cranks rotations in a range of motion between -30° (maximum extension) and 120° (maximum flexion), obtained from the geometry of the system rotating the cranks until having interference with the shafts. These values are higher than the values normally reached by human body, following the ideal of "transparent exoskeleton" followed from the very beginning. Indeed, the maximum ROM when walking is around [-15÷35] and the maximum angle that it's possible to reach when bending forward with the vertical legs is less than 90°. Nevertheless, these values are not reachable simultaneously: these results must be evaluated considering the leg crank fixed with the leg and the trunk perpendicular with the rods.

## 5.4 Kinematic Simulations of the Gait Cycle

Having a suitable 3D model, it's been possible to simulate the four-bar linkage behavior imposing as only input a velocity to the leg crank, equal to the angular velocity of the hip during the gait cycle.
A first simulation was performed in SolidWorks itself using the SolidWorks Motion© tool. An eight seconds long cycle was developed (*fig.73*), with the purpose of simulating a brief gait cycle. This cycle may be considered as divided into two part: a first part in which the peak velocities of the input are comparable with the comfortable walking speed, and a second part related to the maximum walking velocity. The trends of position, speed, acceleration and jerk of the leg crank were plotted, and the output video confirmed what was found in the previous kinematic analysis.

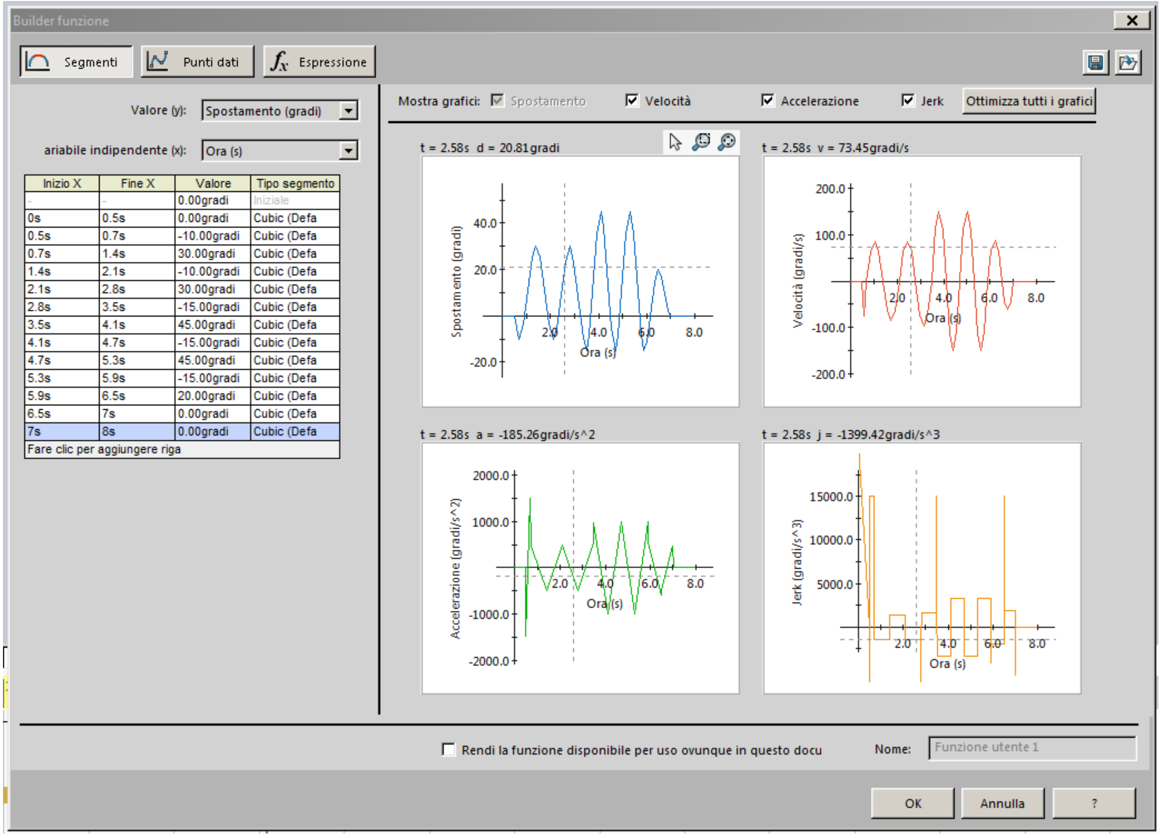


| Inizio X | Fine X | Valore | Tipo segmento |
|---|---|---|---|
| - | | 0.00gradi | Iniziale |
| 0s | 0.5s | 0.00gradi | Cubic (Defa |
| 0.5s | 0.7s | -10.00gradi | Cubic (Defa |
| 0.7s | 1.4s | 30.00gradi | Cubic (Defa |
| 1.4s | 2.1s | -10.00gradi | Cubic (Defa |
| 2.1s | 2.8s | 30.00gradi | Cubic (Defa |
| 2.8s | 3.5s | -15.00gradi | Cubic (Defa |
| 3.5s | 4.1s | 45.00gradi | Cubic (Defa |
| 4.1s | 4.7s | -15.00gradi | Cubic (Defa |
| 4.7s | 5.3s | 45.00gradi | Cubic (Defa |
| 5.3s | 5.9s | -15.00gradi | Cubic (Defa |
| 5.9s | 6.5s | 20.00gradi | Cubic (Defa |
| 6.5s | 7s | 0.00gradi | Cubic (Defa |
| 7s | 8s | 0.00gradi | Cubic (Defa |

*Figure 73. Kinematic Simulation in SolidWorks Motion*

A second simulation was performed in MATLAB© Simulink. By means of the Simscape Multibody toolbox was possible to import the four solid body elements composing the four-bar linkage in .STEP file format. For each element was imposed the density, supposing the four-bar linkage made of steel, in order to have realistic mass and inertia values, automatically calculated from the geometry by the software. A reference frame was created in correspondence of each rotational joint connection hole, with the z-axis along the cylindric surface. The four elements were connected by using “rotational joints” blocks and “reference frame transformation” blocks, to couple them as designed, avoiding interferences. For the kinematic simulation the line crossing the central rotational joints of the two cranks lies on a horizontal plane, supposing the trunk always vertical. Both cranks are anyway free to rotate, dragging the rods with them. Simulink/Simscape signal converters (and vice versa) were used to let the two environments communicate.

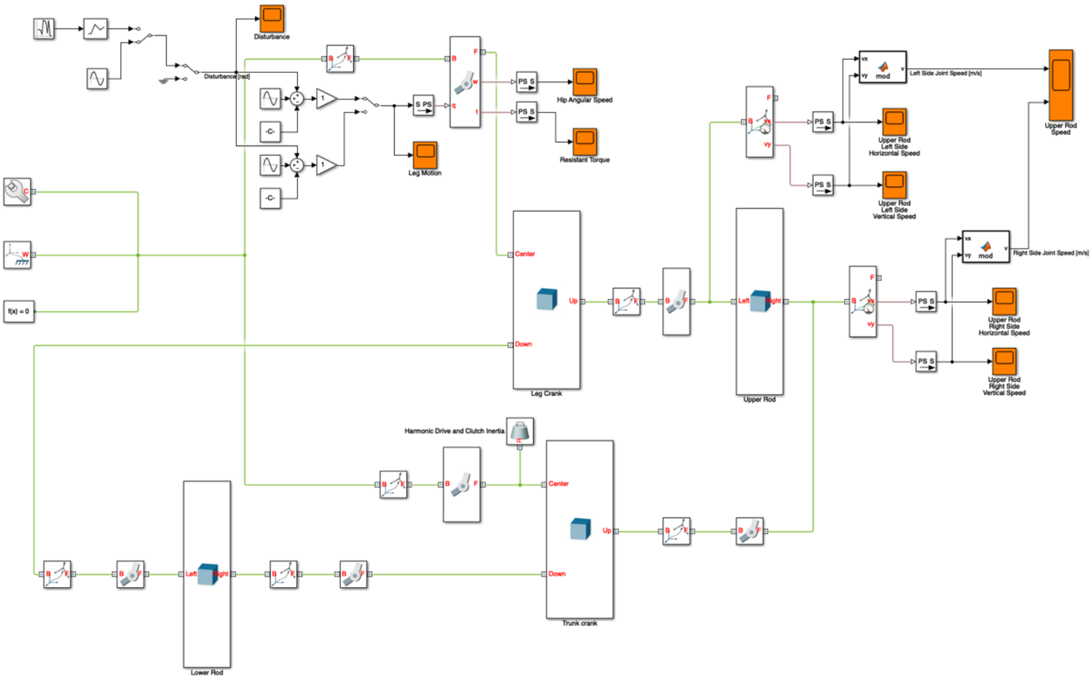


*Figure 74. Simulink/Simscape Kinematic Model*

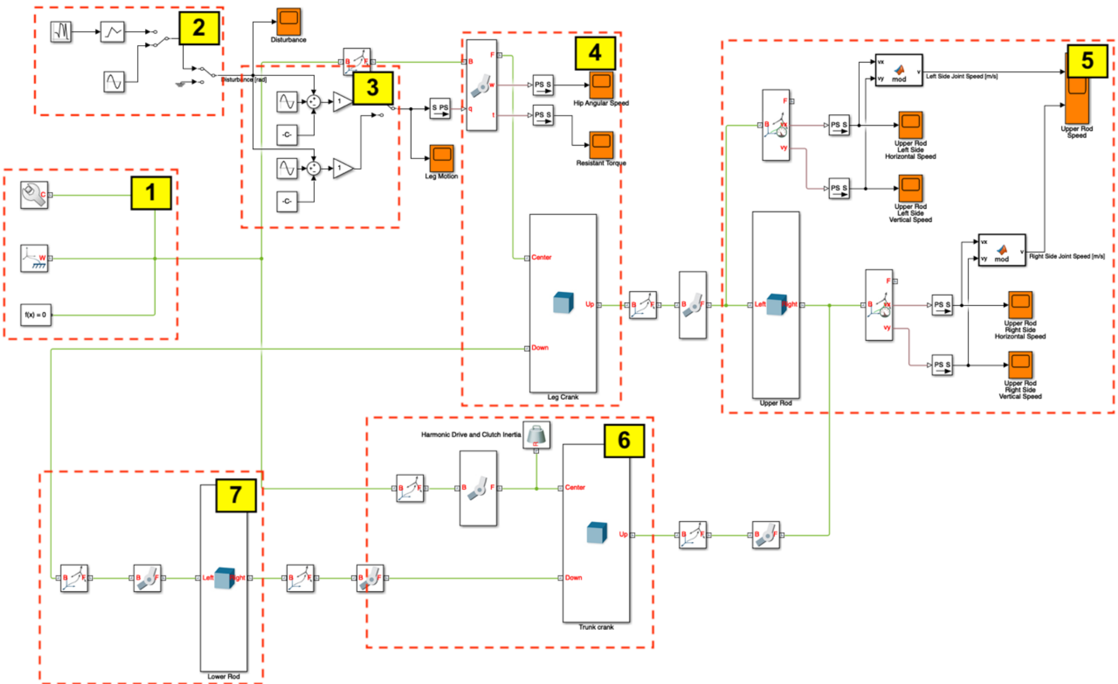


*Figure 75. Simulink/Simscape Kinematic Model with Enumeration*

Analyzing the model in *fig.75* it's possible to see that in the highlighted section 1 it's located the world reference frame and the configuration solver, necessary blocks to make the Simscape model working properly. In the section 2 the input disturbance is located; both sinusoidal and random disturbances were tested, to simulate vibrations while walking due to the muscular activity, a disconnected ground or other types of uncertainties. The section 3 contains the walking angular input, realized by a sinusoidal signal, considering both the maximum flexion/extension performed within the gait cycle and the frequency of the steps, for a comfortable and maximum walking speed. The section 4 includes the leg crank, which central joint is connected with a rotational joint block to the world frame, whereas the other joints are connected to upper and lower rods. Speed and torque sensors were located in the central joint of the crank to have a feedback of its behavior during walking. The section 5 includes the upper rod, connected to both cranks with rotational joints. In each rotational joint of this element were put sensors for both vertical and horizontal speed. The sensed values are the input of a block that returns the module. The absolute speeds of the joints were then compared to understand if the motion of the rod is truly a pure translation motion. The section 6 incorporates the trunk crank, connected to the world reference frame, and also the inertia of the rotating parts connected to the trunk crank, that are the harmonic drive and one of the two main subsystems of the clutch. Nevertheless, due to the HD, the clutch rotates faster than the input, then its inertia was multiplicated by the square of the transmission ratio $i$, for a reason that will be discussed in the next chapter. The last highlighted section, the 7$^{th}$ one, represents the lower rod.

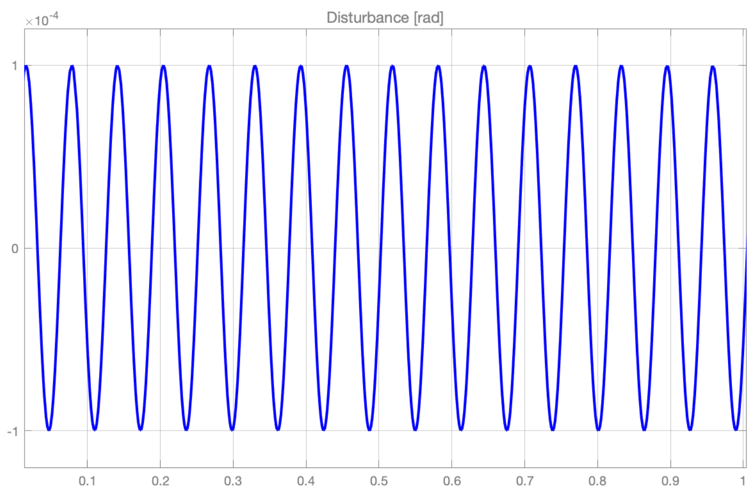


*Figure 76. Kinematic Simulation - Input Disturbance as a Function of Time [s]*

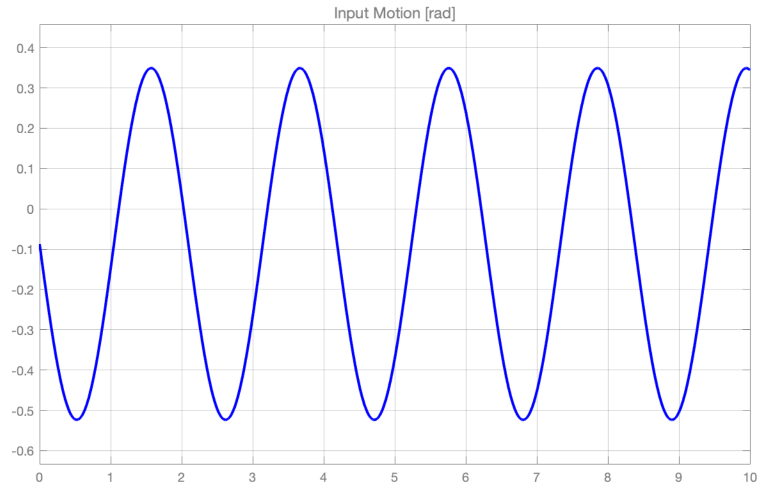


*Figure 77. Kinematic Simulation - Input Motion as a Function of Time [s]*

Taking into account a sinusoidal disturbance (*fig.76*), added to a comfortable walking speed input (*fig.77*), the sensed outputs are given in the following pictures.

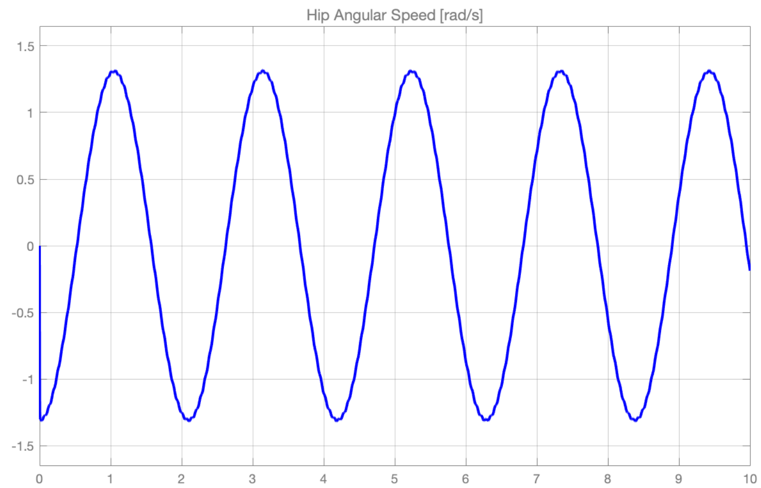


*Figure 78. Kinematic Simulation - Hip Angular Speed as a Function of Time [s]*

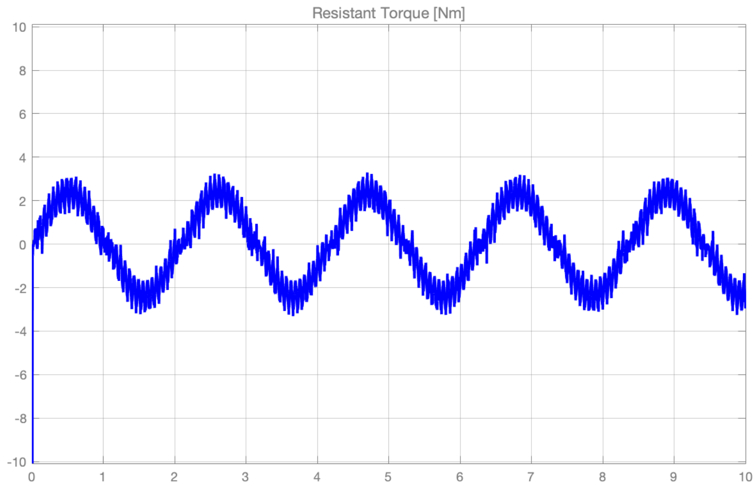


*Figure 79. Kinematic Simulation - Hip Resistant Torque as a Function of Time [s]*

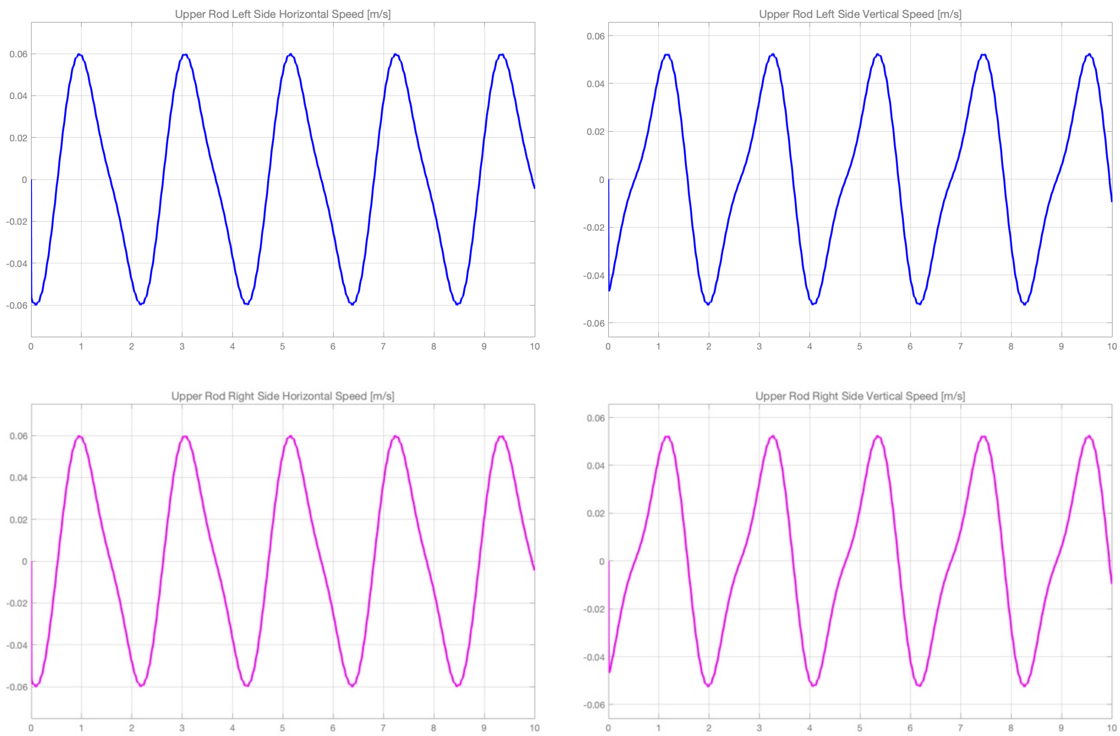


*Figure 80. Kinematic Simulation - Upper Rod Velocities as a Function of Time [s]*

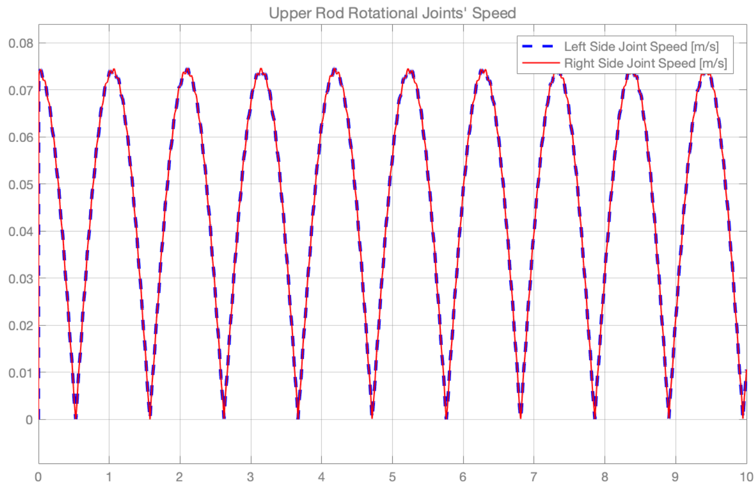


*Figure 81. Kinematic Simulation - Upper Rod Absolute Velocities as a Function of Time [s]*

A small torque (*fig.79*) with peaks of 3 Nm for each leg opposes resistance to the gait cycle, due to the inertia of the clutch, of the harmonic drive and of the four-bar linkage. This is a small interference with the gait cycle, considering the high hip torque produced by the human beings while walking. The actual resistant torque will be higher, because different elements were not considered, such as the spring, the shaft and the links, each one of them having its own inertia, to be added to the friction losses, also neglected. From *fig.80* and *fig.81* it's possible to notice that, as it was predicted, the rod motion is a pure translation while walking, demonstrated by the fact that the speed of left and right side of the rod are identical.

# Chapter 6

# "Active Modes" Analysis and Control

## 6.1 Dynamics Introduction

In this chapter a study of the dynamics of the system was performed, considering the clutch engaged and so the torque transmission from the actuation unit allowed. For making this, the legs were considered always parallel as fixed rigid bodies, with the torsional spring directly clamped at one end to them. The leg crank is then fixed, with the rods free to rotate when a torque is applied to the trunk crank by the actuation unit. The study was firstly developed from an analytical point of view, and then different simulations was performed on Simulink. However, to obtain reasonable results, a suitable control system was created, to impose the desired behavior to the whole system. A two-levels control system was designed: the high-level control system gives the optimal torque to provide to the joint to achieve the desired position with the desired speed and acceleration; the low-level control system performs the control of the electric motor.

### 6.1.1 Body Inertia Calculation

A better knowledge of the load is required for studying the system. As it's already known, the load in this case is a human being. The upper body of the user will be modeled representing it as a moment of inertia rotating around the hip joint. The upper body inertia will then be calculated for a 99 percentile Italian man reference subject, reference subject of the project, with a procedure comparable to the one in [93].
The head, neck, torso and arms will be represented as sticks in a free body diagram and will be considered all lying on the same plane. The only motion contemplated will be the one in the sagittal plane.
For each segment is calculated the partial length and partial mass of the segment itself by means of the coefficients found in [80], starting from the already found total mass M=103 kg and total height H=1.883 m of the considered reference subject.

$L_{hn} = H \cdot (1 - 0.818) = 0.343\ m$ Head and neck length

$L_t = H \cdot (0.818 - 0.530) = 0.542\ m$ Torso length

$L_{ua} = H \cdot (0.186) = 0.350\ m$ Upper arm length

$L_{la} = H \cdot (0.146) = 0.275\ m$ Lower arm length

$L_h = H \cdot (0.108) = 0.203\ m$ Hand length

$m_{hn} = M \cdot (0.081) = 8.343\ kg$ Head and neck mass

$m_t = M \cdot (0.497) = 51.191\ kg$ Torso mass

$m_{ua} = M \cdot (0.028) = 2.884\ kg$ Upper arm mass

$m_{la} = M \cdot (0.016) = 1.648\ kg$ Lower arm mass

$m_h = M \cdot (0.006) = 0.618\ kg$ Hand mass

For the calculation of the moment of inertia it's necessary the radius of gyration of each body segment. The radii of gyration are found by means of the coefficients in *fig.82* according to the sagittal axis, that have to be multiplied by the length of each segment.

| Segment | Radius of gyration according to the axis | | |
|---|---|---|---|
| | Sagittal | Frontal | Longitudinal |
| Head & Neck | 30.3 | 31.5 | 26.1 |
| Torso | 48.2 | 38.3 | 46.8 |
| Upper arm | 32.8 | 31.0 | 18.2 |
| Lower arm | 29.5 | 28.4 | 13.0 |
| Hand | 28.5 | 23.3 | 18.2 |
| Thigh | 26.7 | 26.7 | 12.1 |
| Calf | 28.1 | 27.5 | 11.4 |
| Foot | 25.7 | 24.5 | 12.4 |

*Figure 82. Radii of Gyration Coefficients [93]*

$k_{hn} = L_{hn} \cdot (0.303) = 0.1038\, m$ Head and neck radius of gyration

$k_t = L_t \cdot (0.482) = 0.2614\, m$ Torso radius of gyration

$k_{ua} = L_{ua} \cdot (0.328) = 0.1149\, m$ Upper arm radius of gyration

$k_{la} = L_{la} \cdot (0.295) = 0.0811\, m$ Lower arm radius of gyration

$k_h = L_h \cdot (0.285) = 0.0580\, m$ Hand radius of gyration

After doing this, it's possible to determine the moment of inertia of each body segment in its own center of gravity.

$J_{hn,CoG} = m_{hn} \cdot k_{hn}{}^2 = 0.090\ kg \cdot m^2$ Head and neck MOI in its own CoG

$J_{t,CoG} = m_t \cdot k_t{}^2 = 3.498\ kg \cdot m^2$ Torso MOI in its own CoG

$J_{ua,CoG} = m_{ua} \cdot k_{ua}{}^2 = 0.038\ kg \cdot m^2$ Upper arm MOI in its own CoG

$J_{la,CoG} = m_{la} \cdot k_{la}{}^2 = 0.011\ kg \cdot m^2$ Lower arm MOI in its own CoG

$J_{h,CoG} = m_h \cdot k_h{}^2 = 0.002\ kg \cdot m^2$ Hand MOI in its own CoG

It's now necessary to determine the MOI of each segment with respect to the hip axis. For making this, it's firstly essential to know the exact location of the CoG of each segment. The location of the segments' center of gravity with respect to their proximal end were found with the Hall investigator coefficients in *fig.83*. By having each precise location, it's possible to determine the offset of each segment with respect to the hip joint axis from the human body geometry.

| Segment | Investigators | |
|---|---|---|
| | Dempster | Hall |
| **Head & Neck** | 43.3 | 56.7 |
| **Torso** | 49.5 | 56.2 |
| **Upper arm** | 43.6 | 43.6 |
| **Lower arm** | 43.0 | 43.0 |
| **Hand** | 49.4 | 46.8 |
| **Thigh** | 43.3 | 43.3 |
| **Calf** | 43.3 | 43.4 |
| **Foot** | 42.9 | 50.0 |

*Figure 83. Center of Gravity Location Coefficients [93]*

$d_{hn} = L_{hn} \cdot (0.567) = 0.194\, m$ Head and neck CoG location

$d_t = L_t \cdot (0.562) = 0.305\, m$ Torso CoG location

$d_{ua} = L_{ua} \cdot (0.436) = 0.153\, m$ Upper arm CoG location

$d_{la} = L_{la} \cdot (0.430) = 0.118\, m$ Lower arm CoG location

$d_h = L_h \cdot (0.468) = 0.095\, m$ Hand CoG location

$r_{hn} = d_{hn} + L_t = 0.737\, m$ Head and neck CoG offset

$r_t = d_t = 0.305\, m$ Torso CoG offset

$r_{ua} = L_t - d_{ua} = 0.390\, m$ Upper arm CoG offset

$r_{la} = L_t - L_{ua} - d_{la} = 0.074\, m$ Lower arm CoG offset

$r_h = L_t - L_{ua} - L_{la} - d_h = -0.178\, m$ Hand CoG offset

It's now possible to apply the Huygens-Steiner theorem, also known as the parallel axis theorem, to determine the moment of inertia of each segment in the sagittal plane around the hip joint axis.

$J_{hn} = J_{hn,CoG} + m_{hn} \cdot {r_{hn}}^2 = 4.617\, kg \cdot m^2$ Head and neck MOI in hip axis

$J_t = J_{t,CoG} + m_t \cdot {r_t}^2 = 8.253\, kg \cdot m^2$ Torso MOI in hip axis

$J_{ua} = J_{ua,CoG} + m_{ua} \cdot {r_{ua}}^2 = 0.476\, kg \cdot m^2$ Upper arm MOI in hip axis

$J_{la} = J_{la,CoG} + m_{la} \cdot {r_{la}}^2 = 0.020\, kg \cdot m^2$ Lower arm MOI in hip axis

$J_h = J_{h,CoG} + m_h \cdot {r_h}^2 = 0.022\, kg \cdot m^2$ Hand MOI in hip axis

The upper body moment of inertia can be now easily found as the sum of the moments of inertia of each body segment.

$$J_{HIP} = J_{hn} + J_t + 2 \cdot (J_{ua} + J_{la} + J_h) = 13.904\ kg \cdot m^2 \tag{19}$$

### 6.1.2 Dynamic Model

The system can be represented with a simplified model, but some assumptions have to be made: the internal losses inside the components were not considered, modeling each element as an ideal element, the friction between the components was neglected, the damping effect was not considered, due to the impossibility to estimate it, and also the inertia of the shafts and of the exoskeleton links were neglected. Even with these simplifications it's possible to write a dynamic equation of the system that returns the behavior of the system broadly.

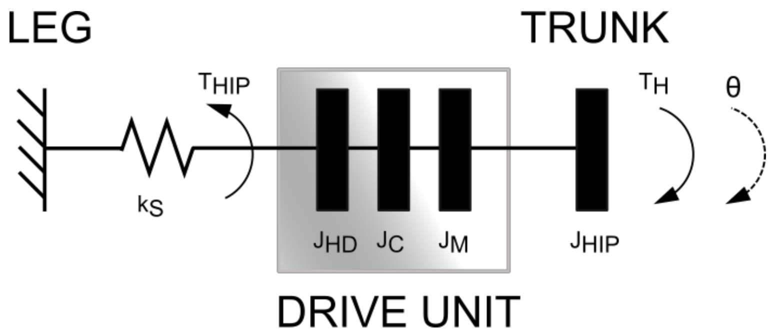


*Figure 84. Dynamic Simplified Model of the System*

The torsional spring was considered clamped at one end to the fixed leg, and its torsional stiffness was considered known, even if the actual custom spring is not available yet. The inertia of the harmonic drive $J_{HD}$, the inertia of the clutch $J_C$ and the inertia of the electric motor $J_M$ are known from the datasheets, whereas the inertia of the human upper body was determined in the previous paragraph. The torques applied to the system are the actuation torque $T_{HIP}$, provided by the drive unit, and the resistant torque $T_H$ due to the weight of the human upper body and depending on the torso angle θ.

The system dynamic equation can be found through the Lagrange formulation so, firstly, it's necessary to write the kinetic and potential energy of the evaluated system. The kinetic energy $\mathcal{T}$ of the system is:

$$\mathcal{T} = \frac{1}{2} \cdot J_{HIP} \cdot \dot{\vartheta}^2 + \frac{1}{2} \cdot J_M \cdot {\omega_M}^2 + \frac{1}{2} \cdot J_C \cdot {\omega_M}^2 + \frac{1}{2} \cdot J_{HD} \cdot \dot{\vartheta}^2 \tag{20}$$

Where $\omega_M$ is the speed of the motor. At a first look one could think that there are two different state variables, $\theta$ and $\omega_M$, and this is a 2-DoF system. Actually, one is dependent from the other one by means of the harmonic drive and its transmission ratio $i$, and this is a single DoF system.

$$\omega_M = i \cdot \dot{\vartheta} \tag{21}$$

The corrected kinetic energy of the system is:

$$\mathcal{T} = \frac{1}{2} \cdot J_{HIP} \cdot \dot{\vartheta}^2 + \frac{1}{2} \cdot J_M \cdot i^2 \cdot \dot{\vartheta}^2 + \frac{1}{2} \cdot J_C \cdot i^2 \cdot \dot{\vartheta}^2 + \frac{1}{2} \cdot J_{HD} \cdot \dot{\vartheta}^2 \tag{22}$$

It's possible to write the kinetic energy expression as:

$$\mathcal{T} = \frac{1}{2} \cdot J_{TOT} \cdot \dot{\vartheta}^2 \tag{23}$$

With

$$J_{TOT} = J_{HIP} + J_{HD} + i^2 \cdot (J_M + J_C) \tag{24}$$

The potential energy $\mathcal{U}$ is expressed by:

$$\mathcal{U} = \frac{1}{2} \cdot k_S \cdot \vartheta^2 \tag{25}$$

Actually, the spring deformation corresponds to the difference between the angle upstream the spring (harmonic drive side) and the angle downstream the spring (leg side), but being

the leg assumed as fixed then the whole output angle of the drive unit corresponds to the deformation of the spring itself.
The Euler-Lagrange equation [94] can now be applied. Its formulation follows.

$$\frac{d}{dt}\left(\frac{\partial \mathcal{L}}{\partial \dot{\vartheta}}\right) - \frac{\partial \mathcal{L}}{\partial \vartheta} + \frac{\partial \mathcal{D}}{\partial \dot{\vartheta}} = \mathcal{F}_i \tag{26}$$

Where $\mathcal{F}_i$ are the generalized forces, in this case the external torques, and $\mathcal{D}$ is the dissipative energy, here neglected. The Lagrangian $\mathcal{L}$ is defined as a function of the generalized coordinates:

$$\mathcal{L} = \mathcal{T} - \mathcal{U} \tag{27}$$

Developing the needed derivatives, the dynamic equation of the system results to be:

$$J_{TOT} \cdot \ddot{\vartheta} + k_S \cdot \vartheta = T_{HIP} - T_H \tag{28}$$

## 6.2 Dynamic Control

Starting from the Simulink kinematic model in *fig.74*, a modified model was created in order to study the behavior of the system when the exoskeleton is working in stooping or bending mode. As it was assumed in the analytical analysis, the legs were considered as fixed, with their position that will remain stable for all the duration of the simulation.
Two types of control systems were created. A high-level control system, equivalent to the outer loop, which controls the plant composed by the four-bar linkage and the human, giving as output the desired torque to provide to the hip joint, in order to achieve the desired trunk motion. The input of the system are the initial condition of the leg and the initial condition of the trunk, for any aim that the exoskeleton must accomplish, both uprising and stooping. For now, the “bending mode” only will be considered, with the aim to bring the upper body of the user in vertical position. Any other case is always attributable to these ones, with a suitable manipulation of the inputs. A low-level control system, equivalent to the inner loop, was developed to control the electric motor, performing a torque control which becomes a position control, thanks to the series elastic actuator system.

A suitable sensorization system must be developed both for the high-level control and for the low-level control. To properly make working the high-level control system, different angles have to be detected time-by-time. In *fig.85* it's shown a suitable sensorization system.

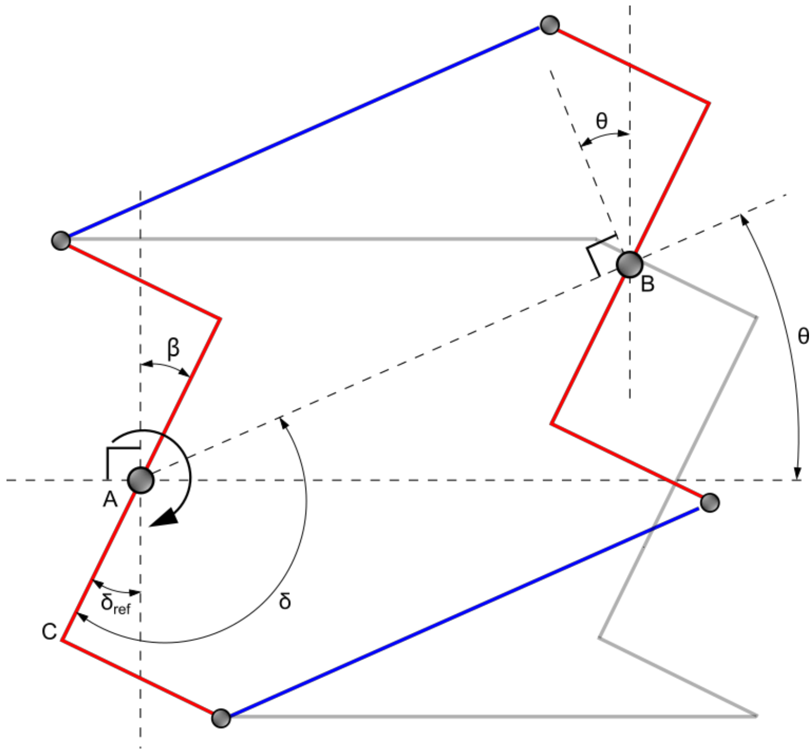


*Figure 85. High-Level Control System Sensorization*

The angle θ, equivalent to the inclination of the trunk is detected only when the control starts. This is made because the angle θ is detected by an accelerometer, located as close as possible to the point in which the upper body reaction forces are applied. Indeed, when a torque is provided the trunk starts moving, causing a loss of precision in the angle detection and then in the feedback, which may bring the system to instability. This is why the initial trunk displacement $\theta_0$ only is detected by the accelerometer.

The angle δ is detected time-by-time by an encoder/potentiometer. Its initial position $\delta_0$ is acquired and used to achieve the leg initial position $\delta_{ref}$.

$$\delta_{ref} = \delta_0 - {}^{\pi}/_{2} - \vartheta_0 \tag{29}$$

The model was built to take this value as reference to bring the trunk in vertical position.

When the system starts working, providing a torque, the hip joint starts rotating, and δ varies as a function of time. From this, it's possible to achieve the angle θ as a function of time, which represents the high-level control feedback.

$$\vartheta(t) = \delta(t) - \pi/_2 - \delta_{ref} = \delta(t) - \delta_0 + \vartheta_0 \qquad (30)$$

What just said it's valid for the bending mode, when the aim is to bring the trunk in vertical position. If the target is to bring the trunk in any other final position, equal to a generic angle γ to the vertical axis, the generalized reference has to be modified adding this angle as follows:

$$\delta_{ref,gen} = \delta_{ref} + \gamma \qquad (31)$$

As it's easy to deduce, the reference angle in stooping mode, when the aim is to maintain the initial position, becomes:

$$\delta_{ref,stooping} = \delta_0 - \pi/_2 \qquad (29)$$

Because $\gamma = \vartheta_0$.

## 6.3 High-Level Control System

The high-level model was designed in order to determine the ideal desired torque to provide time-by-time. It was modeled starting from the kinematic model, changing the revolute joint relationship with the world reference, creating subsystems to increase the clarity of the model and adding the needed elements. It is highlighted in *fig.86* and *fig.87*.

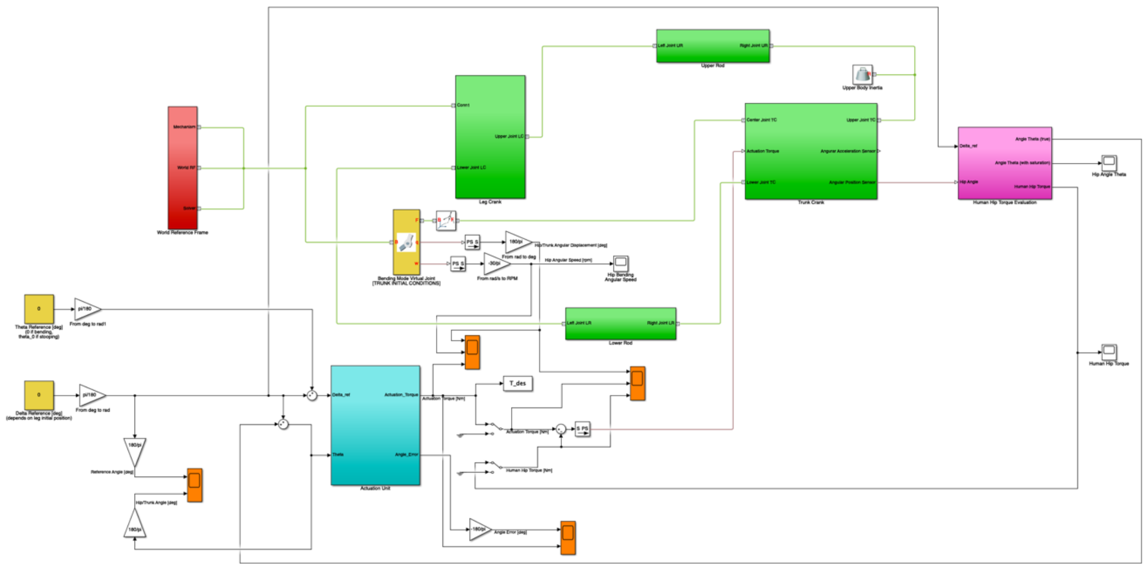

*Figure 86. Simulink/Simscape Dynamic Model*

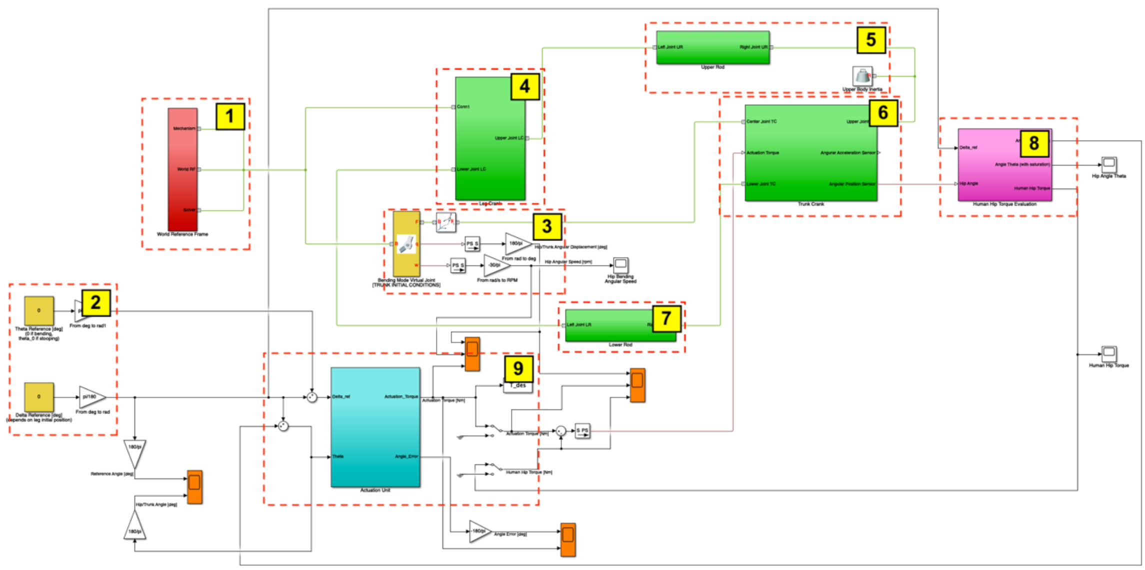


*Figure 87. Simulink/Simscape Dynamic Model with Enumeration*

The green subsystems represent the solid bodies, components of the four-bar linkage, the magenta block is the human action, which provides a resistant hip torque depending on the angle θ, the blue one is the actuation unit, with the scopes of interest highlighted in orange color and, lastly, the yellow block represents both the reference and the initial conditions. As in the previous case, in the highlighted section 1 is present the world reference frame with the configuration solver. The two yellow blocks in section 2 are the initial angle of the leg $\delta_{ref}$ and the reference trunk angle $\theta_{ref}$, which is 0 if the "bending mode" is selected or equal to the initial trunk angle $\theta_0$ if the "stooping mode" is selected. In the highlighted section 3 it's located a revolute joint, which may be considered as a "virtual joint" necessary for the plant building, which imposes to the trunk crank to rotate around the leg crank, fixed. Within this block it's also possible to set the initial conditions of the trunk. The highlighted section 4 includes the leg crank, similarly for what was seen in the kinematic case, with the addition of a series of blocks (*fig.88*) which impose to the leg crank to stay fixed, as already discussed. In the highlighted section 5 it's located the upper rod subsystem and the inertia block. The latter includes the inertia of human upper body, harmonic drive, clutch and electric motor, and it's located on the revolute joint between trunk crank and upper rod, to avoid any trouble with the non-rotating frames due to the virtual joint, without any loss of precision. In section 6 there is the trunk crank subsystem, with receives both the actuation torque and the human resistant torque. Angular acceleration and angular position are sensed in its central revolute joint. The highlighted section 7 includes just the lower rod subsystem, while the section 8 is the subsystem (*fig.89*) devoted to the resistant hip torque calculation due to the human upper body weight. This subsystem takes as input the hip angle and depurates it from the leg angle $\delta_{ref}$, to achieve the actual trunk angle $\theta$, input of a MATLAB function which returns the hip torque of the human. Saturation blocks are used to stay in the desired range of motion. A gain block is located after this, to simulate that the human muscles hold a part of the human weight, because the system is designed to hold up to the 70% of the human upper body. In this case the gain is set to 0.6, then a 40% of the human upper body is held by the human itself. The highlighted section 9 contains the core of the simulation, that is the actuation unit (*fig.90*). In this case it's composed only by the controller which commands the high-level control system. Giving the error between the reference and the actual angle $\theta$ input to a suitably tuned controller, the output will be the desired torque, input of the trunk crank, which will make the system move. The input reference is the sum of the trunk reference $\theta_{ref}$ and the leg initial angle $\delta_{ref}$. The actual angle $\theta$ is obtained by detecting the hip angle on the trunk crank, and adding the leg initial condition, to make the system work properly. The chosen controller, in this case, is a PID controller.

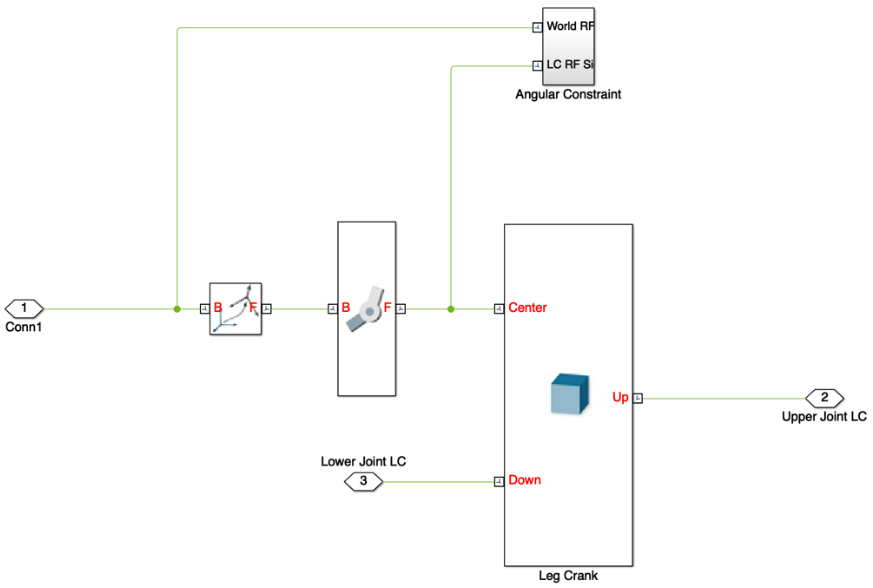


*Figure 88. Leg Crank Subsystem*

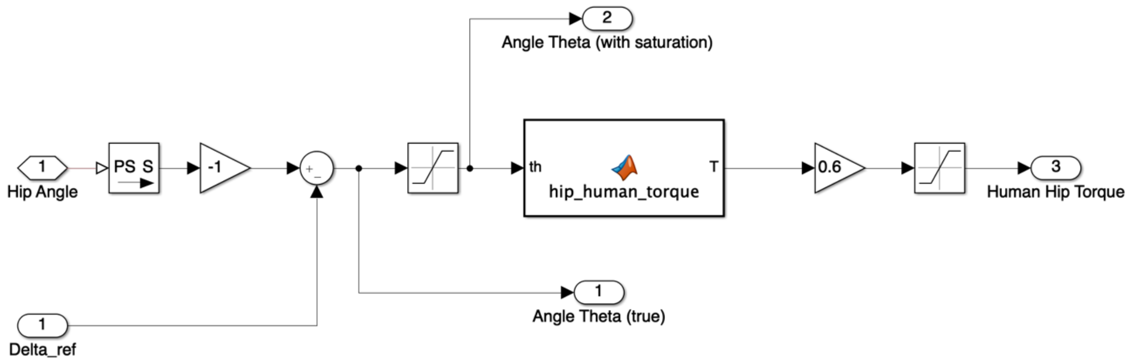


*Figure 89. Human Hip Torque Calculation Subsystem*

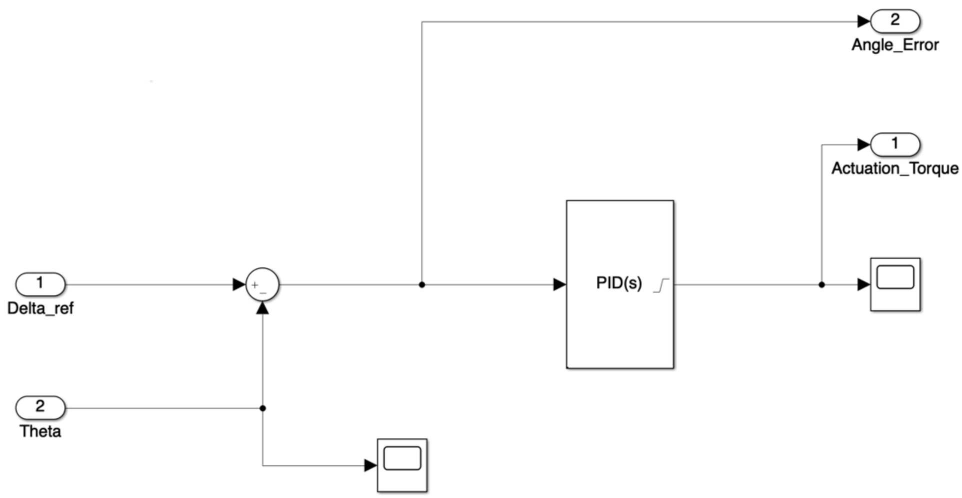


*Figure 90. Actuation Unit Subsystem*

### 6.3.1 High-Level Controller

The PID controller is a simple and very versatile controller, widely used in many application fields. It is composed by three parts, that it's possible to tune separately: proportional, integrative and derivative contributes. Its transfer function is the following:

$$P + I\frac{1}{s} + D\frac{N}{1 + N\frac{1}{s}} \tag{30}$$

After linearizing the plant and setting the output saturation compatible with the prescribed design torque, the parameters were set.

$P = -1463.9$

$I = -1189.3$

$D = -295.3$

$N = 219.7$

A controller designed as described is able to provide, for a unit step input, a rise time of 0.0822 s, with a settling time of 1.29 s. The overshoot is around 23.7% with a peak of 1.24. The gain margin is -18.5 dB, while the phase margin is 65.9 deg. The closed-loop, with this controller, results stable. The Bode plot is reported in *fig.91*.

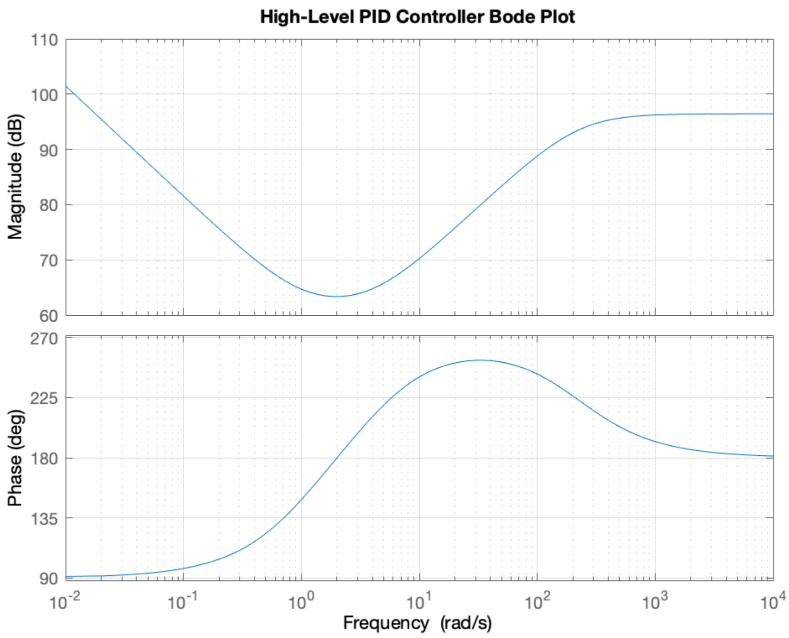


*Figure 91. Bode Plot of the High-Level Controller*

### 6.3.2 Simulations Interpretation Guide

All the simulations including the high-level control system have to be interpreted as follows, considering that only the four-bar linkage will be visible during the simulations. As shown in *fig.92* the human leg must always be considered parallel with the segment of the leg crank passing through the center revolute joint. On the other hand, the user torso has to be imagined perpendicular with the line intercepting the center revolute joints of the two cranks, and then perpendicular with both rods.
Anyway, many graphs are provided to have a correct response of the system behavior within the simulations and to support the obtained results.

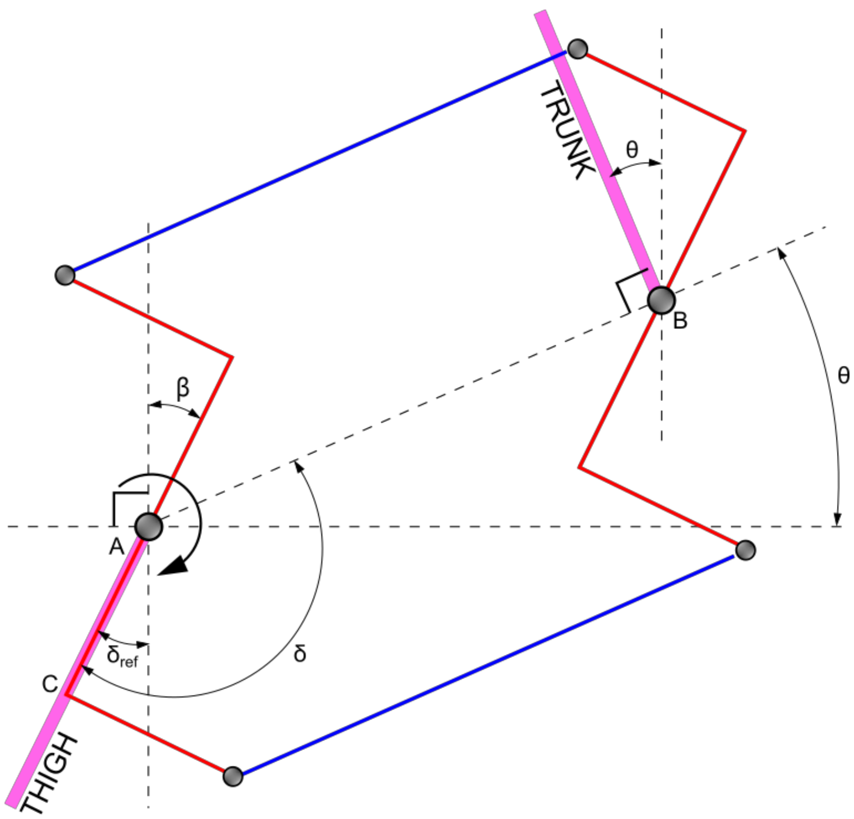


*Figure 92. High-Level Interpretation Scheme*

### 6.3.3 High-Level Model Results

The simulation analyzed in this paragraph was performed assuming the exoskeleton operating in "bending mode", with an initial trunk angle of 45° and the legs kept vertical, condition that is possible to relate to the worst possible case for the actuation unit, considering how the design torque was defined. The results are shown in *fig.93-96*.

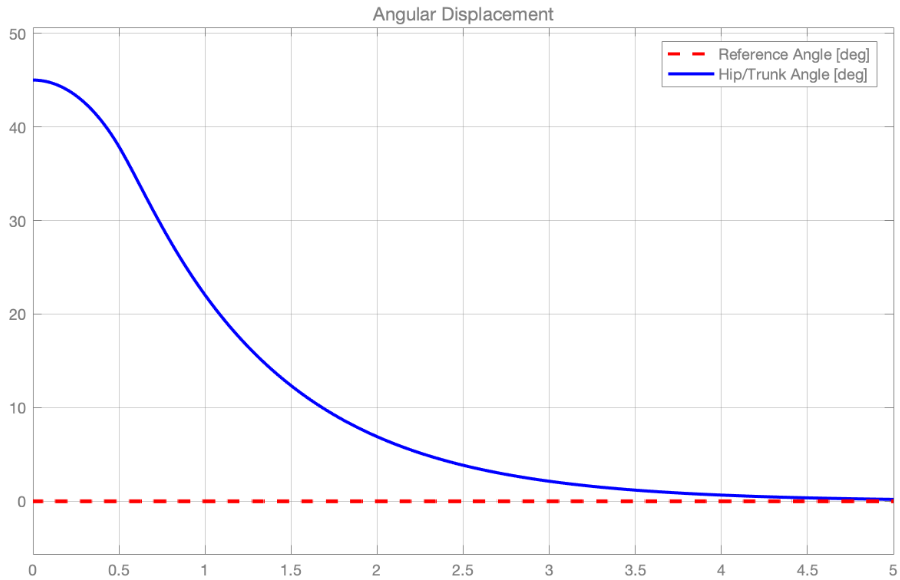


*Figure 93. High-Level Model - Simulation Results 1 as a Function of Time [s]*

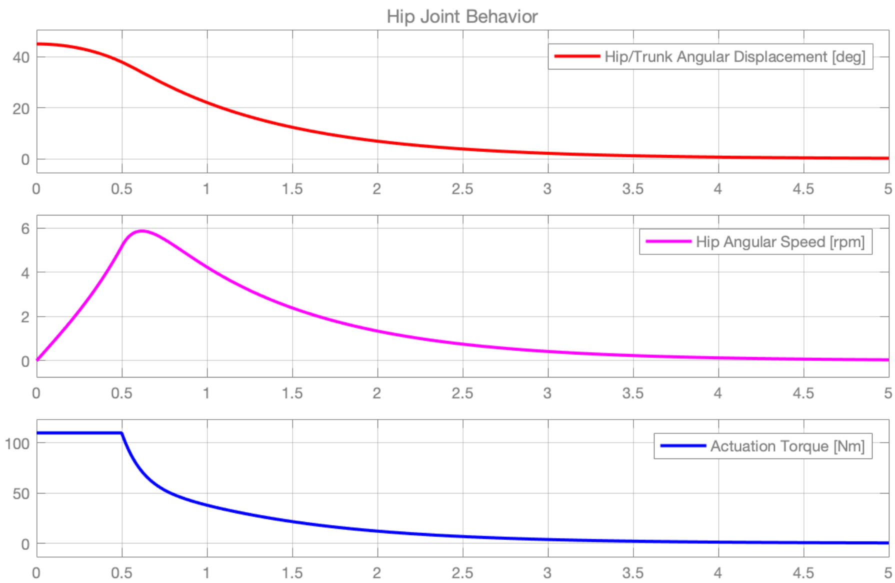


*Figure 94. High-Level Model - Simulation Results 2 as a Function of Time [s]*

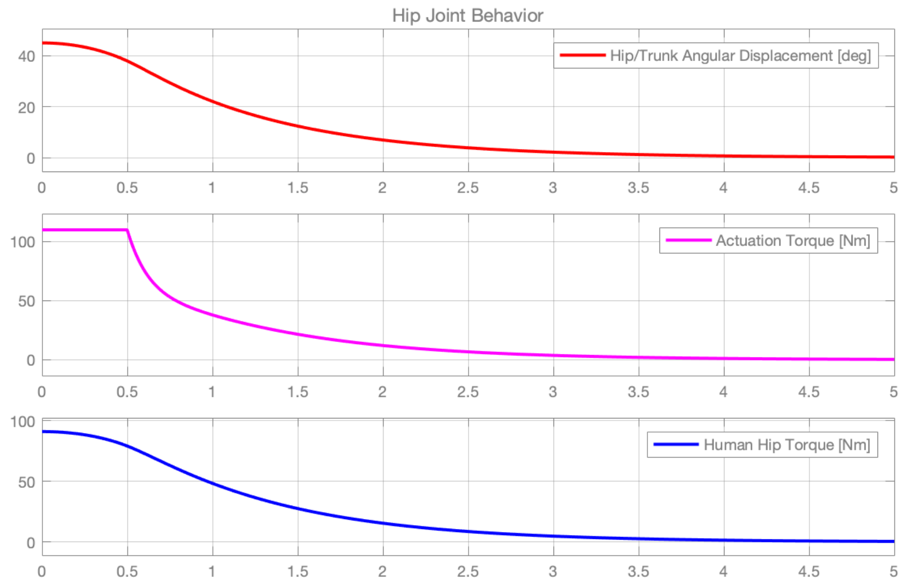


*Figure 95. High-Level Model - Simulation Results 3 as a Function of Time [s]*

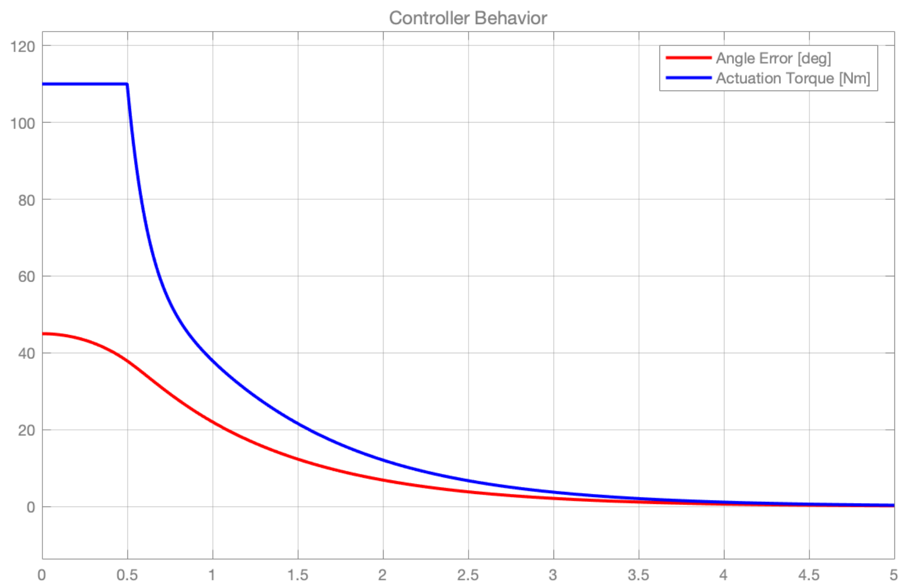


*Figure 96. High-Level Model - Simulation Results 4 as a Function of Time [s]*

All the obtained plots show the results for a five seconds simulation. The *fig.93* shows how the torso angle θ follows the reference, bringing the trunk in vertical position in less than 5 s with a smooth, monotonic and continuous movement. In *fig.94* it's shown the same angular displacement and compared with the hip rotational speed and the desired actuation torque. It's possible to notice that the maximum rotational speed is around 6 rpm, less than the one prescribed in the design phase: this condition is respected. The torque output starts with its maximum saturation value, equal to the total design torque, it maintains this value for 0.5 s and then lowers when the angle decreases.

In *fig.95* it's also shown the resistant torque due to the human upper body weight, while the *fig.96* compares the desired torque with the angle error, input of the PID controller.

## 6.4 Low-Level Control System

A low-level control system was also created. For making this, for simplicity, the model of a series-excitation DC brushed motor was used, which has the following electrical and mechanical characteristic equations:

$$v = K_e\omega + i_m R + L\frac{di_m}{dt} \tag{31}$$

$$T = K_t i_m - K_b\omega - T_f - J\frac{d\omega}{dt} \tag{32}$$

Where v is the input voltage, $i_m$ is the current flowing into the windings, ω is the motor rotor speed, T is the output torque and all the other voices are motor constants, which can be found from any motor datasheet.

To achieve a more accurate result, a real DC brushed motor was chosen from the catalogues, with characteristics comparable with the ones prescribed in the component design phase. The chosen motor is the Maxon Motor© RE 65 Ø65 mm, Graphite Brushes, 250 Watt [95]. From the datasheet many values were taken, such as the nominal voltage $v_n$, the no load speed $s_0$, the no load current $i_0$, the nominal speed $s_n$, the nominal torque $T_n$, the nominal current $i_n$, the stall torque $T_s$, the stall current $i_s$, the terminal resistance R, the terminal inductance L and the rotor inertia J. Some data needed to model the system by means of the characteristic equations are not available from the datasheet, but it's possible to achieve them with the possessed data, with good approximation.

$$K_t = \frac{T_s}{i_s - i_0} \tag{33}$$

$$T_f = K_t i_n - T \tag{34}$$

$$K_e = \frac{v_n - Ri}{s_n} \tag{35}$$

$$K_b = \frac{K_t i_n}{s_n} \tag{36}$$

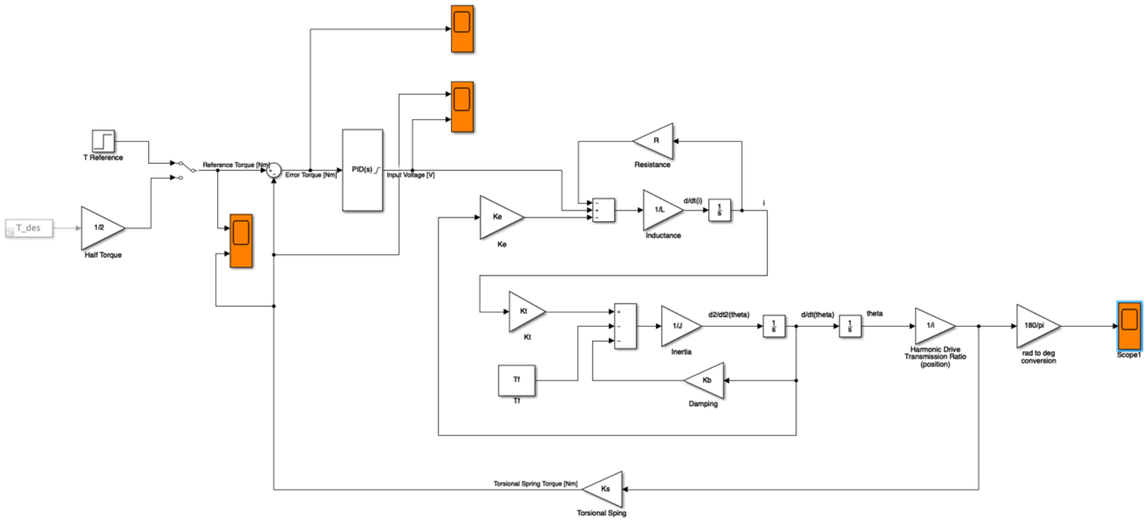


*Figure 97. Simulink Low-Level Model*

By having all the needed motor data, it's now possible to build the low-level control model. In *fig.97* it's presented the low-level control model. On the left there is the torque reference that the motor has to follow. It will be compared with the current measured torque. The torque is not directly measured: it's assumed that all the motor rotation corresponds to the deformation of the torsional spring, considering the harmonic drive transmission ratio. In the real case the deformation of the spring will be measured with a couple of encoders, one located upstream the spring and the other downstream the spring, to obtain the difference between the two detected values, and then the real spring deformation. For this ideal case it's a good approximation. The torque control has then become a position control. The torque error is the input of the low-level controller, a PID controller also in this case. Its output is the input voltage of the motor, which saturate at a voltage equal to -24/+24 V. The rest of the model represents the equations 31 and 32, describing the brushed DC motor. The output of the motor is its angular displacement that, as already said, when multiplied by the harmonic drive transmission ratio corresponds to the torsional spring deformation.

### 6.4.1 Low-Level Controller

After linearizing the plant and setting the output saturation compatible with the prescribed nominal voltage of the motor, the parameters were set.

$P = 11.96$

$I = 491.70$

$D = 0.0335$

$N = 35086.06$

A controller designed as described is able to provide, for a unit step input, a rise time of 0.00585 s, with a settling time of 0.0482 s. The overshoot is around 9.76% with a peak of 1.1. The gain margin is 41.1 dB, while the phase margin is 77 deg. The closed-loop, with this controller, results stable. The Bode plot is reported in *fig.98*.

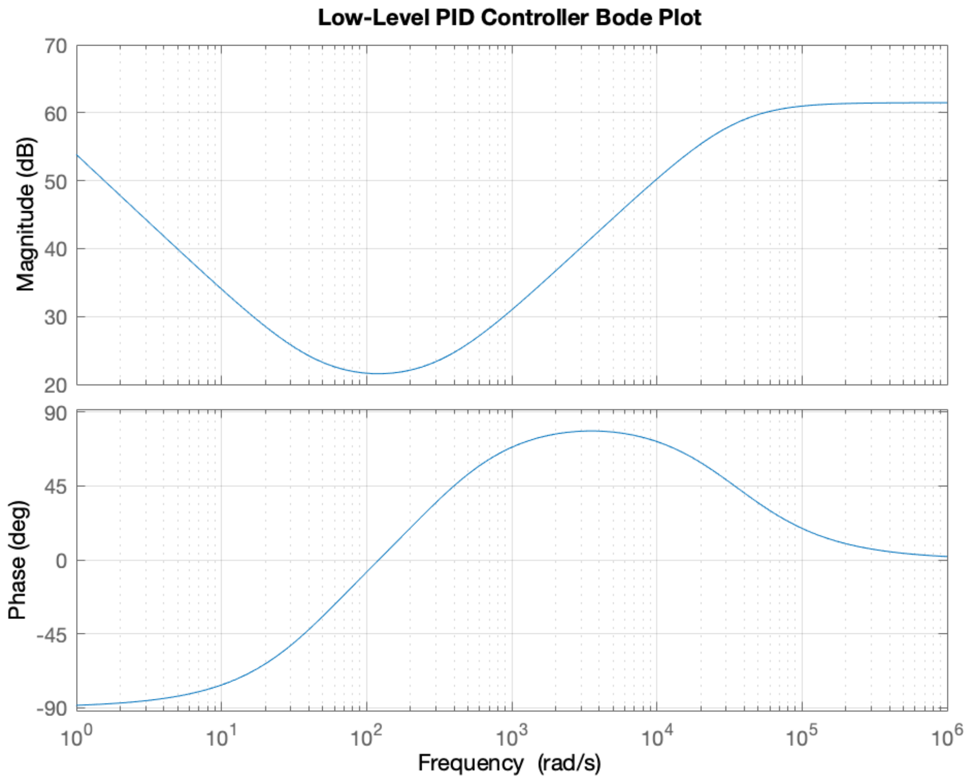


*Figure 98. Bode Plot of the Low-Level Controller*

### 6.4.2 Low-Level Model Results

The simulation analyzed in this paragraph was performed assuming a step input as reference, with amplitude equal to the design torque of a single actuation unit, that is 55 Nm. The results are shown in *fig.99-102*.

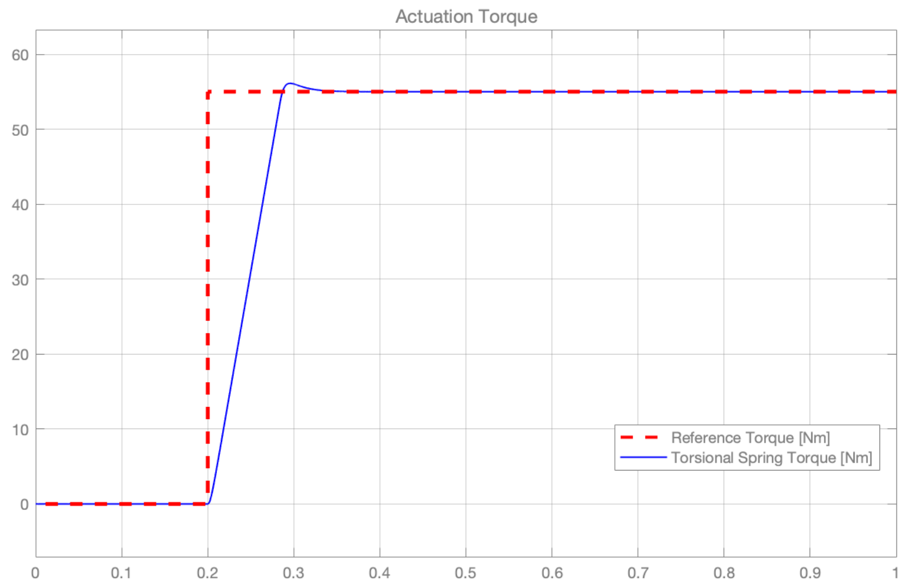


*Figure 99. Low-Level Model - Simulation Results 1 as a Function of Time [s]*

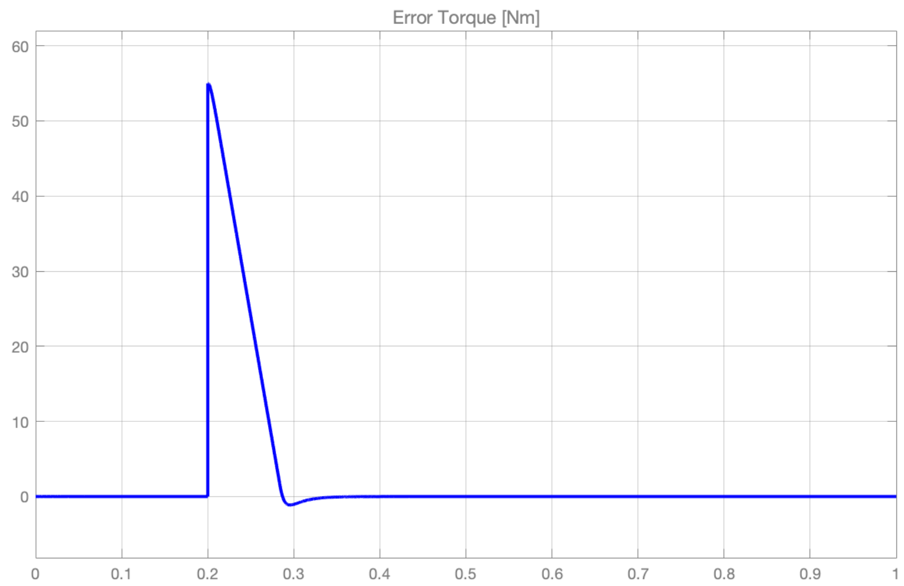


*Figure 100. Low-Level Model - Simulation Results 2 as a Function of Time [s]*

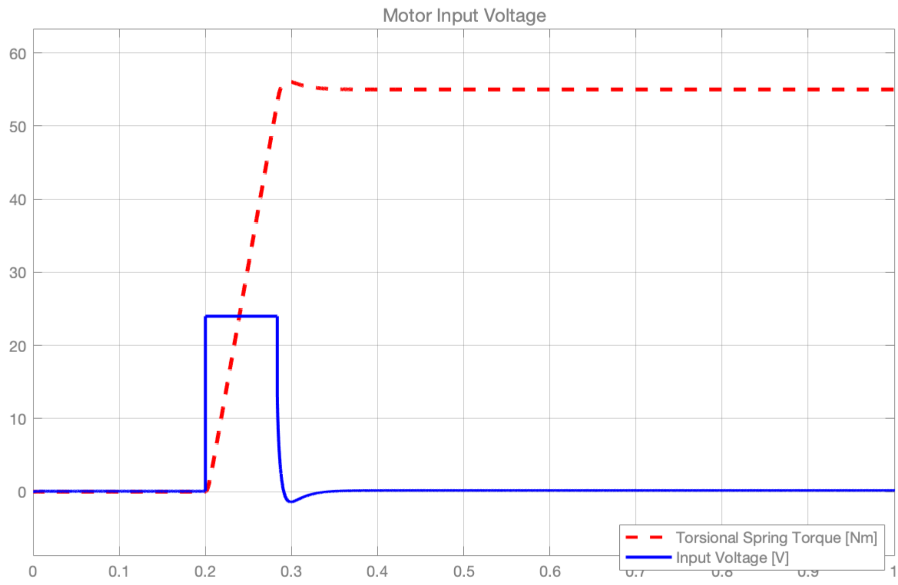


*Figure 101. Low-Level Model - Simulation Results 3 as a Function of Time [s]*

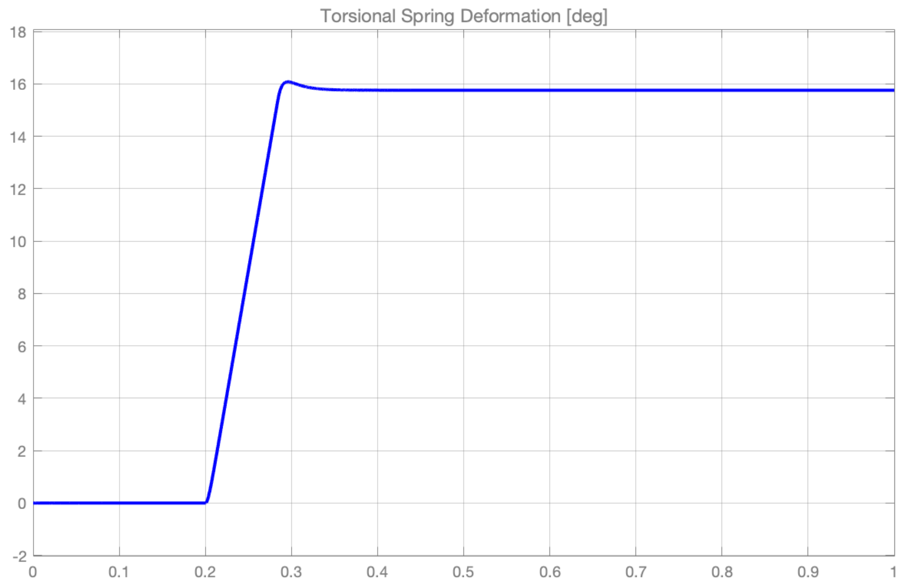


*Figure 102. Low-Level Model - Simulation Results 4 as a Function of Time [s]*

The outputs are shown for a 1 s long simulation. In *fig.99* it's reported how the motor output torque follows the step reference, and as it's possible to see that in just 0.1 s the motor is able to provide the required torque. In *fig.100* it's shown the error torque, input of the PID controller. The *fig.101* shows motor input voltage, output of the PID controller, compared with the output torque. It's possible to see that, to maintain the torque constant, the electric motor performs a sort of ripple around the null voltage. Lastly, the *fig.102* reports the torsional spring deformation, proportional to the output torque. The maximum spring deformation is around 16°.

## 6.5 Implementation of the Two-Levels System

To have a more realistic idea about the behavior of the system, it's possible to implement the low-level control into the high-level control system.
It's assumed to maintain the human legs always parallel, in order to have a single initial condition for the legs, and then a single high-level control system.
Inside the actuation unit subsystem of the high-level model (highlighted section 9 in *fig.87*) it's possible to integrate the low-level control system. The output of the high-level controller becomes the input reference of the low-level control subsystem (*fig.103*). This reference has to be halved, becoming the two low-level control systems reference (*fig.104*), one per side, because a single motor is not able to provide all the torque that the system needs. The output torques of the two motors are summed, becoming the input of the trunk crank revolute joint.

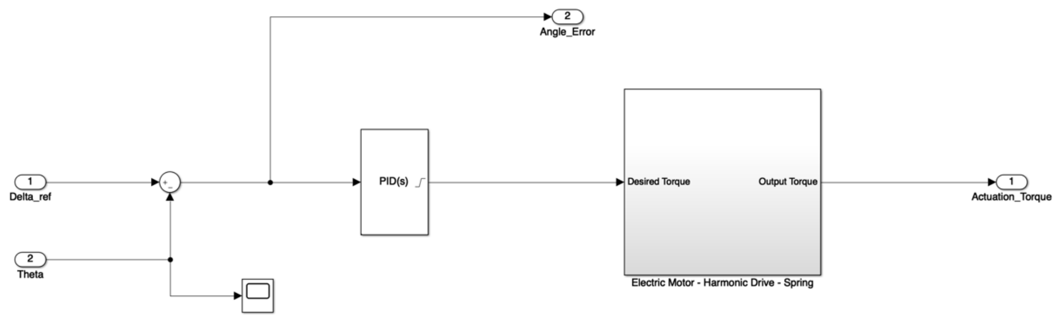


*Figure 103. Simulink Model of the Actuation Unit Implementing the Low-Level Control System*

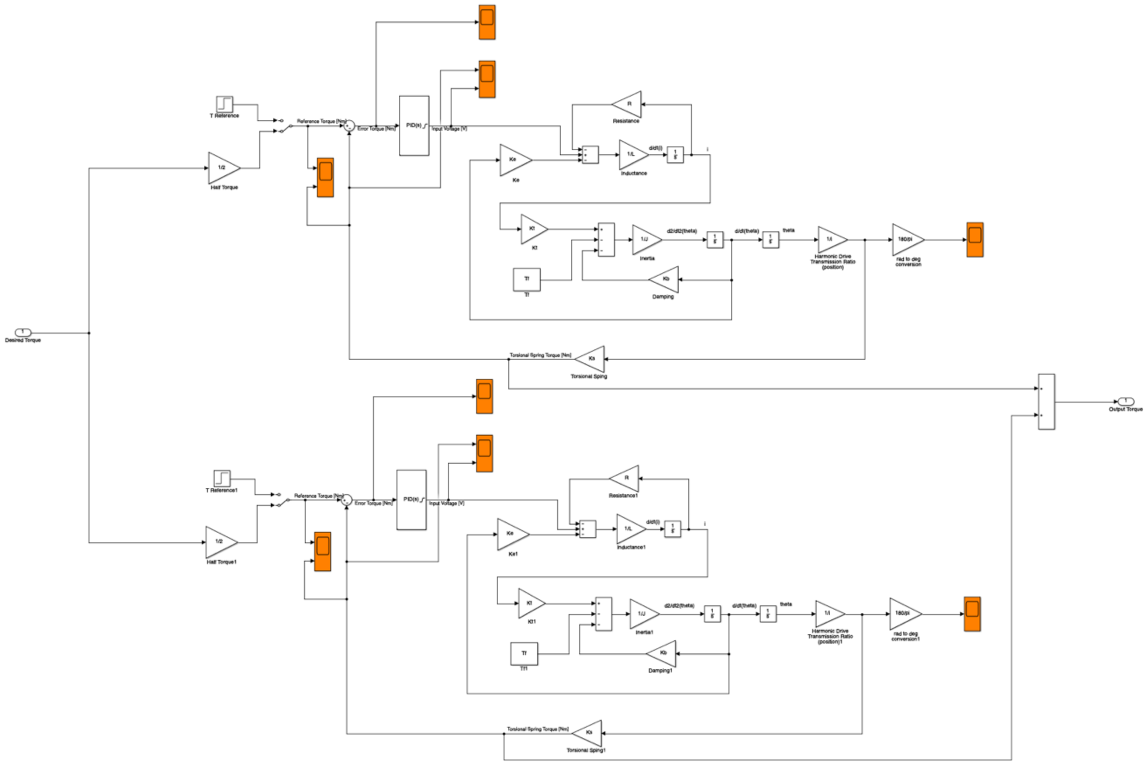

*Figure 104. Simulink Model of the Low-Level Control System Implemented in the High-Level*

### 6.5.1 Results

The plotted results (*fig.105-112*) are the same of the previous cases, when high-level and low-level were studied separately. The simulation was performed for 5 s, with an initial trunk angle of 45°, the parallel legs, and the aim of bringing the trunk in vertical position, being the exoskeleton working in "bending mode".

In *fig.105-106* it's possible to see the trunk angular displacement and it's easy to notice that the exoskeleton, in the first 0.4 s of the simulation, is not capable to provide all the torque that the system needs to hold the human upper body. In fact, before starting the uprising, there is a phase in which the trunk bends forward because the hip torque due to the human weight is higher than the actuation torque. The maximum angular speed of the trunk is around 6.3 rpm.

From *fig.109* it's possible to see that the low-level control system is able to provide the desired torque to the system, reaching the reference torque in just 0.2 s, and following it well when the reference starts changing. The motor input voltage needs to change its sign in order to follow the reference torque as desired (*fig.111*).

From the collected data it’s possible to assert that the whole system behaves as expected.

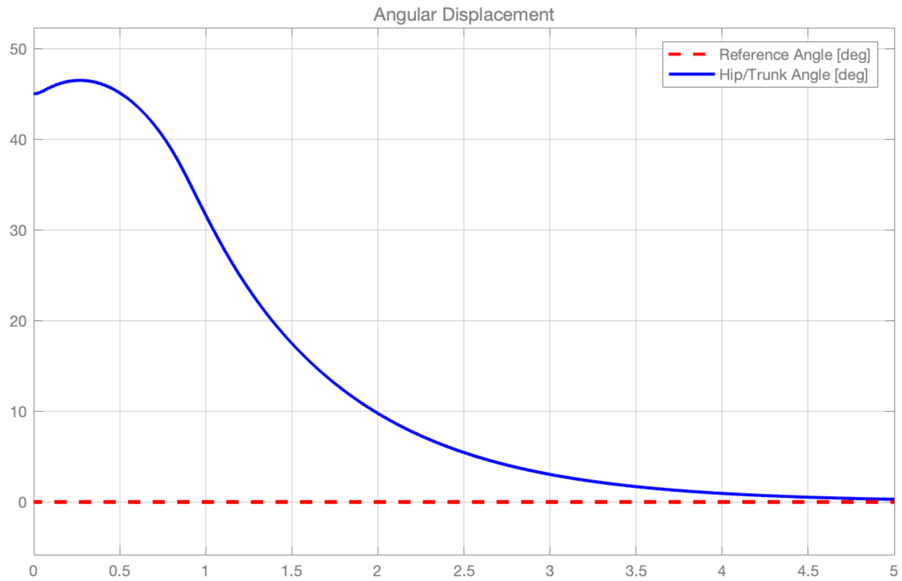


*Figure 105. Complete Control System Model – Simulation Results 1 as a Function of Time [s]*

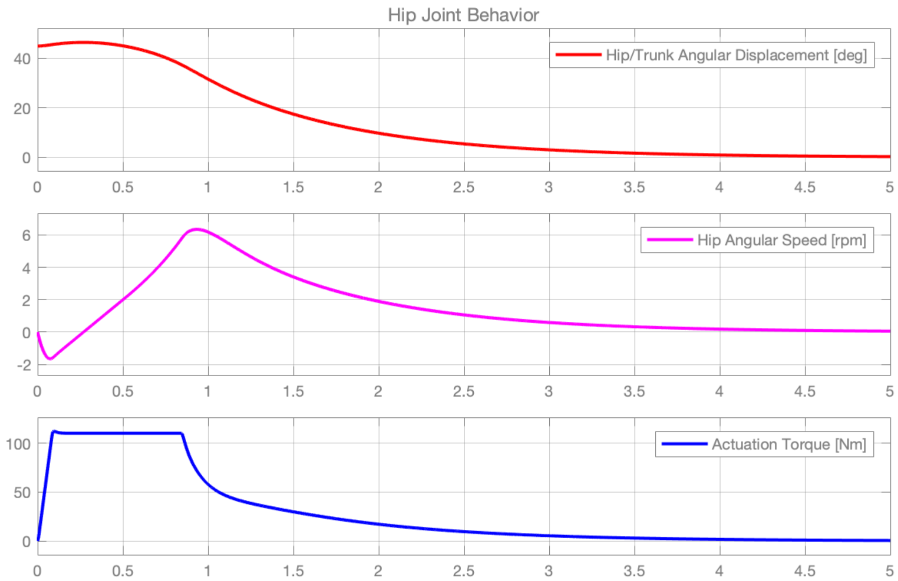


*Figure 106. Complete Control System Model – Simulation Results 2 as a Function of Time [s]*

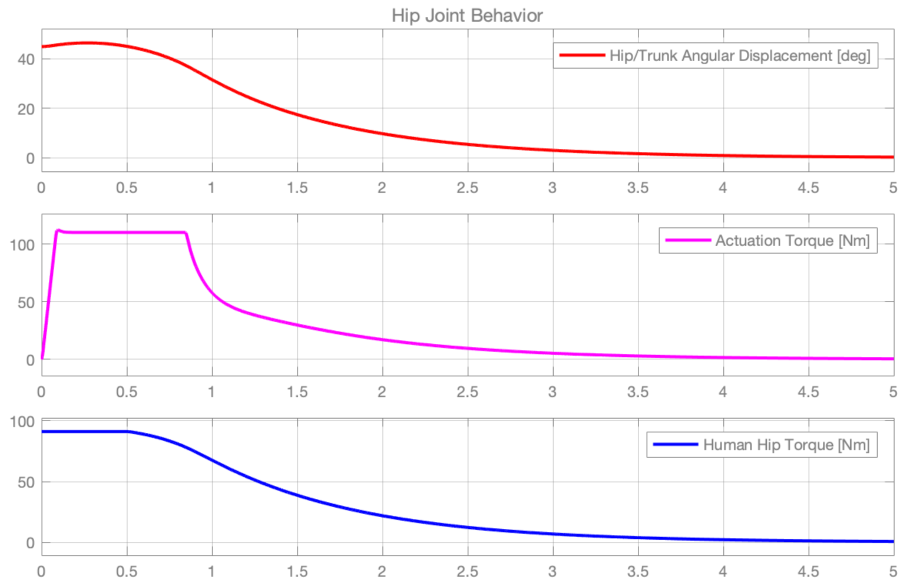


*Figure 107. Complete Control System Model – Simulation Results 3 as a Function of Time [s]*

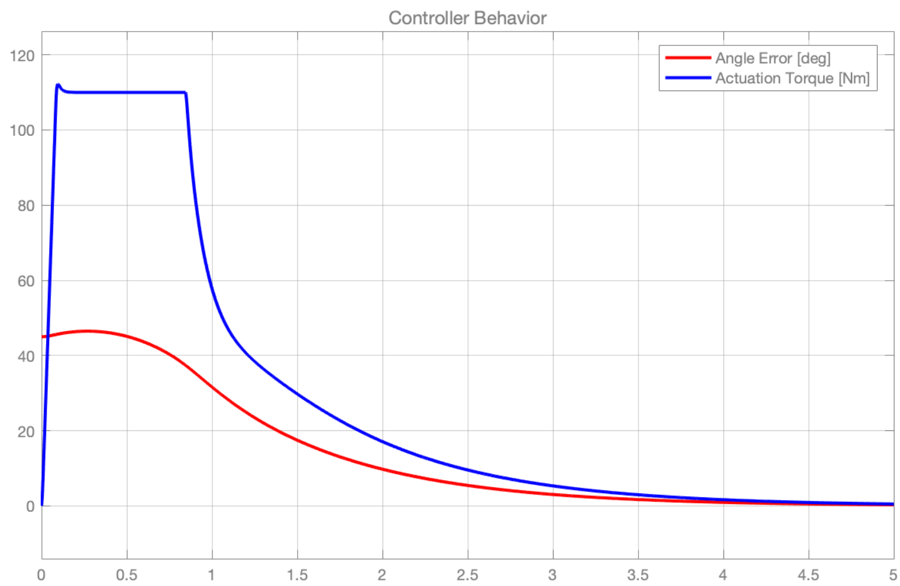


*Figure 108. Complete Control System Model – Simulation Results 4 as a Function of Time [s]*

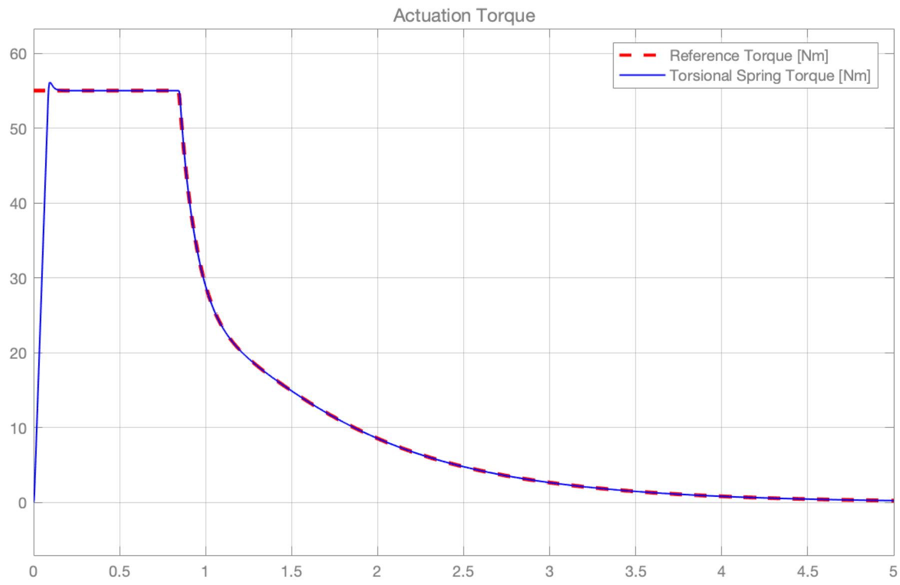


*Figure 109. Complete Control System Model – Simulation Results 5 as a Function of Time [s]*

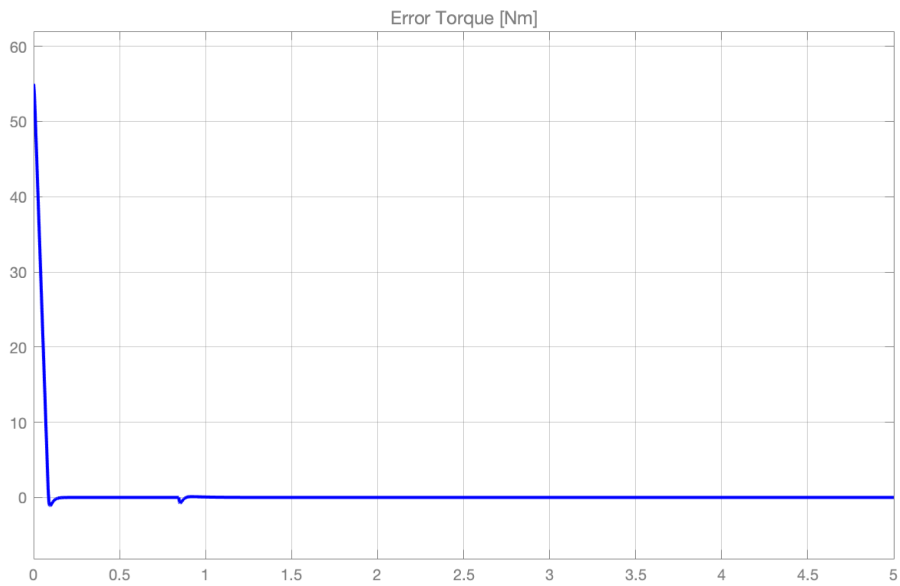


*Figure 110. Complete Control System Model – Simulation Results 6 as a Function of Time [s]*

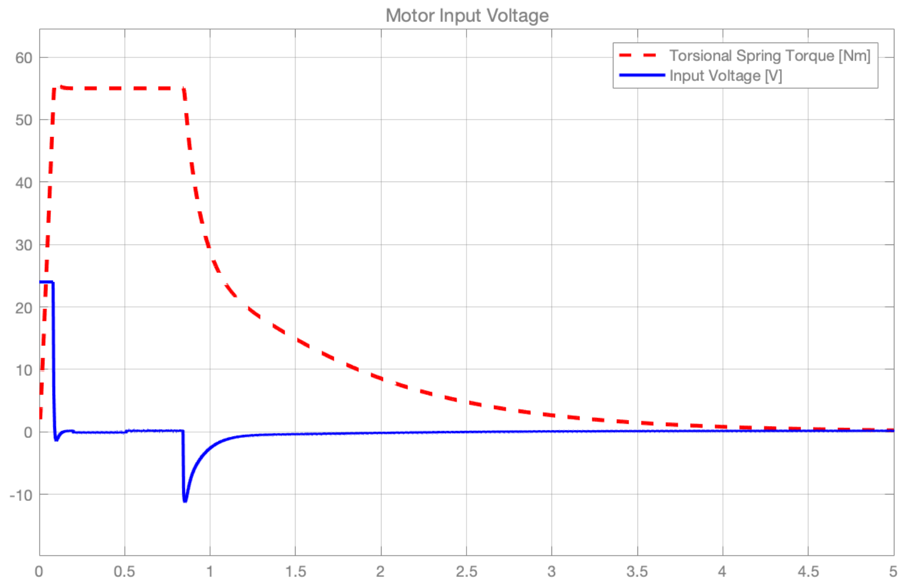


*Figure 111. Complete Control System Model – Simulation Results 7 as a Function of Time [s]*

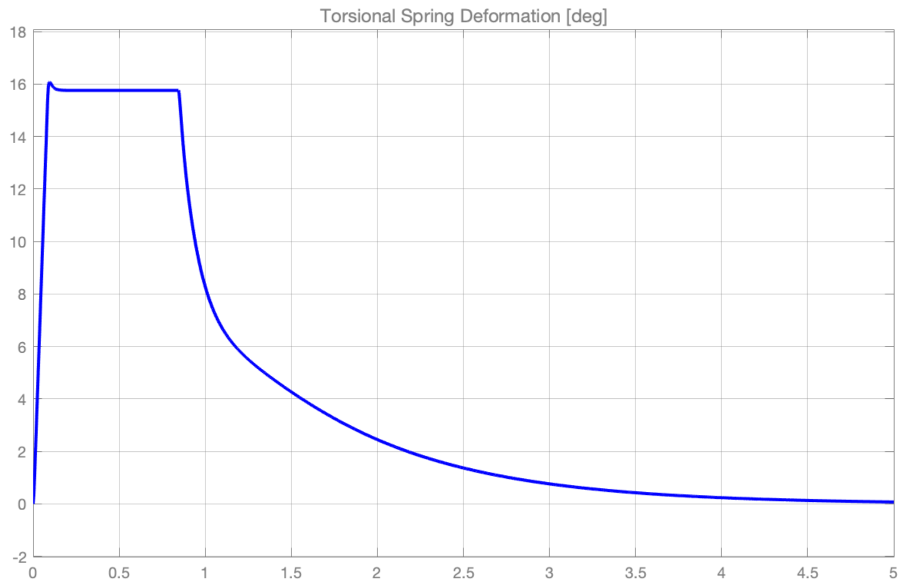


*Figure 112. Complete Control System Model – Simulation Results 8 as a Function of Time [s]*

## 6.5.2 Conclusive Tests

It's possible to simulate the final system with different input references and different initial conditions to test its robustness.

The first performed test considers the legs always parallel, but with a 10° angle from the vertical axis. The initial condition of the trunk is 30°, corresponding to an initial angle with respect to the vertical axis equal to $\theta_0$=30°-10°=20°. In *fig.113* it's shown that also in this case the system is able to reach the reference easily, the movement is smooth as desired with a maximum speed of 2.6 rpm. In this case, there isn't a constant torque phase, with a local maximum of 86 Nm.

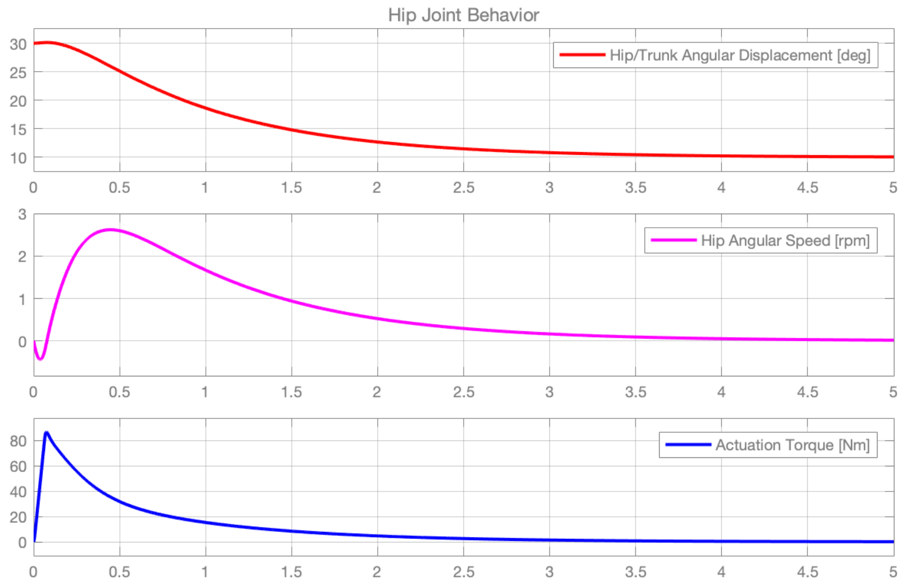


*Figure 113. Simulation Plots – Leg Not Vertical and Different Trunk Reference as a Function of Time [s]*

Another possible test is performing the "bending mode" simulation, with vertical legs and initial trunk angle of 45°, changing the gain of the resistant hip torque due to the user upper body weight. The maximum percentage for which the system is capable to bring the trunk in vertical position is 71%, a really good value considering that the actuation unit was designed to hold the 70% of the upper body weight. The resulting output (*fig.114*) of a 10 s long simulation shows a long constant torque phase, almost 5.3 s, due to the fact that the resistant torque is really high, enough to bring the torso angle to 61° before starting the uprising. The system reaches the target in 8.3 s, much more than any other case. The maximum speed is exactly 6 rpm.

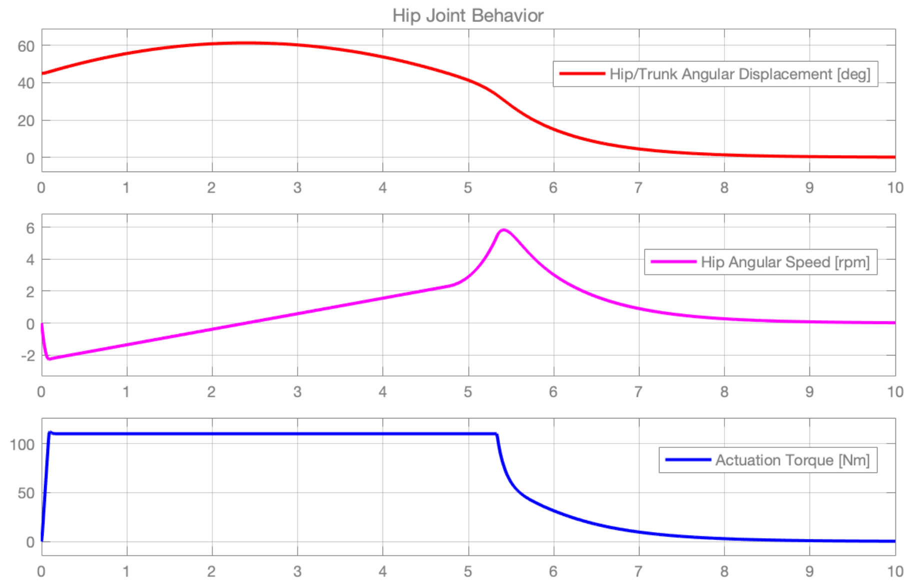


*Figure 114. Simulation Plots – Human Holding the 29% of Upper Body Weight as a Function of Time [s]*

As already said, the designed system can also work in "stooping mode", setting the reference equal to the initial torso angle. The performed simulation considers the system operating in stooping mode with a starting trunk angle of 45°. As it's reported in *fig.115,* at the beginning the trunk starts bending forward, reaching a displacement of 3.2° beyond the desired equilibrium position. In 0.6 s the actuation unit is capable to provide the needed constant torque, bringing the trunk to 45° in just 4 s, with a maximum speed of 0.3 rpm.

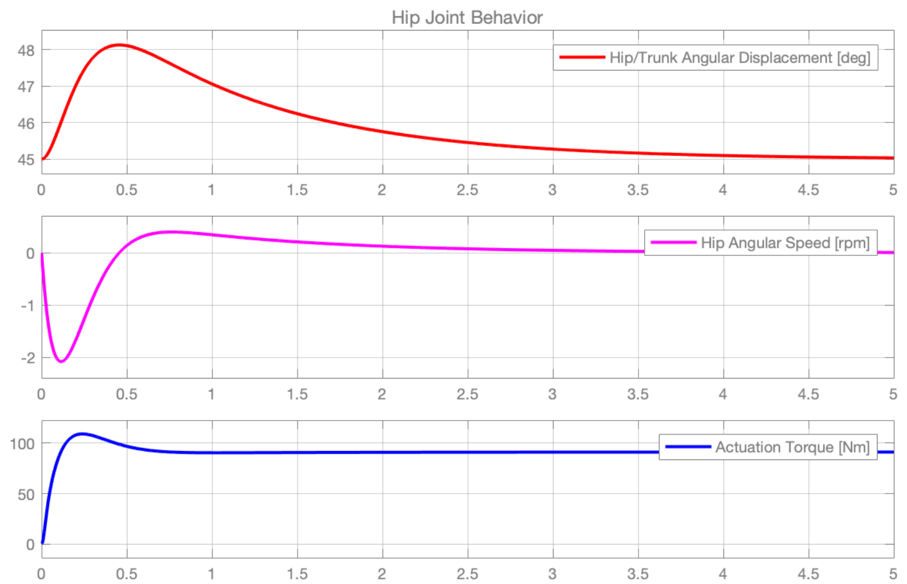


*Figure 115. Simulation Plots – Stooping Mode at 45° as a Function of Time [s]*

A last simulation can be made, hypothesizing to start with a null torso angle (trunk in vertical displacement), with the aim of reaching an angle of 30°, value that may be inserted manually by the user in practice, with a so designed control system. The target is then to perform a controlled bending forward movement, with a final stooping operation. The *fig.116* demonstrates that it's possible to perform this kind of operation with a smooth and controlled movement. After just 3.5 s the system reaches the reference, with a maximum speed of 4.2 rpm, and a torque in the stooping phase of 59 Nm.

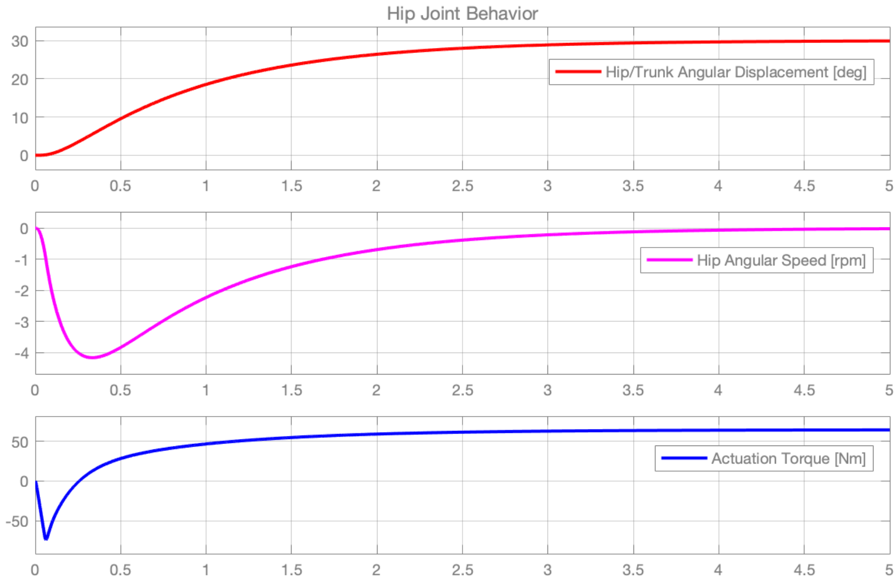


*Figure 116. Simulation Plots – Reverse Bending Mode (Bending Forward and Stooping) as a Function of Time [s]*

# Chapter 7

# Conclusions and Future Works

## 7.1 Conclusions

A study of the past and current environment surrounding the wearable robotics was performed, in particular for what concerns the exoskeleton intended for operating on legs and trunk, with a specific focus on their shape, actuation system, materials, control system, joints and degrees of freedom. This research brought to have a wide view of the state of the art, allowing to understand the starting problem, set a design target and develop the optimal solution to realize it between different proposals. The choice was to provide a hip torque to achieve the desired results. Many studied exoskeletons were taken into account, considering their proposed solutions from different points of view. A 99 percentile Italian man was chosen as reference subject, with the aim to design an exoskeleton able to work in three different modes. The first chosen working mode is the “free mode”, in which the actuation unit is decoupled with the legs, allowing the user to walk. Besides, the “stooping mode" was studied to detect the trunk angle of the user and maintaining it, providing a hip torque. The last working mode, the "bending mode", has the aim of aiding the user to bringing back the trunk to the vertical position, performing the uprising, providing a hip torque also in this case. After defining the design torque, the focus was then aimed on the hip joint development, designing the actuation unit system, and then choosing each component from different companies' catalogues. The encumbrance of the system with the chosen components amounts to 11.9 cm of lateral width, with the interaxle spacing between the two shafts equal to 12 cm, and an overall weight of the actuation unit of 1 kg, neglecting the components not yet designed.

Kinematics of the gait cycle, associated with "free mode", and dynamics, related to "stooping mode" and "bending mode", were then studied. These studies were performed both analytically and with simulations on different tools. In this way, all the three operating modes of the system were studied. For making this, a model composed by the four-bar linkage and the attached inertia was considered, imposing suitable boundary conditions. For the dynamic study, a control system was developed. It was necessary to design a structured control system, composed by an outer loop which controller returns the reference torque for the inner loop, which controls the motor. The employment of the series elastic actuator allowed to transform the torque control problem into a position control problem.

The design target was to have a system able to hold up to the 70% of the human upper body of the considered reference subject. The simulations return that the system is capable to hold up to the 71% of the subject's weight, respecting all the criteria in terms of displacement, velocity and torque. Indeed, the aim of the project was to design an actuation system able to perform all the required actions safely, without torques and velocities excessively high and potentially dangerous for the user, maintaining a good response time. The system was demonstrated to be stable and efficient in any situation, for any set of reference and initial conditions having a physical meaning, in any designed operating mode.

## 7.2 Future Works

The system may still be refined, starting with the implementation of a different motor in the low-level control, such as the stepper motor, finding a suitable control system for the new inner loop. The high-level control system may also be modified, splitting it into two parts, one per leg, having two initial conditions for the legs but still a single initial condition for the trunk. In this way there will be a second actuation unit and also its inertia, that was neglected in this treatise with a small loss of precision. All the models may be implemented together, with a stateflow chart controlled by the user, to select the current working mode. It's also important to proceed with more detailed drawings of the hip joint, without neglecting the chance to design a specific test bench, equipped with force sensors, in order to have empirical results to compare with the simulations. The actual sensors of the exoskeleton must also be chosen accurately, in order to make the system work properly. Lastly, the rest of the exoskeleton has to be designed, paying attention to the materials, the size adjustments, the contact surfaces and the resistance of the links.

# List of Abbreviations

| | |
|---|---|
| ALEX | Active Leg Exoskeleton |
| APO | Active Pelvis Orthosis |
| BCI | Brain-Computer Interface |
| BLEEX | Berkeley Lower Extremity Exoskeleton |
| BLERE | Bionic Lower Extremity Rehabilitation Exoskeleton |
| cHRI | Cognitive Human-Robot Interaction |
| CYBERLEGs | Cybernetic Lower-Limb Cognitive Ortho-Prothesis |
| DoF | Degree of Freedom |
| EMG | Electromyography |
| EXO | Exoskeleton |
| HAL | Hybrid Assistive Limb |
| HD | Harmonic Drive |
| HJC | Hip Joint Center |
| ICR | Instantaneous Center of Rotation |
| IEMG | Integral Electromyography |
| IHMC | Institute for Human and Machine Cognition |
| MOI | Moment of Inertia |
| PD | Proportional Derivative |
| pHRI | Physical Human-Robot Interaction |
| PID | Proportional Integral Derivative |
| PLC | Programmable Logic Controller |
| PMA | Pneumatic Muscle Actuator |
| ROM | Range of Motion |

| | |
|---|---|
| RSEA | Rotary Series Elastic Actuator |
| SEA | Series-Elastic Actuator |
| SERKA | Series Elastic Remote Knee Actuator |
| VR | Virtual Reality |
| w/ | With |
| w/o | Without |
| WR | Wearable Robot |
| wrt | With Respect To |

# References


[1] N. Cetin, M. Bayramoglu, A. Aytar, O. Surenkok and O. Umit Yemisci (2008), "*Effects of Lower-Extremity and Trunk Muscle Fatigue on Balance*", The Open Sports Medicine Journal, pp. 16-22

[2] Asbjørn Roaas & Gunnar B. J. Andersson (1982), "*Normal Range of Motion of the Hip, Knee and Ankle Joints in Male Subjects, 30–40 Years of Age*", Acta Orthopaedica Scandinavica, 53:2, 205-208, DOI: 10.3109/17453678208992202

[3] D. Saravanakumar, B. Mohan, T. Muthuramalingam (2017), "*A review on recent research trends in servo pneumatic positioning systems*", Precision Engineering 49, p. 483

[4] Wei YANG, Can-jun YANG, Ting XU (2016), "*Human hip joint center analysis for biomechanical design of a hip joint exoskeleton*", Front Inform Technol Electron Eng, pp. 792-802

[5] Schiele A., et al. (2006), "*Kinematic design to improve ergonomics in human machine interaction*", IEEE Transaction on Neural Sysems and Rehabilitation Engineer, pp. 456-469.

[6] Stienen A.H.A., et al. (2009), "*Self-aligning exoskeleton axes through decoupling of joint rotations and translations*", IEEE Transaction on Robotics, pp. 628-633.

[7] Zinn M., et al. (2004), "*A new actuation approach for human friendly robot design*", The International Journal of Robotics Research, pp. 379-398.

[8] Gill A. Pratt and Matthew M. Williamson (1995), "*Series Elastic Actuators*", MIT Artificial Intelligence Laboratory and Laboratory for Computer Science, pp. 399-406

[9] N. Jarrasse and G. Morel (2009), "*A methodology to design kinematics of fixations between an orthosis and a human member*", Intelligent Mechatronics, pp. 1958–1963

[10] Aaron M. Dollar and Hugh Herr (2008), "*Lower Extremity Exoskeletons and Active Orthoses: Challenges and State-of-the-Art*", IEEE Transactions On Robotics, Vol. 24, pp. 144-158

[11] Yagin Nicholas (1890), "*Apparatus for Facilitating Walking*", U.S. Patent 440,684, November 18, 1890

[12] General Electric Company Corporate Research and Development (1971), "*Research and Development Prototype for Machine Augmentation of Human Strength and Endurance, Hardiman I Project*", National Technical Information Service

[13] Jerry E. Pratt, Benjamin T. Krupp, Christopher J. Morse, Steven H. Collins, (2004), "*The RoboKnee: An Exoskeleton for Enhancing Strength and Endurance During Walking*", International Conference on Robotics and Automation, pp. 2430-2435

[14] H. Kazerooni and R. Steger (2005), "*The Berkeley Lower Extremity Exoskeleton*", Journal of Dynamic Systems, Measurement, and Control Vol. 128, March 2006, pp. 14-25

[15] Adam B. Zoss, H. Kazerooni and Andrew Chu (2006), "*Biomechanical Design of the Berkeley Lower Extremity Exoskeleton (BLEEX)*", IEEE/ASME TRANSACTIONS ON MECHATRONICS, VOL. 11, NO. 2, APRIL 2006, pp. 128-138

[16] Nelson Costa and Darwin G. Caldwell (2006), "*Control of a Biomimetic "Soft-actuated" 10DoF Lower Body Exoskeleton*", Centre for Advanced Robotics Research Department of Computing, Science and Engineering – University of Salford, M5 4WT, United Kingdom

[17] Kyoungchul Kong and Doyoung Jeon (2006), "*Design and Control of an Exoskeleton for the Elderly and Patients*", E/ASME Transactions On Mechatronics, Vol. 11, No. 4, August 2006, pp. 428-432

[18] Saso Jezernik, Gery Colombo, Thierry Keller, Hansruedi Frueh and Manfred Morari (2003), "*Robotic Orthosis Lokomat: A Rehabilitation and Research Tool*", International Neuromodulation Society, Neuromodulation, Volume 6, Number 2, pp. 108–115

[19] Jan F. Veneman, Rik Kruidhof, Edsko E. G. Hekman, Ralf Ekkelenkamp, Edwin H. F. Van Asseldonk, and Herman van der Kooij (2007), "*Design and Evaluation of the LOPES Exoskeleton Robot for Interactive Gait Rehabilitation*", IEEE Transactions On Neural Systems And Rehabilitation Engineering, Vol. 15, No. 3, September 2007, pp. 379-386

[20] Claysson Bruno Santos Vimieiro, Breno Gontijo do Nascimento, Danilo Alves Pinto Nagem and Marcos Pinotti (2005), "*Development Of A Hip Orthosis Using Pneumatic Artificial Muscles*", Proceedings of TMSi 2005

[21] Breno Gontijo do Nascimento, Claysson Bruno Santos Vimieiro, Danilo Alves Pinto Nagem, and Marcos Pinotti (2008), "*Hip Orthosis Powered by Pneumatic Artificial Muscle: Voluntary Activation in Absence of Myoelectrical Signal*", Journal compilation 2008, International Center for Artificial Organs and Transplantation and Blackwell Publishing, pp. 317-322

[22] Sai K. Banala, Seok Hun Kim, Sunil K. Agrawal, and John P. Scholz (2009), "*Robot Assisted Gait Training with Active Leg Exoskeleton (ALEX)*", IEEE Transactions On Neural Systems And Rehabilitation Engineering, Vol. 17, No. 1, February 2009, pp. 2-8

[23] H. Kawamoto and Y. Sankai (2002), "*Power assist system HAL-3 for gait disorder person*", inLecture Notes Computer Science, vol 2398: Proc. 8th Int. Conf. Computers Helping People with Special Needs. Berlin, Germany: Springer-Verlag

[24] H. Kawamoto, S. Kanbe and Y. Sankai (2003), "*Power assist method for HAL-3 estimating operator's intention based on motion information*", inProc. IEEE Int. Workshop on Robot and Human Interactive Communication, Millbrae, CA, USA, Oct. 31–Nov. 2, 2003, pp. 67–72.

[25] H. Kawamoto and Y. Sankai (2004), "*Power assist method based on phase sequence driven by interaction between human and robot suit*", inProc.IEEE Int. Workshop on Robot and Human Interactive Communication, Okayama, Japan, Sep. 20–22, 2004, pp. 491–496.

[26] Kawamoto H. et al. (2009), "*Development of single leg version of HAL for hemiplegia*", Conference proceedings IEEE Engineering in Medicine and Biology Society, pp. 5038-5043.

[27] CYBERDYNE INC. all rights reserved (2018), www.cyberdyne.jp/english/ [ONLINE]

[28] Hiromasa Hara and Yoshiyuki Sankai (2010), "*Development of HAL for Lumbar Support*", SCIS & ISIS 2010, Dec. 8-12, 2010, Okayama Convention Center, Okayama, Japan, pp. 416-421

[29] Hiromasa Hara and Yoshiyuki Sankai (2012), "*HAL Equipped with Passive Mechanism*", 2012 IEEE/SICE International Symposium on System Integration (SII), pp. 1-6

[30] Kousei Miura, Hideki Kadone, Masao Koda, Tetsuya Abe, Hiroshi Kumagai, Katsuya Nagashima, Kentaro Mataki, Kengo Fujii, Hiroshi Noguchi, Toru Funayama, Hiroaki Kawamoto, Yoshiyuki Sankai and Masashi Yamazaki (2018), "*The hybrid assistive limb (HAL) for Care Support successfully reduced lumbar load in repetitive lifting movements*", Journal of Clinical Neuroscience 53, pp. 276–279

[31] Kousei Miura, Hideki Kadone, Masao Koda, Tetsuya Abe, Hirooki Endo, Hideki Murakami, Minoru Doita, Hiroshi Kumagai, Katsuya Nagashima, Kengo Fujii, Hiroshi Noguchi, Toru Funayama, Hiroaki Kawamoto, Yoshiyuki Sankai, Masashi Yamazaki (2018), "*The hybrid assisted limb (HAL) for Care Support, a motion assisting robot providing exoskeletal lumbar support, can potentially reduce lumbar load in repetitive snow-shoveling movements*", Journal of Clinical Neuroscience 49, pp. 83–86

[32] Hian Kai Kwa, Jerryll H. Noorden, Matthew Missel, Travis Craig, Jerry E. Pratt and Peter D. Neuhaus (2009), "*Development of the IHMC Mobility Assist Exoskeleton*", IEEE International Conference on Robotics and Automation, Kobe International Conference Center Kobe, Japan, pp. 2556-2562

[33] James S. Sulzer, Ronald A. Roiz, Michael A. Peshkin and James L. Patton (2009), "*A Highly Backdrivable, Lightweight Knee Actuator for Investigating Gait in Stroke*", IEEE Transactions On Robotics, Vol. 25, No. 3, pp. 539-548

[34] Ryan J. Farris, Hugo A. Quintero and Michael Goldfarb (2011), "*Preliminary Evaluation of a Powered Lower Limb Orthosis to Aid Walking in Paraplegic Individuals*", IEEE Transactions On Neural Systems And Rehabilitation Engineering, Vol. 19, No. 6, pp. 652-659

[35] Ryan J. Farris, Hugo A. Quintero and Michael Goldfarb (2012), "*Performance Evaluation of a Lower Limb Exoskeleton for Stair Ascent and Descent with Paraplegia*", 34th Annual International Conference of the IEEE EMBS San Diego, California USA, pp. 1908-1911

[36] Peter D. Neuhaus, Jerryll H. Noorden, Travis J. Craig, Tecalote Torres, Justin Kirschbaum and Jerry E. Pratt (2011), "*Design and Evaluation of Mina, a Robotic Orthosis for Paraplegics*", IEEE International Conference on Rehabilitation Robotics Rehab Week Zurich, ETH Zurich Science City, Switzerland

[37] (2018), https://mindwalker-project.eu/ [ONLINE]

[38] Shiqian Wang, Cor Meijneke and Herman van der Kooij (2013), "*Modeling, Design, and Optimization of Mindwalker Series Elastic Joint*", IEEE International Conference on Rehabilitation Robotics, Seattle, Washington USA

[39] Sang-Ho Hyon, Takuya Hayashi, Atsutoshi Yagi, Tomoyuki Noda and Jun Morimoto (2013), "*Design of Hybrid Drive Exoskeleton Robot XoR2*", IEEE/RSJ International Conference on Intelligent Robots and Systems (IROS), pp. 4642-4648

[40] Wei Yang, Can-jun Yang, and Qian-xiao Wei (2014), "*Design of an Anthropomorphic Lower Extremity Exoskeleton with Compatible Joints*", Proceedings of the 2014 IEEE International Conference on Robotics and Biomimetics, pp. 1374-1379

[41] Nicola Vitiello, Francesco Giovacchini, Mario Cortese, Andrea Parri, Tingfang Yan, Marko Munih, Dirk Lefeber and Raffaele Molino-Lova (2015), "*CYBERLEGs: un nuovo sistema robotico per gli amputati di arto inferiore*", pp. 53-92

[42] Francesco Giovacchini, Federica Vannetti, Matteo Fantozzi, Marco Cempini, Mario Cortese, Andrea Parri, Tingfang Yan, Dirk Lefeber and Nicola Vitiello (2015), "*A light-weight active orthosis for hip movement assistance*", Robotics and Autonomous Systems 73, pp. 123–134

[43] Marco Cempini, Dario Marconi, Marco Muscolo, Matteo Moisè, Matteo Fantozzi, Mario Cortese, Andrea Parri, Tingfang Yan, Simona Crea, Francesco Giovacchini, Federico Posteraro, Maria Chiara Carrozza, and Nicola Vitiello (2015), "*Relevance of Series-Elastic Actuation in Rehabilitation and Assistance Robotic: two Cases of Study*", 978-1-4673-8167-3/15 2015 IEEE

[44] (2018), https://innophys.jp/ [ONLINE]

[45] Chie Sato, Juji Yokoya, Hiromi Watanabe, Hideyuki Umehara, Hiroki Nakamura and Hiroshi Kobayashi (2013), "*Field Test of the Back Support Muscle Suit (Application in the Material Handling Field)*", 2013 The Japan Society of Mechanical Engineers, pp. 3525-3538

[46] Y. Muramatsu, H. Umehara, and H. Kobayashi (2013), "*Improvement and Quantitative Performance Estimation of the Back Support Muscle Suit*", 35th Annual International Conference of the IEEE EMBS Osaka, Japan, pp. 2844-2849

[47] Yoshiki Muramatsu and Hiroshi Kobayashi (2014), "*Assessment of local muscle fatigue by NIRS - development and evaluation of muscle suit -*", Muramatsu and Kobayashi ROBOMECH Journal, pp. 1-11

[48] Takahiro Ito, Ko Ayusawa, Eiichi Yoshida, and Hiroshi Kobayashi (2016), "*Stationary Torque Replacement for Evaluation of Active Assistive Devices using Humanoid*", 2016 IEEE-RAS 16th International Conference on Humanoid Robots (Humanoids), Cancun, Mexico, pp. 739-744

[49] Eita Nakamura, Kouki Ichinose and Hiroshi Kobayashi (2017), "*Development and Evaluation of Muscle Suit for Arms and Lower Back Support*", 17th International Conference on Control, Automation and Systems (ICCAS 2017), Ramada Plaza, Jeju, Korea, pp. 1462-1465

[50] (2018), http://rewalk.com/ [ONLINE]

[51] A. Esquenazi, M. Talaty, A. Packel and M. Saulino (2012), "*The ReWalk Powered Exoskeleton to Restore Ambulatory Function to Individuals with Thoracic-Level Motor-Complete Spinal Cord Injury*", American Journal of Physical Medicine & Rehabilitation: November 2012 - Volume 91, pp. 911–921

[52] (2018), http://www.indego.com/indego/en/home [ONLINE]

[53] Katherine A. Strausser and H. Kazerooni (2011), "*The Development and Testing of a Human Machine Interface for a Mobile Medical Exoskeleton*", IEEE/RSJ International Conference on Intelligent Robots and Systems September 25-30, 2011. San Francisco, CA, USA, pp. 4911-4916

[54] Tobias Nefa, Marco Guidalic, and Robert Rienerc (2009), "*ARMin III – arm therapy exoskeleton with an ergonomic shoulder actuation*", Applied Bionics and Biomechanics Vol. 6, No. 2, June 2009, pp. 127–142

[55] Hyung-Soon Park, Yupeng Ren, and Li-Qun Zhang (2008), "*IntelliArm: An Exoskeleton for Diagnosis and Treatment of Patients with Neurological Impairments*", Proceedings of the 2nd Biennial IEEE/RAS-EMBS International Conference on Biomedical Robotics and Biomechatronics, pp. 109-114

[56] Joaquin Blaya, Dava Newman and Hugh Herr (2002), "*Active Ankle Foot Orthoses (AAFO)*", pp. 275-277

[57] Hutter M., Remy C. D., Hoepflinger M. A., and Siegwart R. (2011). "*High compliant series elastic actuation for the robotic leg ScarlETH*", In Proc. of the International Conference on Climbing and Walking Robots (CLAWAR)

[58] (2018), http://asimo.honda.com/innovations/feature/body-weight-support-assist/ [ONLINE]

[59] Carolyn Buesing, Gabriela Fisch, Megan O'Donnell, Ida Shahidi, Lauren Thomas, Chaithanya K. Mummidisetty, Kenton J. Williams, Hideaki Takahashi, William Zev Rymer and Arun Jayaraman (2015), "*Effects of a wearable exoskeleton stride management assist system (SMA©) on spatiotemporal gait characteristics in individuals after stroke: a randomized controlled trial*", Buesing et al. Journal of NeuroEngineering and Rehabilitation

[60] Yasushi Ikeuchi, Jun Ashihara, Yutaka Hiki, Hiroshi Kudoh and Tatsuya Noda (2009), "*Walking Assist Device with Bodyweight Support System*", The 2009 IEEE/RSJ International Conference on Intelligent Robots and Systems, pp. 4073-4079

[61] (2018), www.army-technology.com/projects/human-universal-load-carrier-hulc/ [ONLINE]

[62] (2018), https://www.sarcos.com/ [ONLINE]

[63] (2018), http://www.20knots-plus.com/marine-mojo/ [ONLINE]

[64] (2018), https://www.bionic-power.com/ [ONLINE]

[65] (2018), https://www.noonee.com/en/ [ONLINE]

[66] (2018), https://www.rb3d.com/en/exo/ [ONLINE]

[67] (2018), http://www.suitx.com/ [ONLINE]

[68] (2018), http://atoun.co.jp/products/atoun-model-a [ONLINE]

[69] (2018), https://www.strongarmtech.com/products [ONLINE]

[70] (2018), https://www.hyundai.news/eu/technology/hyundai-motor-leads-personal-mobility-revolution-with-advanced-robots/?L=0 [ONLINE]

[71] (2018), http://en.laevo.nl/laevo-v2-product-information/ [ONLINE]

[72] (2018), http://marvel.com/characters/29/iron_man [ONLINE]

[73] (2018), http://marvel.com/movies/movie/19/iron_man [ONLINE]

[74] (2018), https://www.alienuniverse.com/film/aliens [ONLINE]

[75] (2018), https://www.gundam.info/ [ONLINE]

[76] (2018), http://www.evangelion.co.jp/neon_genesis.html [ONLINE]

[77] (2018), https://www.konami.com/games/eu/it/products/mgs/ [ONLILNE]

[78] (2018), https://www.ea.com/it-it/games/crysis/crysis [ONLINE]

[79] ISO/TR 7250-2:2010 – Basic human body measurements for technological design – Part 2: Statistical summaries of body measurements from individual ISO populations

[80] "*Physics of the Human Body*", Herman Irving P, Springer Verlag 2007

[81] David W. Robinson, Jerry E. Pratt, Daniel J. Paluska, and Gill A. Pratt (1999), "*Series Elastic Actuator Development for a Biomimetic Walking Robot"*, International Conference on Advanced Intelligent Mechatronics

[82] Kyoungchul Kong, Joonbum Bae, and Masayoshi Tomizuka (2009), "*Control of Rotary Series Elastic Actuator for Ideal Force-Mode Actuation in Human – Robot Interaction Applications"*, IEEE/ASME Transactions On Mechatronics

[83] Kyoungchul Kong, Joonbum Bae, and Masayoshi Tomizuka (2012), "*A Compact Rotary Series Elastic Actuator for Human Assistive Systems"*, IEEE/ASME Transactions On Mechatronics

[84] Marco Cempini, Dario Marconi, Marco Muscolo, Matteo Moisè, Matteo Fantozzi, Mario Cortese, Andrea Parri, Tingfang Yan, Simona Crea, Francesco Giovacchini, Federico Posteraro, Maria Chiara Carrozza, and Nicola Vitiello (2015), "*Relevance of Series-Elastic Actuation in Rehabilitation and Assistance Robotic: two Cases of Study"*, IEEE

[85] Fabio Antonaci, Gurmar Bovim, Maria Luisa Fasano, Lucas Bonamico, and Jie-Ming Shen (1992), "*Pain Threshold in Humans. A Study with the Pressure Algometer*, Functional Neurology" (7)4

[86] Marja Mikkelsson, Pirjo Latikka, Hannu Kautiainen, Risto Isomeri, and Heikki Isomtiki (1992), *"Muscle and Bone Pressure Pain Threshold and Pain Tolerance in Fibromyalgia Patients and Controls"*, Arch Phys Med Rehabil Vol.73

[87] Maxon Motor© (2017), *EC frameless 90 flat Ø90 mm, brushless, 160 Watt,* September 2017 product catalogue

[88] Maxon Motor© (2011), *Motori Maxon DC e Maxon EC, Le Cose Più Importanti*, August 2011 product catalogue, pp. 36-43

[89] Altra Industrial Motion© (2018), *Clutches and Brakes*, 2018 product catalogue

[90] Harmonic Drive© AG (2014), *Engineering Data CPL-2A Components Sets*, December 2014 product catalogue

[91] Schneider Electric Motion USA© (2018), *Stepper Motors - 1.8° 2-phase stepper motors*, Product catalogue

[92] Richard W. Bohannon (1997), "*Comfortable and maximum walking speed of adults aged 20-79 years: reference values and determinants"*, Age and Ageing 1997, pp. 15-19

[93] R. Hari Krishnan, V. Devanandh, Aditya Kiran Brahma and S. Pugazhenthi (2016), "*Estimation of Mass Moment of Inertia of Human Body, When Bending Forward, For The Design Of A Self-Transfer Robotic Facility*", Journal of Engineering Science and Technology Vol. 11, No. 2, pp. 166-176

[94] Bruno Siciliano, Lorenzo Sciavicco Luigi Villani and Giuseppe Oriolo (2009), "*Robotics - Modelling, Planning and Control*", Springer-Verlag London Limited, pp. 247-289

[95] Maxon Motor© (2018), *RE 65 Ø65 mm, Graphite Brushes, 250 Watt*, May 2018 product catalogue, p. 134

[96] Wibawa Adhi (2014), "*Lower limb musculoskeletal modeling during normal walking, one-legged forward hopping, side jumping and knee flexion*", University of Groningen

# Acknowledgements

My heartful thanks to my thesis supervisor Professor Luigi Mazza for providing me with professional guidance during study period. I am also great indebted to my thesis co-supervisors, Professor Terenziano Raparelli, Professor Gabriella Eula and Professor Alexandre Ivanov, for their valuable suggestions to accomplish the study. I am also grateful to the researcher Riccardo Mala for the cooperation received during the study period.

*% English language → Italian language*

E quindi eccoci qui, al termine di una strada che all'inizio pareva sfociare all'orizzonte. Eppure, eccoci qui. Se scrivo queste ultimissime righe in lingua italiana è perché voglio parlare a voi, in maniera più calda ed intima, come se fossimo tutti insieme in una spiaggia solitaria durante una chiara notte estiva, con le braccia protese verso un falò. Voglio farlo perché i protagonisti di queste parole siete proprio voi. Voi, che mi avete dato tutto, e dopo anche di più. Voi, che mi siete stati sempre accanto, sia nei momenti luminosi che in quelli più bui. Voi, che mi avete insegnato più di quanto qualunque libro potesse mai fare. Voi, che con la potenza di un sorriso, di una lacrima o di un abbraccio, siete riusciti a svoltarmi prima la giornata, e poi la vita. Quello che sono è frutto di ciò che siete voi, ed è solo grazie alla vostra influenza che oggi posso dire di essere moderatamente orgoglioso di me stesso. Sapete, sono fermamente convinto che la fortuna di un uomo si misuri sulla base della qualità delle persone di cui si circonda. Sono un ragazzo fortunato. Grazie a voi.

Vostro,
Gabriele